



**MONASH** University

# **Controlled drug release from porous silicon nanomaterials**

**Yufei Xue**

B. Sc.

A thesis submitted in fulfilment of the requirements for the Degree of  
Doctor of Philosophy

Department of Drug Delivery, Disposition and Dynamics  
Faculty of Pharmaceutical Sciences  
Monash University

381 Royal Parade Parkville, Victoria, Australia, 3052

April, 2021

## **Copyright notice**

© Yufei Xue (2021).

I certify that I have made all reasonable efforts to secure copyright permissions for third-party content included in this thesis and have not knowingly added copyright content to my work without the owner's permission.

# *Table of contents*

Statement of originality.....	4
Publications during enrolment .....	5
Thesis including published works declaration .....	5
Acknowledgements .....	7
Abbreviations .....	8
Abstract .....	11
Chapter 1.0: Introduction .....	12
1.1 Overview of traditional drug delivery systems .....	12
1.2 Porous silicon nanoparticles and versatile surface functionalisation .....	12
1.3 Emerging challenges of porous silicon nanoparticles in delivering small molecule drugs .....	14
1.4 Stimulus-cleavable linkers in the field of controlled drug delivery .....	15
1.4.1 Photo-cleavable linkers (PCLs) .....	16
1.4.2 Acid-cleavable linkers (ACLs) .....	18
1.4.3 Enzyme-cleavable linkers (ECLs) .....	19
1.4.4 Self-immolative spacers.....	20
1.4.5 The application of SCLs in controlled drug release .....	21
1.5 Project aims/hypothesis of incorporating SCLs into pSiNP-based DDSs .....	22
1.5.1 Drug selection.....	24
1.5.2 Conjugation strategy .....	25
Chapter 2.0: Design and synthesis of SCL-DOX conjugates .....	27
2.1 Synthetic approach to Photo-cleavable linker (PCL).....	27
2.2 Synthetic approach to Acid-cleavable linker (ACL).....	29
2.2.1 Synthetic approach to <b>ACL-Vanillin</b> .....	29
2.2.2 Synthetic approach to <b>ACL-DOX</b> .....	30
2.3 Synthetic approach to Enzyme-cleavable linker (ECL).....	31
2.3.1 Synthetic approach to <b>ECL-Benzylamine</b> .....	31
2.3.2 Synthetic approach to <b>ECL-DOX</b> .....	35
Chapter 3.0: Fabrication and surface functionalisation of porous silicon nanoparticles .....	37
3.1 Preparation of freshly etched pSiNPs.....	37
3.2 Surface functionalisation of pSiNPs .....	38
3.3 Preparation of pSiNP-SCL-DOX.....	38
3.4 pSiNP-SCL-DOX Characterisation .....	38
3.4.1 TEM and SEM result .....	38
3.4.2 DLS result.....	39

3.4.3 Surface chemistry characterisation .....	40
3.4.4 Drug loading capacity characterisation .....	41
Chapter 4.0: Linker cleavage study.....	43
4.1 Study on the stimulus-responsive linker cleavage .....	43
4.1.1 Cleavage of <b>PCL-DOX</b> .....	43
4.1.2 Cleavage of <b>ACL-Vanillin</b> .....	44
4.1.3 Cleavage of <b>ACL-DOX</b> .....	45
4.1.4 Cleavage of <b>ECL-Benzylamine</b> .....	47
4.1.5 Cleavage of <b>ECL-DOX</b> .....	47
4.2 DOX release from pSiNP-SCL-DOX upon exposure to corresponding stimuli.....	48
Chapter 5.0: In vitro and in vivo test of pSiNP-SCL-DOX .....	50
5.1 Cytotoxicity test .....	50
5.2 Cellular uptake study.....	51
5.3 In vivo test.....	52
Chapter 6.0: Conclusion, supplementary experiment and future work.....	53
6.1 Conclusion.....	53
6.2 Supplementary experiment and future work .....	53
Chapter 7.0: Experimental Section .....	59
7.1 Synthesis of test compounds general chemistry.....	59
7.1.1 Synthesis of <b>PCL-DOX</b> .....	60
7.1.2 Synthesis of <b>ACL-Vanillin</b> and <b>ACL-DOX</b> .....	62
7.1.3 Synthesis of <b>ECL-Benzylamine</b> and <b>ECL-DOX</b> .....	63
7.1.4 Synthesis of deep red light-cleavable linker .....	69
7.2 Surface functionalisation of pSiNPs .....	71
7.3 Biological assays .....	72
7.3.1 C32 cell viability assays .....	72
7.3.2 In vivo test .....	73
<b>Chapter 8.0: References .....</b>	<b>74</b>
<b>Appendix.....</b>	<b>81</b>

## *Statement of originality*

To the best of the author's knowledge and belief, this thesis contains no material which has been accepted for the award for any other degree or diploma in any University or other institution, and contains no material previously published or written by another person except where due reference is made.

Yufei Xue

April, 2021

## *Publications during enrolment*

**Yufei Xue**, Hua Bai, Bo Peng, Bin Fang, Jonathan Baell, Lin Li, Wei Huang and Nicolas Hans Voelcker. Stimulus-cleavable chemistry in the field of controlled drug delivery. *Chemical Society Reviews*. **2021** March doi:10.1039/d0cs01061h.

## *Thesis including published works declaration*

I hereby declare that this thesis contains no material which has been accepted for the award of any other degree or diploma at any university or equivalent institution and that, to the best of my knowledge and belief, this thesis contains no material previously published or written by another person, except where due reference is made in the text of the thesis.

This thesis includes 1 review paper published in review journal.

In the case of Chapter 1, my contribution to the work involved the following:

<b>Thesis Chapter</b>	<b>Publication Title</b>	<b>Status</b>	<b>Nature and % of student contribution</b>	<b>Co-author name(s) Nature and % of Coauthor's contribution</b>	<b>Co-author(s), Monash student Y/N*</b>
1	Stimulus-cleavable chemistry in the field of controlled drug delivery	Published	60% Literature writing	BH, BP, BF, JB, LL, WH, NHV edited and provided input into manuscript preparation (40%)	N

I have not renumbered sections of submitted or published papers in order to generate a consistent presentation within the thesis.

**Student name:**

**Student signature:**

**Date:**

I hereby certify that the above declaration correctly reflects the nature and extent of the student's and co-authors' contributions to this work.

**Main Supervisor name:**

**Main Supervisor signature:**

**Date:**

## *Acknowledgements*

I would like to begin by acknowledging my supervisor Professor Nicolas Voelcker and Dr Bo Peng. Words do not give justice to the continual guidance, wisdom and support you have provided me throughout this research effort. Your constant dedication and enthusiasm are truly inspiring and have played a significant role in the progression of the project to where it is today. I cannot help but share in this enthusiasm which has driven me to achieve my best. I am extremely thankful for all the knowledge and opportunities you have given me, not least the opportunity to work with you on this project.

I further wish to acknowledge my panel members –Professor Jonathan Baell, Dr Beatriz Prieto-Simon and Dr Helmut Thissen – for all your advice and encouragement, it is greatly appreciated.

Considerable thanks go to the many collaborators who worked on this project, without whom this research would not stand. Particularly, Dr Terence Tieu for his work on preparation of porous silicon nanoparticles and Dr Bai Hua for her work on *in vivo* experiments.

I wish to especially thank Dr Jason Dang, without you no work would simply get done at Monash. Thank you for your tireless dedication to your work in looking after the NMR and HPLC/MS machinery, for your patience in helping me, and for being my friend. Special thanks to Winfield Jugo for his commitment to safety, and to Nicole Penny.

## Abbreviations

$\mu\text{g}$	microgram
$\mu\text{M}$	micromolar
$^{13}\text{C}$ NMR	carbon nuclear magnetic resonance spectroscopy
$^1\text{H}$ NMR	proton nuclear magnetic resonance spectroscopy
ACL	acid-cleavable linker
AcOH	acetic acid
ADCs	antibody-drug conjugates
$\text{Ag}_2\text{O}$	silver oxide
APTES	3-Aminopropyltriethoxy-silane
(BimC4A) <sub>3</sub>	tris(benzimidazole)
$\text{Boc}_2\text{O}$	di-tert-butyl dicarbonate
$\text{CaCO}_3$	calcium carbonate
$\beta\text{-CD}$	$\beta$ -cyclodextrin
$\text{CH}_2\text{O}_2$	formic acid
MeCN	acetonitrile
CLP	clathrin-mediated endocytosis inhibitor
$\text{CO}_2$	carbon dioxide
CPT	camptothecin
$\text{Cs}_2\text{CO}_3$	cesium carbonate
CuAAC	Cu(I)-catalysed azide alkyne cycloaddition
Cu(I)	copper(I) iodide
DCC	N, N'-dicyclohexylcarbodiimide
DCM	dichloromethane
DDSs	drug delivery systems
DIPEA	N, N-diisopropylethylamine
DLS	dynamic light scattering
DMAP	4-Dimethylaminopyridine
DMF	dimethylformamide
DOX	doxorubicin
DSC	N, N-disuccinimidyl carbonate
DMSO	dimethyl sulfoxide

EDCI·HCl	N-ethyl-N'-(3-dimethylaminopropyl)carbodiimide hydrochloride
ECL	enzyme-cleavable linker
EPR	enhanced permeability and retention
Et <sub>3</sub> N	triethylamine
EtOAc	ethyl acetate
EtOH	ethanol
FDA	Food and Drug Administration
Fe	iron
FTIR	Fourier transform infrared spectroscopy
5-FU	5-fluorouracil
GHs	glycoside hydrolases
GNPs	gold nanoparticles
H <sup>+</sup>	hydrogen ion
HATU	2-(7-Azabenzotriazol-1-yl)-N, N, N', N'-tetramethyluronium hexafluorophosphate
HF	hydrofluoric acid
H <sub>2</sub> SO <sub>4</sub>	sulfuric acid
HBr	hydrobromic acid
HCl	hydrochloric acid
HNO <sub>3</sub>	nitric acid
HOBt	1-Hydroxybenzotriazole
HR-ESI	high-resolution electrospray ionisation mass spectrometry
K <sub>2</sub> CO <sub>3</sub>	potassium carbonate
KOH	potassium hydroxide
LC-MS	liquid chromatography/mass spectrometry
LiOH.H <sub>2</sub> O	lithium hydroxide monohydrate
<i>m</i> CPBA	meta-chloroperoxybenzoic acid
MDR	multidrug resistance
MeOH	methanol
MgSO <sub>4</sub>	magnesium sulfate
MPTES	3-Mercaptopropyltriethoxy-silane
MSNs	mesoporous silica nanoparticles
MTT	Methylthiazolyldiphenyl-tetrazolium bromide
MTX	methotrexate

MW	molecular weight
Na <sub>2</sub> S <sub>2</sub> O <sub>4</sub>	sodium dithionite
NaBH <sub>4</sub>	sodium borohydride
NaCl	sodium chloride
NADPH/NADP <sup>+</sup>	nicotinamide adenine dinucleotide phosphate
NaHCO <sub>3</sub>	sodium bicarbonate
NaN <sub>3</sub>	sodium azide
NaOH	sodium hydroxide
Na <sub>2</sub> SO <sub>4</sub>	sodium sulphate
NH <sub>4</sub> Cl	ammonium chloride
NHS	N-hydroxysuccinimide
Noc	nocodazole
NPs	nanoparticles
Ny	nystatin
mM	millimolar
O <sub>3</sub>	ozone
ONB	<i>o</i> -nitrobenzyl
PCL	photo-cleavable linker
PDCs	polymers-drug conjugates
PK	pharmacokinetics
pKa	negative logarithm of the acid dissociation constant
pSiNP	porous silicon nanoparticle
RT	room temperature
SCL	stimulus-cleavable linker
SEM	scanning electron microscopy
TEM	transmission electron microscopy
TFA	trifluoroacetic acid
TGA	thermogravimetric analysis
THF	tetrahydrofuran
THPTA	tris(hydroxypropyltriazolylmethyl)amine
XTT	2,3-Bis-(2-methoxy-4-nitro-5-sulfohenyl)-2H-tetrazolium-5-carboxanilide

## Abstract

Over the past few years, there has been increased interest in introducing stimulus-cleavable linkers (SCLs) into the nanoparticle-based drug delivery systems (DDSs) for cancer therapy. This has led to the development of novel SCLs showing robust responsiveness to different stimuli, which can be implicated in achieving controlled drug release behaviour on nanoparticles.

Chapter 1 provides an overview of the current landscape of SCLs for controlled drug release. Then, the introduction of porous silicon nanoparticles (pSiNPs) and their advantages as drug carriers are given. Lastly, the aim and project design are detailed.

In Chapter 2, the design and synthesis of SCLs is reported. As the bridge between the small molecules drug doxorubicin (DOX) and pSiNP, the SCLs are designed to be cleaved upon exposure to both endogenous and exogenous stimuli, which also exist as the biomarkers of cancerous cells. Here, we designed and synthesised three SCLs which can be cleaved by UV irradiation, acidic pH and enzyme respectively. The cleavage of SCLs will lead to the release of DOX, which has been identified to display cytotoxicity and cause cell apoptosis.

In Chapter 3, the fabrication of pSiNP for controlled size is described. The preparation of pSiNP following the anodic electrochemical etching method was previously reported, and freshly anodised pSi was further functionalised, providing a chemical handle for further SCL-DOX conjugate attachment. The synthesised SCL-DOX conjugates were further articulated to the surface of pSiNP based on catalysed alkyne-azide cycloaddition (CuAAC, i.e. click reaction). The successful conjugation and corresponding loading capacity (LC) of pSiNPs were confirmed by various characterisation methods.

Following Chapter 3, Chapter 4 demonstrates the controlled drug release from pSiNP modified with three SCL-DOX conjugates (pSiNP-SCL-DOX). The drug released from pSiNP-SCL-DOX was found to occur in a stimuli-dependent order, with full drug release being observed upon exposure to the corresponding stimuli but no drug release in the absence of stimuli.

In Chapter 5, the pSiNP-SCL-DOX was tested in the absence and presence of corresponding stimuli both *in vitro* and *in vivo* to confirm the stimulus-dependent drug release behaviour.

Conclusion and future work of this project are provided at the end.

## Chapter 1.0: Introduction

### 1.1 Overview of traditional drug delivery systems

Over the past few decades, significant progress has been achieved in the field of drug discovery, affording new candidates with high efficacy and safety for the treatment of different diseases.<sup>2-7</sup> However, traditional pharmaceuticals, especially small molecule drugs, follow a non-specific distribution path within the human body when administered *via* traditional drug formulations, leading to unacceptable toxicity at healthy tissues, as well as severe side effects and narrow therapeutic indexes.<sup>8</sup> Moreover, several other drawbacks also prevent promising drug candidates from moving to clinical application, such as hydrophobicity,<sup>9-12</sup> development of multidrug resistance (MDR),<sup>13-16</sup> and low cell/tissue permeability.<sup>17-20</sup> The problems associated with traditional pharmaceuticals have provided an impetus to the discovery of DDSs, methods, or devices designed to decrease the exposure of healthy organs or cells to the drugs<sup>21, 22</sup> and improve the pharmacokinetic (PK) parameters of drugs, such as bioavailability<sup>23, 24</sup> and plasma clearance.<sup>25</sup> For instance, anti-cancer drugs loaded nanosized materials (e.g. engineered nanoparticles<sup>26</sup> and polymers-drug conjugates (Polymer-DCs)<sup>27</sup>) showed promising accumulation at tumour sites by enhanced permeability and retention (EPR) effect, contributing to an increase in specific targeting ability and a decrease in cytotoxicity to normal cells.

Although substantial advances have been made in the development of DDSs, uncontrolled drug release behaviour from DDSs emerged as a main issue, which causes undesired premature drug release to the healthy tissue and thus impairs the therapeutic effect.<sup>28</sup> To achieve an ideal concentration of drugs at target sites, the concept of controlled drug release was incorporated into the DDSs.<sup>29</sup> Early efforts have been devoted to exploring materials capable of releasing the drugs in a controlled manner, and numerous materials have attracted significant attention. Particularly, nanomaterials, such as porous nanoparticles,<sup>30, 31</sup> liposomes,<sup>32-34</sup> and polymers,<sup>35-38</sup> have been well studied for their potential to establish a controlled drug release order and some received promising results.<sup>39-41</sup>

### 1.2 Porous silicon nanoparticles and versatile surface functionalisation

pSiNPs (**Figure 1**) have gained increasing popularity for their potential applications in the drug delivery field. Firstly discovered in 1956, pSiNPs were found to be biocompatible and biodegradable, which is considered one of its most appealing features as a drug carrier.<sup>42</sup> Other characteristics of pSiNPs such as high porosity<sup>43</sup> and tuneable pore size<sup>44</sup> also make this type of nanomaterial a promising carrier for encapsulating therapeutic payloads for drug delivery purpose. pSiNPs used for biomedical applications are commonly prepared through electrochemical etching of silicon wafers in aqueous or ethanolic HF electrolytes, also known as anodisation. The nanostructure of pSiNPs can be manipulated by adjusting the fabrication parameters such as current density, level of doping, and electrolyte composition to meet the specific requirement.<sup>45, 46</sup> Notably, pSiNPs are an attractive

platform for drug delivery where versatile surface chemistry can be utilised to stabilise the loaded drug while prolonging the half-time of the drug delivery carrier in circulation.<sup>47</sup>

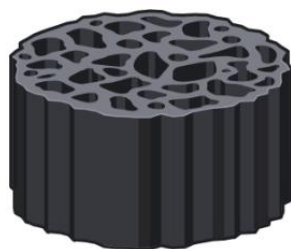


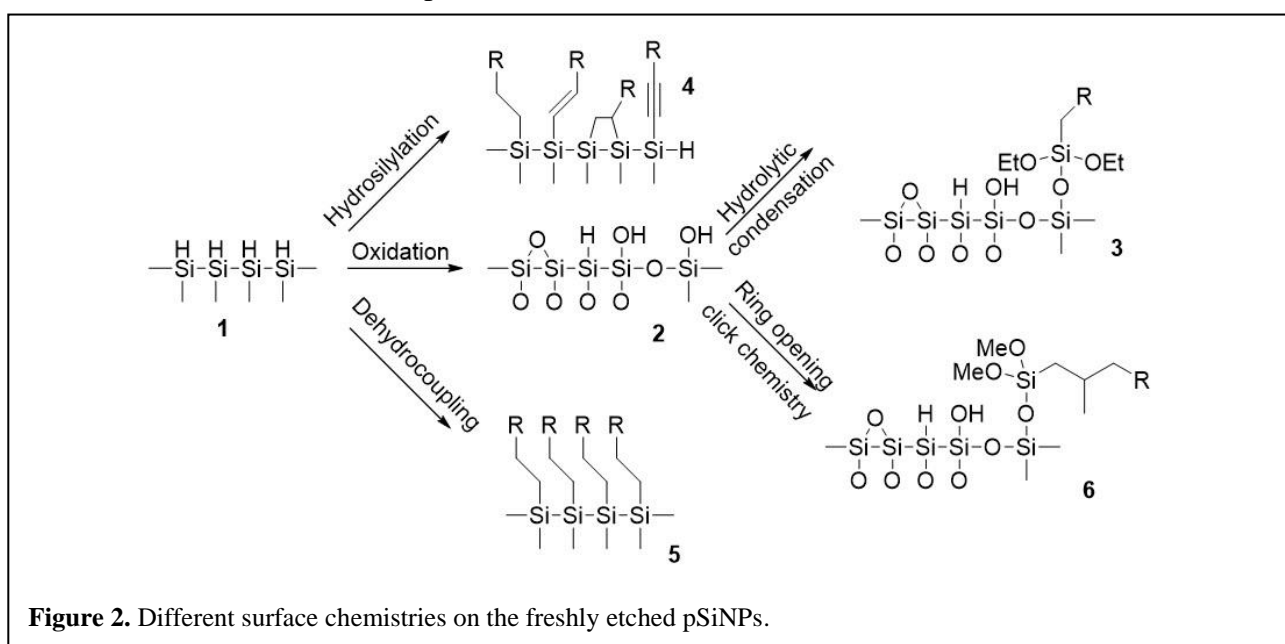
**Figure 1.** Image of porous silicon nanoparticles (pSiNPs).

Although the electrochemical etching of Si wafers affords pSiNPs with unique and tuneable properties, the freshly etched pSiNP is highly reactive due to its hydride terminated (Si-H, Si-H<sub>2</sub>, Si-H<sub>3</sub>) surface.<sup>48</sup> To make pSiNPs a better candidate for drug delivery, further surface modification to stabilise the pSiNPs is required. Conventional surface modification methods for pSiNPs involve oxidation, hydrolytic condensation, and hydrosilylation reaction. Among those three modification methods, oxidation is the most commonly used one to stabilise the surface of pSiNPs, by breaking the silicon-hydride (Si-H) and silicon-silicon (Si-Si) bond (**1** in **Figure 2**) on the surface of pSiNP to produce hydrated silicon oxide (Si-OH) and silicon oxide (Si-O-Si) bonds (**2** in **Figure 2**). Given the low bonding energy of the Si-Si bond compared with Si-H bond, the addition of mild oxidants like dimethyl sulfoxide (DMSO)<sup>49</sup> and pyridine<sup>50</sup> is able to break the Si-Si bond, resulting in the generation of Si-O-Si bond at room temperature (RT). The increase in oxidant reactivity can lead to an increase in oxidation degree. For instance, ozone (O<sub>3</sub>)<sup>51</sup> can break both the Si-Si and Si-H bonds to generate Si-O-Si and Si-OH at RT. Apart from chemical-based oxidation, thermal oxidation serves as another popular method to stabilise the surface of pSiNP. In the presence of dry oxygen, the back-bond oxidation mainly occurs at 300-400°C, whereas the oxidation at 600°C and above completely converts the pSiNP into silicon oxide.<sup>52</sup> As a result of oxidation, the hydrophobic nature of pSiNP changes to hydrophilic, which is a favourable feature for the construction of DDSs.

The oxidised pSiNP can serve as a promising platform for further modification, and the most commonly used method refers to hydrolytic condensation. The main efforts have been made on two silanes, 3-Aminopropyltriethoxy-silane (APTES)<sup>53</sup> and 3-Mercaptopropyltriethoxy-silane (MPTES),<sup>54</sup> for hydrolytic condensation with oxidised pSiNP materials, producing the primary amine and thiol terminals on their surface, respectively (**3** in **Figure 2**). Both the amine and thiol groups allow further conjugation with other molecules *via* amide coupling<sup>55</sup> or thiol-Michael addition<sup>56</sup> with a high yield.

Apart from surface oxidation, the hydrosilylation reaction is another strategy to stabilise the surface of pSiNP, where Si-H reacts with unsaturated compounds such as alkynes, alkenes, and aldehydes to form the silicon-carbon (Si-C) bond (**4** in **Figure 2**).<sup>57</sup> Owing to the low electronegativity of carbon, the Si-C bond possesses greater kinetics stability compared with Si-O bond, leading to more stable

pSiNP surface.<sup>58</sup> Hydrosilylation can be catalysed through a variety of means including thermal, photon, chemical catalyst, and microwave, some of which can even occur under mild conditions. More importantly, hydrosilylation can provide versatile functional groups on the pSiNP surface for further modification.<sup>47, 59, 60</sup> However, one of the disadvantages of hydrosilylation refers to the production of silicon oxide during the modification process. Therefore, it usually proceeds in the absence of oxidants. A replacement for hydrosilylation has been recently proposed, namely dehydrocoupling, which can occur under mild thermal conditions through dehydrogenative coupling with a trihydridosilane reagent (**5** in **Figure 2**).<sup>61</sup> The dehydrocoupling shows tolerance to oxidants like oxygen and H<sub>2</sub>O, while various functional groups such as bromide, azide, and amine are allowed to be installed on the surface of pSiNP.



As mentioned before, the Si-H bond on pSiNP surface is usually oxidised to the Si-O bond, which can be further modified through hydrolytic condensation. However, there are several drawbacks of this modification method, including long reaction time, production of by-products due to cross-linking, and low coupling efficiency.<sup>62</sup> To overcome these limitations, a novel alternative of hydrolytic condensation, known as ring-opening click chemistry, was introduced.<sup>63</sup> The general mechanism is illustrated in **Figure 2**, where the Si-OH on the pSiNP surface attacks the silicon core of cyclic-silane reagent to break the Si-X (X= S or N) bond, giving rise to the new terminals like primary amine or thiol on the pSiNP surface (**6**). The ring-opening click chemistry provides an advance in bio-conjugation applications due to its high yield without by-products and under mild reaction conditions.<sup>63, 64</sup>

### 1.3 Emerging challenges of porous silicon nanoparticles in delivering small molecule drugs

Although pSiNP-based DDSs have made great success in the treatment of various types of diseases, it has been hindered dramatically by several issues such as premature drug release and the degradation

of loaded active agent.<sup>65</sup> These drawbacks are caused by the conventional drug loading methods, especially when pSiNPs are used to deliver small molecule drugs.

Commonly used methods to load drugs into pSiNPs can be categorised into three types: physical adsorption, noncovalent bond stacking, and drug/particle entrapment.<sup>31,66</sup> Among all the approaches, physical adsorption has been extensively used for drug loading due to the simplicity of this method and large surface area of pSiNPs.<sup>67</sup> Based on the “like dissolves like” principle between the loaded drug and pSiNPs, the hydrophobic pSiNPs tend to load more hydrophobic drugs.<sup>68</sup> Although physical adsorption plays a critical role in the drug loading process, the noncovalent bonding between the cargo and carrier is considered unstable in circulation. In this case, a considerable fraction of therapeutics may leak out from the pSiNPs, resulting in potential damage to healthy organs or tissues.<sup>67</sup>

In comparison to physical adsorption methods, increased loading efficiency can be achieved *via* drug entrapment by oxidation.<sup>40</sup> Upon oxidation of freshly etched pSiNPs, a volume expansion was observed to accommodate the extra oxygen atoms, and the pore structure tends to shrink and collapse, causing the entrapment of drug molecules. Nevertheless, the oxidation of pSiNPs requires a relatively harsh environment where strong oxidants such as peroxide and nitrite are used, and this may affect the original structure of the loaded drug and result in drug inactivation.<sup>67</sup>

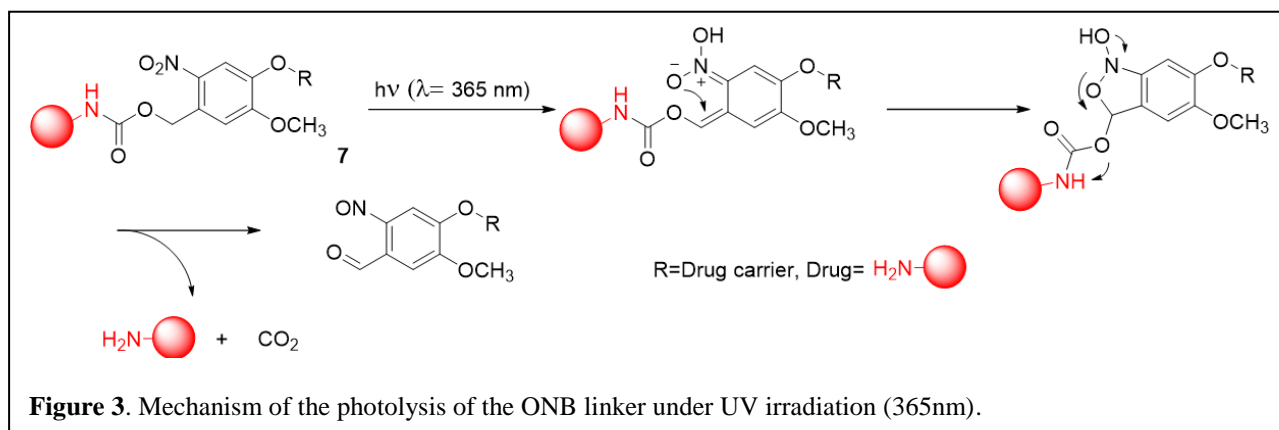
Although the aforementioned methods have delivered positive outcomes in some cases, the limitations, such as lack of controlled drug release manner, high drug leakage, limited drug selection, and low drug LC, hinder the application of these pSiNPs in clinics.

#### **1.4 Stimulus-cleavable linkers in the field of controlled drug delivery**

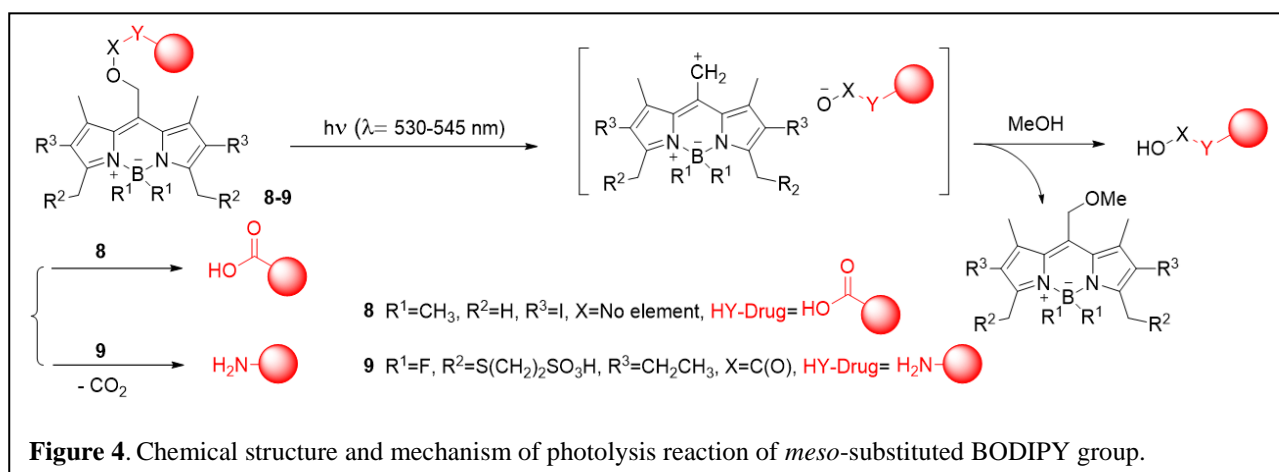
SCLs are defined as chemical structures with sensitivity to single or multiple stimuli, the cleavage of which only occurs after the exposure to corresponding stimuli.<sup>69</sup> This unique relationship between the linker and stimuli has attracted significant attention for realising controlled drug release in DDSs, where the SCLs bridge the drug molecules or capping agents to drug carriers. The SCLs can remain stable in the circulation, while the exposure of them to the corresponding stimuli can induce the cleavage of the linker and result in drug release. The stimuli to trigger the cleavage of the linkers can be categorised as exogenous stimuli and endogenous stimuli, both of which can be exploited for DDSs construction. The exogenous stimuli cover light,<sup>70</sup> temperature,<sup>71</sup> magnetic field,<sup>72</sup> high energy radiation<sup>73</sup>, and ultrasound<sup>74</sup>, possessing tremendous advantages including ease of tuning and precision of control.<sup>75</sup> As a result of on-demand linker cleavage, the system shows a promising way to overcome inter-patient variability.<sup>76</sup> From another perspective, since an abnormal increase in enzymatic activity or other changes in microenvironments in cancers or other disease models are common,<sup>77,78</sup> endogenous stimulus-induced linker cleavage is another highly promising strategy and has excellent potential in clinical applications.<sup>79-81</sup>

### 1.4.1 Photo-cleavable linkers (PCLs)

PCLs provide a unique method for precise therapy since photochemistry does not require any additional reagent, just light.<sup>82</sup> Thus, photochemistry can be utilised in an on-demand fashion and a non-invasive manner.<sup>83</sup> Over the past few decades, a variety of PCLs have been developed for drug delivery purpose, where drug release is triggered by light with different wavelengths to enable photochemistry such as covalent bond cleavage, isomerisation, and rearrangement.<sup>84</sup> The pioneering work of PCLs mostly used short wavelength and high energy UV light ( $\lambda = 190\text{--}400\text{ nm}$ ) to disrupt the chemical structure of the linkers and promote drug release.<sup>85</sup> Aromatic compounds such as *o*-nitrobenzyl (ONB) groups found broad applications to directly regulate the drug release *via* UV irradiation. ONB groups have become the focus for drug delivery as its aromatic ring allows versatile modifications for drug attachment and incorporation into DDSs.<sup>86</sup> To sum up, applications of ONB groups have been demonstrated with numerous drug carriers, including mesoporous silica nanoparticles (MSNs),<sup>87, 88</sup> dendrimers,<sup>89, 90</sup> micelles<sup>20, 91</sup>, and gold nanoparticles (GNPs)<sup>92</sup>. Drug and gating molecules, such as methotrexate (MTX),<sup>90</sup> DOX,<sup>89</sup> camptothecin (CPT),<sup>91</sup> 5-fluorouracil (5-FU),<sup>92</sup> and  $\beta$ -cyclodextrin ( $\beta$ -CD)<sup>88</sup>, have been conjugated to ONB groups (**7** in **Figure 3**).



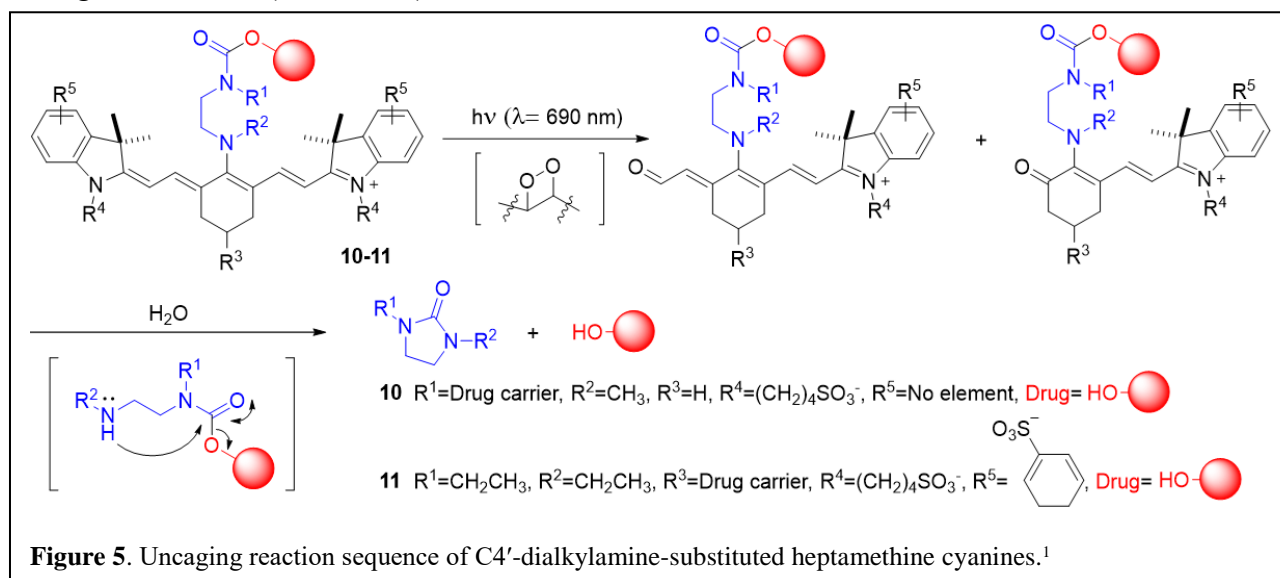
Regarding the mechanism of ONB cleavage, upon UV irradiation (one-photon,  $\lambda = 254\text{--}365\text{ nm}$ ), the nitro group on the aromatic ring undergoes an intramolecular photoreduction to *aci*-nitro tautomers, followed by the formation of benzoxazolidines and subsequent drug release from the benzylic position (**Figure 3**).<sup>93</sup>



Further investigations revealed that two-photon ( $\lambda = 710 \text{ nm}^{94}$  and  $750 \text{ nm}^{95}$ ) excitation can also rupture the ONB groups while there is little research in this regard because the relevant two-photon excitation mechanism is not completely elucidated yet.<sup>96</sup> The benzylic site of ONB groups remains as the key structure for drug attachment. An array of molecules with different functional groups has been successfully articulated to ONB groups, comprising carboxylic acids,<sup>97</sup> phosphoric acids,<sup>98</sup> amines<sup>20</sup> and alcohols<sup>99</sup>, and further showed facile release upon UV irradiation.

Although UV-cleavable linkers had been widely used in various biological approaches, the low tissue penetration depth of UV light<sup>100</sup> critically hindered their clinical applications. Therefore, the PCLs that can be cleaved under a longer wavelength light source are urgently needed. Boron-dipyrromethenes (BODIPY) derivatives serve ideally to rapidly release the payload through one-photon excitation,<sup>101</sup> and the central component in such derivatives is referred to  $\pi$ -extended systems that undergo electronic transitions upon visible light irradiation.<sup>102</sup> BODIPY-based PCLs can be cleaved and subsequently release the drug molecules at different wavelengths (**Figure 4**). To date, drug molecules bearing carboxylic acids (**8**)<sup>103</sup> and amines (**9**)<sup>104</sup> have been successfully tethered to the *meso*-position of BODIPY linkers for prodrug formations.

However, light with deeper tissue penetration will be more beneficial to *in vivo* studies. In this way, a fluorophore with the name of heptamethine cyanine (Cy) attracted our attention. The structure of heptamethine Cy is shown in **Figure 5**, and the central component of this fluorophore is referred to the same  $\pi$ -extended systems featured by the *meso*-substituted BODIPY derivatives. The cyanine-based linkers can be cleaved upon red light irradiation and have shown potential to be utilised in prodrug formations.<sup>1</sup> The photolysis of cyanines relies on a two-step mechanism: photooxidative cleavage (requires access to the singlet oxygen) and subsequent hydrolysis (**Figure 5**). Continuous efforts have been made in developing applications of Cy linker in DDSs, especially in antibody-drug conjugates (ADCs), where combretastain A4 (CA4, **10**)<sup>105</sup> and duocarmycin (DUO, **11**)<sup>106</sup> were successfully installed on Cy linkers and efficient controlled drug release was further realised upon red light irradiation ( $\lambda = 690 \text{ nm}$ ).

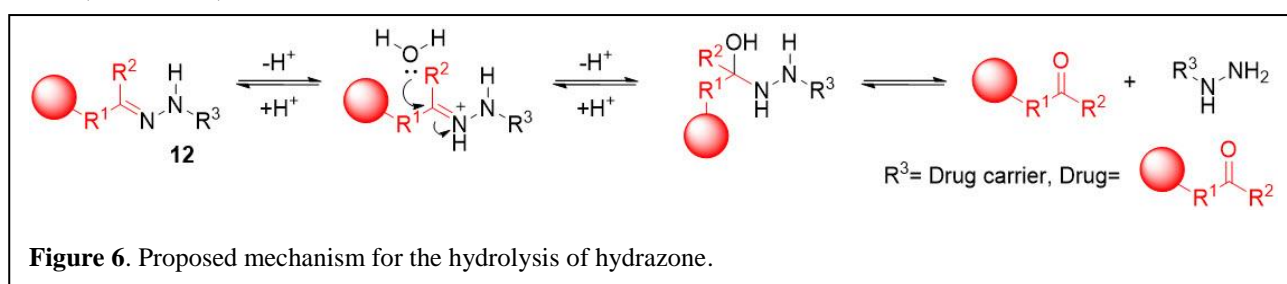


In summary, light provides a powerful and remote stimulus to enable orthogonal drug release, raising concerns from the therapeutic applications that require non-invasive activation of drug release. However, most reported PCLs are far from clinical applications. Therefore, the discovery of a photo-induced DDS with deeper tissue penetration, less energy requirement, decreased tissue damage and higher biostability should be the focus of future research. Moreover, if this problem is solved, we believe that PCLs hold great opportunities in DDSs-based precision therapy.

#### 1.4.2 Acid-cleavable linkers (ACLs)

pH is recognised as a physiological parameter in living organisms.<sup>107</sup> As the smallest but extremely reactive ion, the hydrogen ion ( $H^+$ ) is produced through the balance between protonation and deprotonation of  $H_2O$ , weak acids and weak bases, the regulation of which is affected in particular diseased sites, such as cancerous<sup>108</sup> and inflammatory<sup>109</sup> tissues, due to their intensive respiratory  $CO_2$  and lactic acid production.<sup>110</sup> The resulting excessively higher acidity of these pathological regions compared to blood and healthy tissues provides an appropriate endogenous stimulus for pH-cleavable drug delivery. Besides, organelles with relatively low pH such as endosomes and lysosomes are broadly explored by several DDSs for controlled drug release. Therefore, numerous efforts have been devoted to the design and development of chemical structures with high sensitivity to acidic microenvironments.

Hydrazone linkers (**12** in **Figure 6**), a series of linkers involving acyl hydrazone,<sup>111</sup> alkoxy carbonyl hydrazone<sup>112</sup>, or benzenesulfonyl hydrazone<sup>113</sup> as cores, are widely employed for drug delivery purpose as ACLs, which contributes to their robust hydrolysis rate under acidic conditions and stability at neutral pH.<sup>114</sup> Therefore, the incorporation of hydrazone linkers into the DDSs promises a stable DDS in the circulation and rapid drug release at acidic pH. Hydrazone linkers have been applied in a wide range of drug carriers, including dendrimers,<sup>115, 116</sup> micelles,<sup>117, 118</sup> liposomes,<sup>119, 120</sup> GNPs,<sup>121</sup> MSNs,<sup>122</sup> and antibodies<sup>123, 124</sup>.



The proposed mechanism of hydrolysis of hydrazone linkers is shown in **Figure 6**, where N1 in the  $C1=N1-C$  structure is first protonated at acidic pH, followed by nucleophilic attack by  $H_2O$  molecules. The resulting intermediate undergoes a facile internal  $H^+$  transfer to complete the release of drugs with carbonyl moiety while producing the residue terminated with hydrazide.<sup>125</sup> Limitations still remain, the main of which is the limited flexibility in terms of linker conjugation reactions. As determined by the hydrolysis mechanism, the hydrazone linker is only applicable for drug/gating molecules containing carbonyl group (ketone, aldehyde), like DOX,<sup>121</sup> auristatin E<sup>126</sup> and hydrazide-modified sodium alginate<sup>127</sup>. Although hydroxy group-containing drug molecule such as paclitaxel

(PTX)<sup>128</sup> can be modified with carbonyl group for the construction of hydrazone linkage, further hydrolysis of the carbonyl group by esterase is required to generate the original structure of the drug. Notably, the hydrolysis product of hydrazone, also known as the hydrazide residue, showed a certain degree of cytotoxicity in several cases.<sup>129</sup> This should be considered when a DDS with this cleavable linker type is designed.

### 1.4.3 Enzyme-cleavable linkers (ECLs)

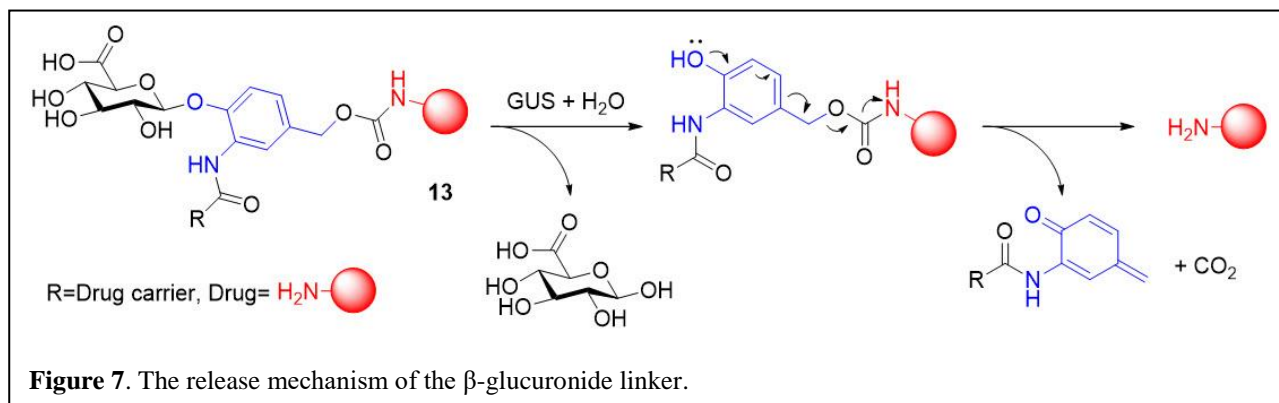
Enzymes are biological molecules (mostly proteins) responsible for accelerating virtually all the chemical reactions within cells.<sup>130</sup> The high substrate specificities and robust enzymatic reactions of enzymes differentiate them from many other chemical stimuli, allowing more specific chemical reactions.<sup>131</sup> Moreover, dysregulation of certain enzymes is a hallmark of pathology for a variety of diseases such as cancer,<sup>132</sup> inflammation,<sup>133</sup> and neurodegenerative diseases<sup>134</sup>. Therefore, using enzymes as stimuli offers a great opportunity in the controlled drug release from DDSs.

There are six different types of enzymes that are well studied in the applications of stimulus-induced drug release, including hydrolases, oxidoreductases, transferases, lyases, isomerases, and ligases.<sup>135</sup> Among them, the hydrolases are capable of cleaving chemical bonds such as ester<sup>136</sup> and peptide<sup>132</sup> bonds using H<sub>2</sub>O as the nucleophile. As the subclass of hydrolases, esterases, proteases, and glycosidases have been extensively explored as the stimuli for controlled drug release, promoting the development of corresponding ECLs.

Glycosidases, also known as glycoside hydrolases (GHs), refer to a large family of enzymes responsible for hydrolytically cleaving the glycosidic bonds in glycoconjugates, oligo- and polysaccharides to form a sugar hemiacetal/hemiketal and the corresponding aglycon.<sup>137</sup> Traditionally, these enzymes are divided into two main groups: the exo-glycosidases releasing a specific monosaccharide from the nonreducing terminus of an oligosaccharide and the endoglycosidases capable of cleaving the glycosidic bonds in the carbohydrate polymer chain.<sup>138</sup> The GHs are mainly involved in glycometabolism, during which they perform both important extracellular and intracellular degradative functions based on two distinct mechanisms.<sup>139</sup> One of the roles for GHs in the targeted drug delivery field is related to their elevated level in cancer cells in contrast to normal cells,<sup>140</sup> where GHs have thus gained significant attention in the study of tumour-specific drug release.

Among the broad spectrum of exo-glycosidases,  $\beta$ -glucuronidase is notable for stimulus-induced drug release/activation due to its elevated activity in various solid tumours including breast,<sup>141</sup> colon,<sup>142</sup> lung,<sup>143</sup> and leukaemia<sup>144</sup>. Human  $\beta$ -glucuronidase is located in lysosomes, where the acidic microenvironment contributes to its optimal activity, and most interestingly,  $\beta$ -glucuronidase exhibits unusual resistance to thermal denaturation, corresponding to their stability up to 70°C.<sup>145</sup> Structurally, human  $\beta$ -glucuronidase is a tetrameric glycoprotein, comprised of four identical monomers.<sup>146</sup>

The main role of  $\beta$ -glucuronidase in biological processes is the deconjugation of  $\beta$ -D-glucuronides (**13** in **Figure 7**) from a variety of natural substrates, such as the deconjugation of chondroitin sulfate to produce  $\beta$ -glucuronic acid and the corresponding aglycone.<sup>147</sup>



The high polarity of glucuronic acid offers advances in improving the hydrophilicity of poorly water-soluble drug molecules, significantly contributing to the prodrug formations.<sup>148</sup> Although glucuronic acid can be directly conjugated to phenol alcohol-bearing molecules like DUO derivatives,<sup>149</sup> self-immolative spacers have been more frequently used. Accordingly, the elongated linkers, such as *N*-phenyl  $\beta$ -*O*-glucuronyl carbamates, and nitrobenzylphenoxy carbamate, showed high susceptibility to  $\beta$ -glucuronidase and have been utilised to conjugate various drug molecules like PTX,<sup>150</sup> DOX<sup>151</sup> and Monomethyl auristatin E (MMAE)<sup>152</sup>. Likewise, these glucuronide-drug conjugates have been attached onto carriers such as antibodies,<sup>153</sup> proteins<sup>154</sup> and micelles<sup>155</sup>. However, the main shortcoming of glucuronide-based linkers is their tedious (usually 10+ steps) synthetic route, which hinders the broad application of these linkers in more material- or biology-oriented labs.<sup>156, 157</sup>

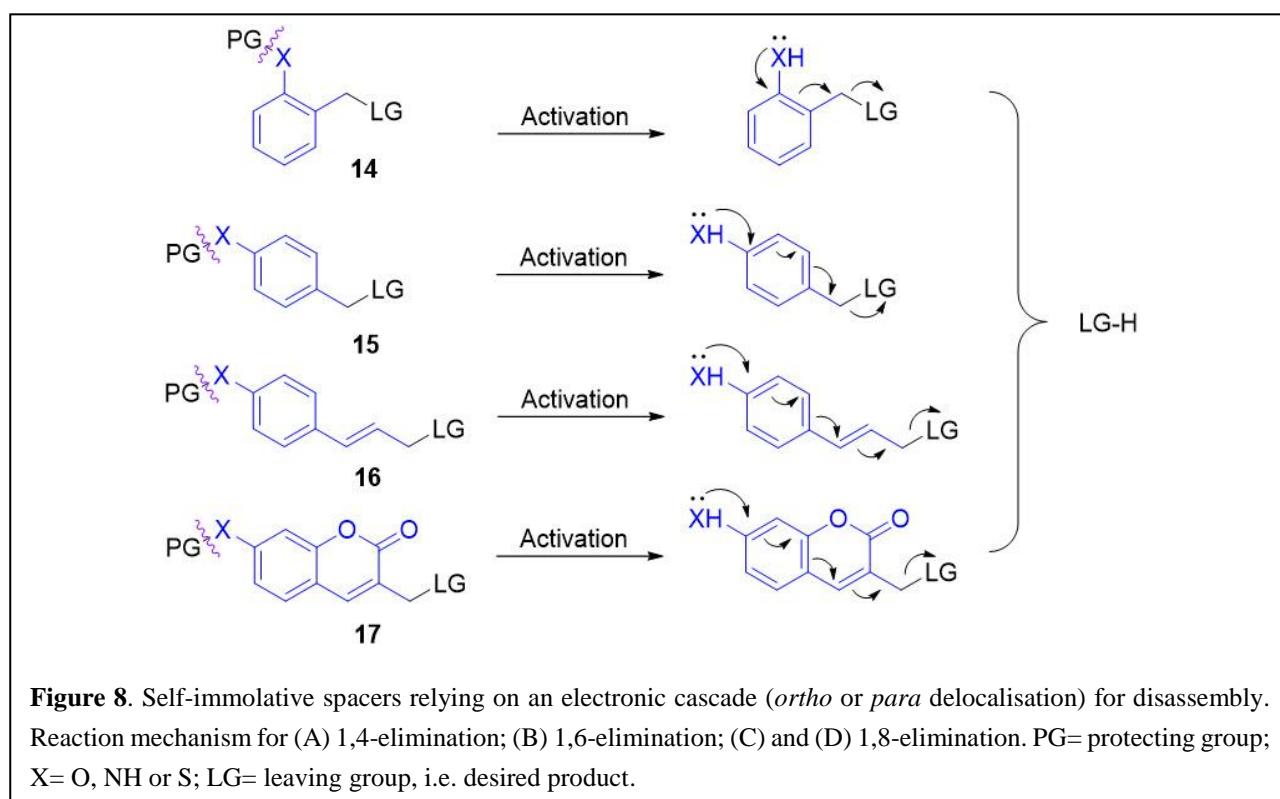
#### 1.4.4 Self-immolative spacers

Spacers, commonly referred to self-immolative spacers, can be introduced between the drug payload and SCL to accommodate drug molecules.<sup>158</sup> The most widely accepted self-immolation process is the electronic delocalisation, which relies on the electron cascade to release the payload with the formation of quinone or azaquinone methide intermediate. The initiating condition of this process requires the generation of nucleophilic functional groups such as hydroxy, amino, or thiol groups after exposure to the stimulus, which subsequently triggers the self-immolation to release the drug payload.

The most widely used electronic delocalisation reactions rely on the 1,4-<sup>159</sup> and 1,6-elimination<sup>160</sup> (**14** and **15** in **Figure 8**), whereas 1,8-elimination reaction (**16** and **17** in **Figure 8**)<sup>161, 162</sup> was only observed in coumarinyl alcohol or *p*-amino/hydroxy cinnamyl alcohol.

The dissociation rate of electronic delocalisation-based self-immolation is believed to be affected by the structural properties of spacer, including the length of the spacer,<sup>163</sup> substituents on the aromatic ring<sup>164</sup> and leaving groups<sup>165</sup>. As the core structure of the self-immolative spacers whose degradation rely on the electronic cascade, the aromatic ring plays a vital role in affecting the disassembly kinetics

since its nature allows for flexible proximity of the leaving group to the activation site, which is independent of the electronic effect. Although the disassembly times for 1,4-elimination and 1,6-elimination were the same,<sup>160</sup> in certain cases where a dual release is involved, the faster release was observed for the leaving group on the *para* site than the *ortho* one.<sup>163</sup> Concerning the substituents on the aromatic ring, electron-withdrawing substituents can decrease the electron density of the aromatic ring to destabilise the partial positive charge at the benzylic position in the transition state of spacer disassembly. Consequently, the increased kinetic stability of the activated spacer contributes to the prolonged half-time, which was observed in self-immolative spacers bearing nitro or methoxycarbonyl group.<sup>166</sup> In contrast, substitution at the benzylic position with the electron-donating group such as methyl group was reported to accelerate the release of the leaving group, while the electron-withdrawing group can prevent the release.<sup>159, 167</sup> Apart from the aromatic core, the leaving group also affects the disassembly rate of self-immolative spaces with its nucleofugacity and the steric hindrance.<sup>168</sup>



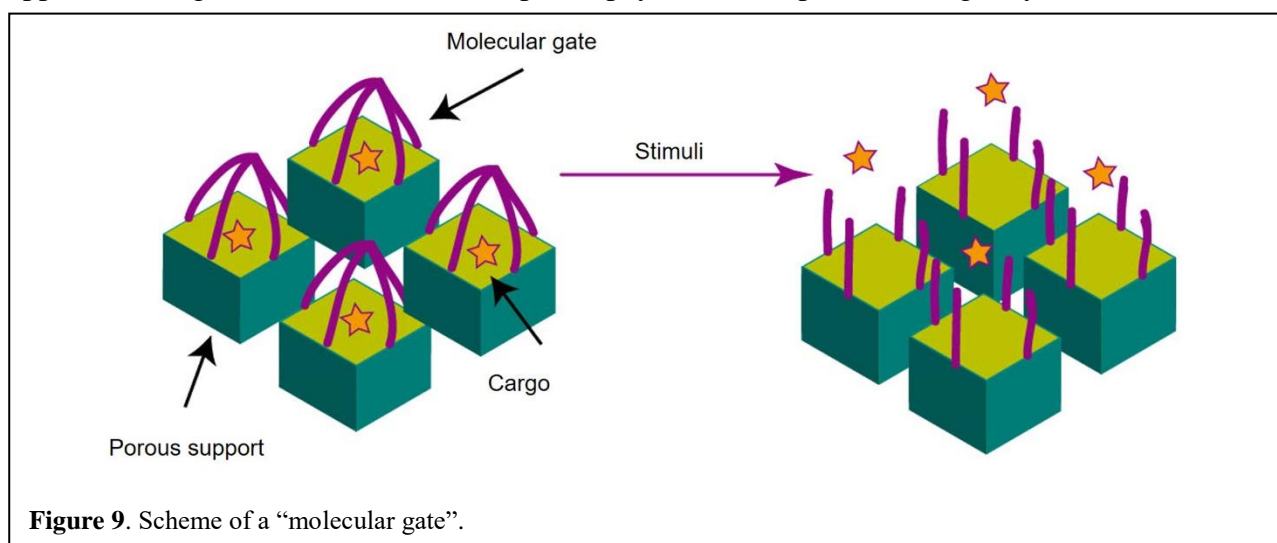
#### 1.4.5 The application of SCLs in controlled drug release

Compared with the administration of free drugs, the combination of SCLs with drug carriers offers a potential alternative to achieve highly controlled drug delivery. More importantly, linker chemistry provides a simpler and more general mechanism of action in comparison with those DDSs requiring complicated design.<sup>169-171</sup> As aforementioned, providing a controlled release of therapeutics at targeted sites is the key challenge for increasing the efficacy of pSiNP-based DDSs. A lot of effort has been made to solve this problem, and the most commonly used method, referring to ‘gating approach’, has attracted interest. The ‘gating approach’ has been widely utilised in the controlled

release from MSNs, depending on a nanovalve anchored onto the external surface of MSN-based material (**Figure 9**).<sup>169, 172</sup>

In this system, multiple drug molecules are kept inside of the porous material with a molecular gate sealing the pores. Upon exposure to the corresponding stimuli, the linkers between the molecular gates and MSNs undergo degradation or isomerisation to open the cap and release the cargo (**Figure 9**).<sup>173-175</sup> Due to the nonselective drug loading character, the gated porous support allows the loading of not only one specific drug but also multiple drugs possessing synergistic effects. Furthermore, the utilisation of stimuli-responsive caps enables a relatively controlled drug release and is promising for the development of more complex DDSs.

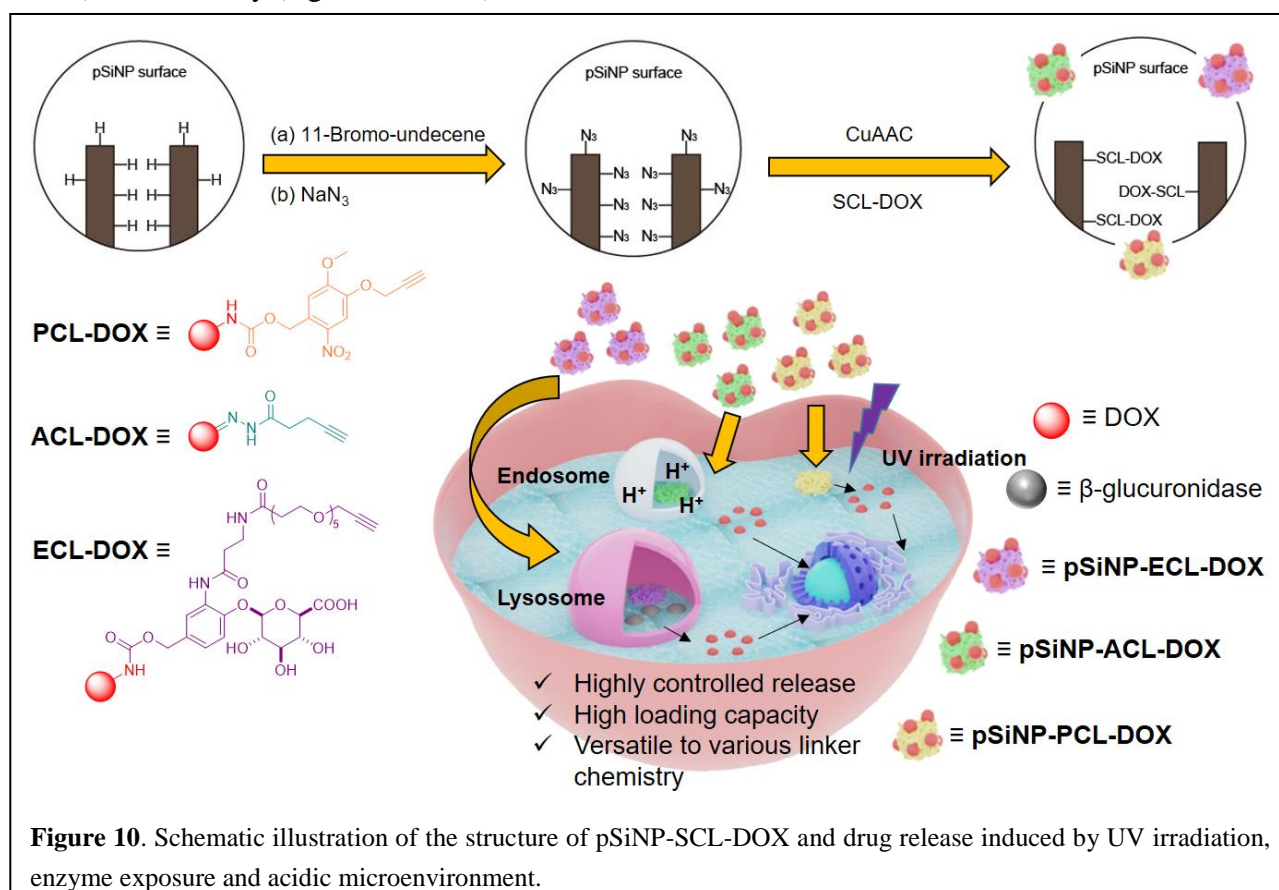
However, the gated nanochemistry has been utilised exclusively in MSNs because the release of the entrapped cargo relies on the average pore size of MSNs. Different from pSiNPs, MSNs are prepared by a templating method resulting in regular morphology; meanwhile, the precise control of pore size and structure enables reliable support for nanovalve.<sup>176</sup> In contrast, the pore size and shape of pSiNPs present a dispersion, which limits the application of nanovalves in pSiNPs. Therefore, a specific approach to regulate the release of therapeutic payloads from pSiNPs is urgently needed.



### 1.5 Project aims/hypothesis of incorporating SCLs into pSiNP-based DDSs

As the medical application of nanotechnology, nanomedicine makes it possible to deliver drugs to target cells using nanoparticles (NPs). Among different nanomaterials applied in nanomedicine, pSiNPs stand out and present a particularly exciting opportunity for drug delivery due to their biocompatibility, biodegradability, high LC/surface area, versatile surface chemistry, and tuneable porous nanostructure.<sup>67</sup> However, as a result of the dispersion in pore size and high biodegradability, the molecular machine widely used in stimulus-responsive controlled release strategies in MSNs have not been successfully applied to pSiNPs. Additionally, nanoparticle encapsulation methods mainly depend on physical, non-covalent capping, and enclosing. Thus, potential leakage or unreleased caps will notably influence the loading and release efficiencies of these systems.

To achieve stimulus-responsive controlled drug release, the incorporation of SCLs has been well studied.<sup>177, 178</sup> SCLs have been well-established in ADCs, peptide-drug conjugates (PDCs), prodrugs, and fluorogenic probes, in which they enable controlled drug release at desired sites upon exposure to different stimuli triggers.<sup>177, 179</sup> As such, these chemical linkers have successfully conjugated small molecule drugs to various drug carriers (e.g. dendrimers, peptides, and antibodies) and showed preferential release profile upon exposure to the relevant stimuli.<sup>180-184</sup> However, these previous studies have been accompanied by unfavourable properties, such as a low LC (e.g. ADCs and PDCs)<sup>185</sup> or toxicity (e.g. dendrimers)<sup>186</sup>.



We hypothesise that we can load drugs through tethering small molecule drugs to the surface of pSiNP *via* SCLs, which in principle can lead to the similar LC to traditional drug loading method due to the high surface area of pSiNPs (up to 580 m<sup>2</sup>/g). In the meanwhile, by taking advantages of linker system's tuneability and selectivity, we would be able to realise much more drug loading stability and responsive controlled drug release. We first use mathematic models to estimate the loading capacities of our covalent and traditional drug encapsulation approaches. The theoretical LC achieved by covalent drug encapsulation<sup>187</sup> can be calculated as follows:

$$LC_{\text{surface loading}} (\%) = A_{pSi} \times M_{W(\text{drug})} / (A_{pSi} \times M_{W(\text{drug})} + A_{\text{drug}} \times N_A) \quad (1)$$

where  $A_{pSi}$  is the surface area of respective pSiNPs (489.17 m<sup>2</sup>/g),<sup>188</sup>  $A_{\text{drug}}$  is the minimal projection area of respective drug ( $7.8 \times 10^{-20}$  m<sup>2</sup>/molecule),  $N_A$  is the Avogadro constant ( $6.022 \times 10^{23}$ /mol), and  $M_{W(\text{drug})}$  is the molecular weight of respective drug (DOX, 543.53 g/mol). Using Eq. (1), the LC achieved by our covalent drug encapsulation is calculated to be 36.8% wt. On the other hand, LC achieved through traditional drug encapsulation method<sup>187</sup> is calculated as follows:

$$LC_{\text{cavity loading}} (\%) = V_{pSi} \times \rho_{drug} / (1 + V_{pSi} \times \rho_{drug}) \quad (2)$$

where  $V_{pSi}$  is the pore volume of the pSiNPs ( $0.741 \text{ cm}^3/\text{g}$ ),<sup>189</sup>  $\rho_{drug}$  is the amorphous density of the loaded drug (DOX,  $1.387 \text{ g/cm}^3$ ). Using Eq. (2), the LC achieved by traditional drug encapsulation method is calculated to be 50.5%. Based on the calculation result, the traditional drug encapsulation method can provide higher LC compared with covalent drug encapsulation. However, the reported LCs achieved through traditional drug encapsulation are usually around 10 wt% in terms of loading small molecule drugs.<sup>190</sup> Therefore, our covalent drug encapsulation strategy may still reach the similar LC to traditional drug encapsulation method.

For the choice of SCLs, after a thorough literature review of SCLs from ADCs,<sup>191-193</sup> MSNs<sup>169, 194, 195</sup> and polymeric nanoparticles (PNPs)<sup>196-198</sup>, we chose three SCLs as a demonstration (**Figure 10**). First, we chose to use a PCL because light as an external trigger has many favourable features, such as being non-invasive, ease of tuning, and high efficiency.<sup>199, 200</sup> Here we chose one of the most commonly applied photolabile group containing ONB as the core structure for the PCL.<sup>201, 202</sup> Apart from using an external stimulus, endogenous stimuli were also chosen to exploit natural stimulants within the human body. In this regard, as a physiological parameter varying across different organelles, pH is a promising endogenous stimulus for targeted drug release. Specifically, the acidity of endosomes (pH 5.5-6.2) and lysosomes (pH 4.5-5.0) has been widely investigated for constructing ACL.<sup>177</sup> We utilised a hydrazone-based ACL owing to its high susceptibility to acidic conditions (extracellular tumour tissues, endosomes and lysosomes) and its stability in a neutral environment.<sup>203, 204</sup> Enzymes are another endogenous stimuli widely exploited due to being involved in various key physiological processes and/or exhibiting altered expression levels in many disease-associated microenvironments.<sup>205, 206</sup> In this context, ECL based on the  $\beta$ -glucuronide motif was chosen to target  $\beta$ -glucuronidase, a lysosomal enzyme overexpressed in many types of cancers, to achieve region-specific drug release inside of the lysosomes in tumour cells.<sup>205, 207</sup>

### 1.5.1 Drug selection

DOX belongs to the anthracycline antibiotic family and was first isolated from *Streptomyces peccetius* bacteria. DOX has been widely used for treating various kinds of cancers including oophoroma, thyroid carcinoma, breast cancer, and lung cancer for 30 years. The drug is comprised of two main parts: aglyconic and sugar moieties. The aglycone possesses a tetracyclic ring, methoxy substituent short side chain followed by the carbonyl group. The daunosamine part is articulated to one of the rings *via* a glycosidic bond (**18** in **Figure 11**).

More importantly, DOX is intrinsically fluorescent. Hence, the drug loading and distribution can be easily tracked *via* fluorescence microscopy and spectroscopy, making it one of the most widely used model drug in DDSs studies.

In terms of the mechanism of action, DOX is believed to bind to DNA-associated enzymes (topoisomerase II), which can relax the supercoil in DNA for transcription.<sup>208</sup> DOX can stabilise the

topoisomerase II after breaking the DNA chain for reproduction, preventing the DNA double helix from being released and thereby stopping the replication.

The only drawback of DOX is the toxicity to healthy tissues in the human body. Since the drug binds to the topoisomerase II non-selectively, a considerable degree of cell death in the human body is caused. Therefore, we speculate that conjugating DOX with SCLs will “cage” the cytotoxicity of DOX to the healthy tissue, resulting in higher therapeutic indexes and fewer side effects.<sup>209</sup>

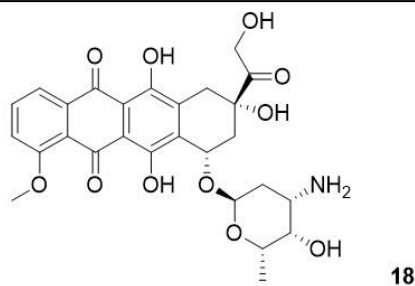


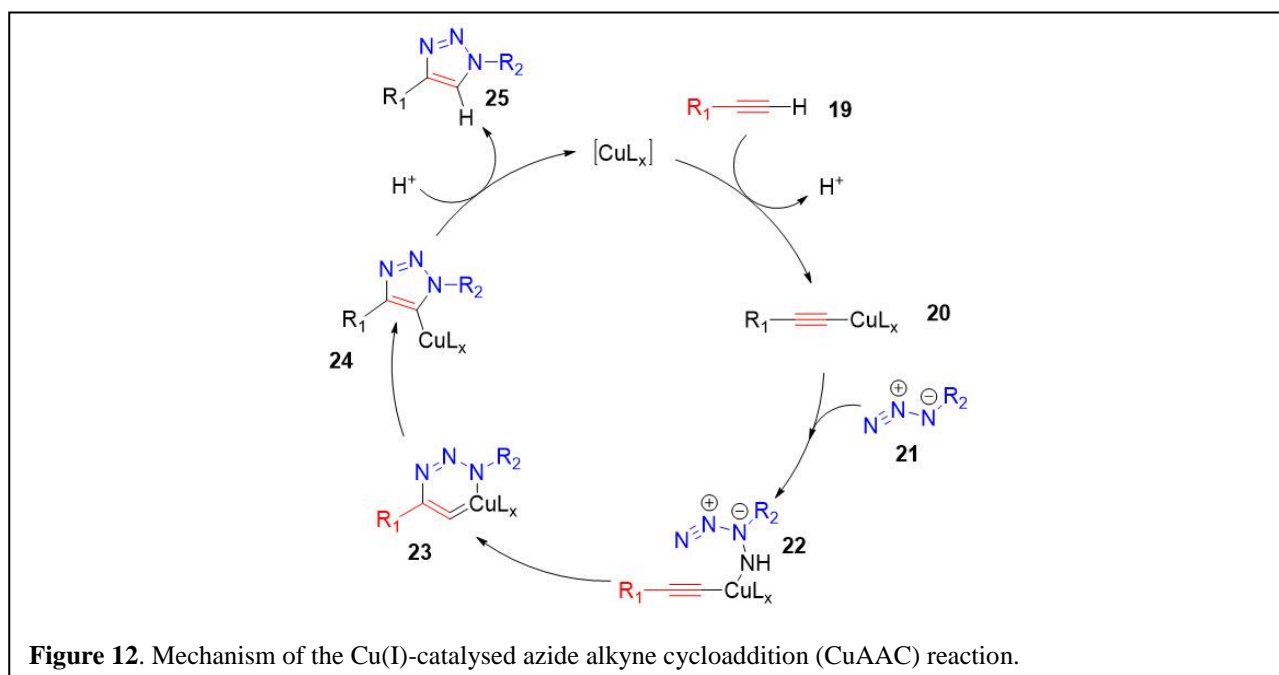
**Figure 11.** Chemical structure of DOX.

### 1.5.2 Conjugation strategy

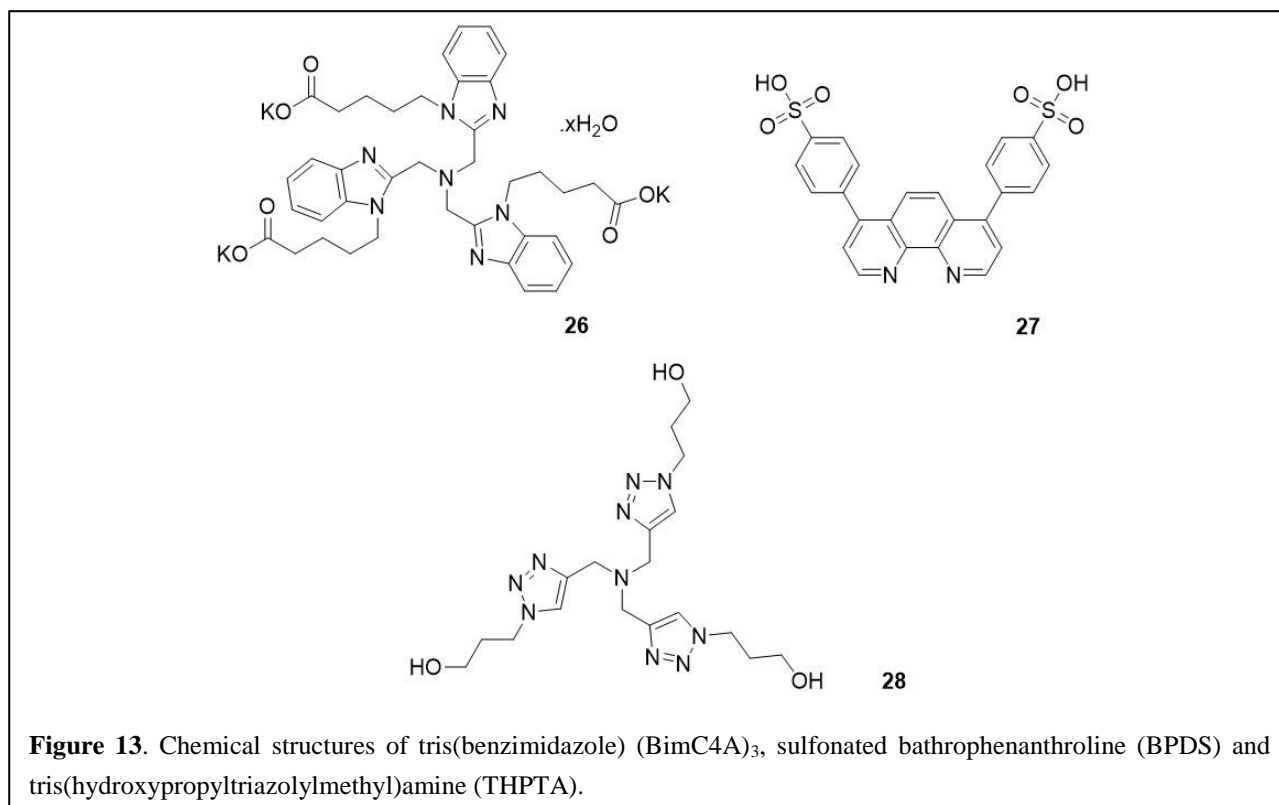
Normally, the initial surface modification of pSiNPs can stabilise their surface while providing a chemical handle, where the general conjugation chemistry is performed to eventually incorporate the linker systems into the nanoparticles. To date, several conjugation strategies have been extensively applied in the construction of DDSs, including amide coupling, maleimide-based reaction, condensation, and ‘click chemistry’.

The concept of ‘click chemistry’ was first introduced in 2001. Its characteristics include high yield, less toxic by-products, and high stereospecificity.<sup>210</sup> Besides, click chemistry proceeds under mild conditions to couple small elements with heteroatoms, and most importantly, the reaction can occur in both aqueous media and organic solvents.<sup>211</sup> Therefore, click chemistry has been widely applied to modify the surface chemistry of various drug carriers for bioimaging<sup>212</sup> and drug delivery<sup>213</sup> purposes.

The CuAAC reaction is the most extensively applied click reaction, probably because of its high orthogonality, reliability and most importantly, the experimental simplicity for researchers without a synthetic chemistry background.<sup>214</sup> The mechanism of the CuAAC reaction is shown in **Figure 12**, where the 1,3-dipolar addition occurs between the terminal alkynes (**19**) and azides (**21**) to afford the 1,2,3-triazole (**25**).<sup>215</sup> Featuring a high tolerance to aqueous solution with a broad range of pH level, CuAAC chemistry has been widely used to conjugate numerous organic functionalities with drug carriers such as antibodies,<sup>216</sup> MSNs,<sup>217</sup> and GNPs<sup>218</sup>. Nevertheless, the Cu(I) used for CuAAC reaction may cause structural damage to biomolecules under standard experimental condition, and the lack of adequate kinetics in some cases also inhibits its further applications in bioconjugation.



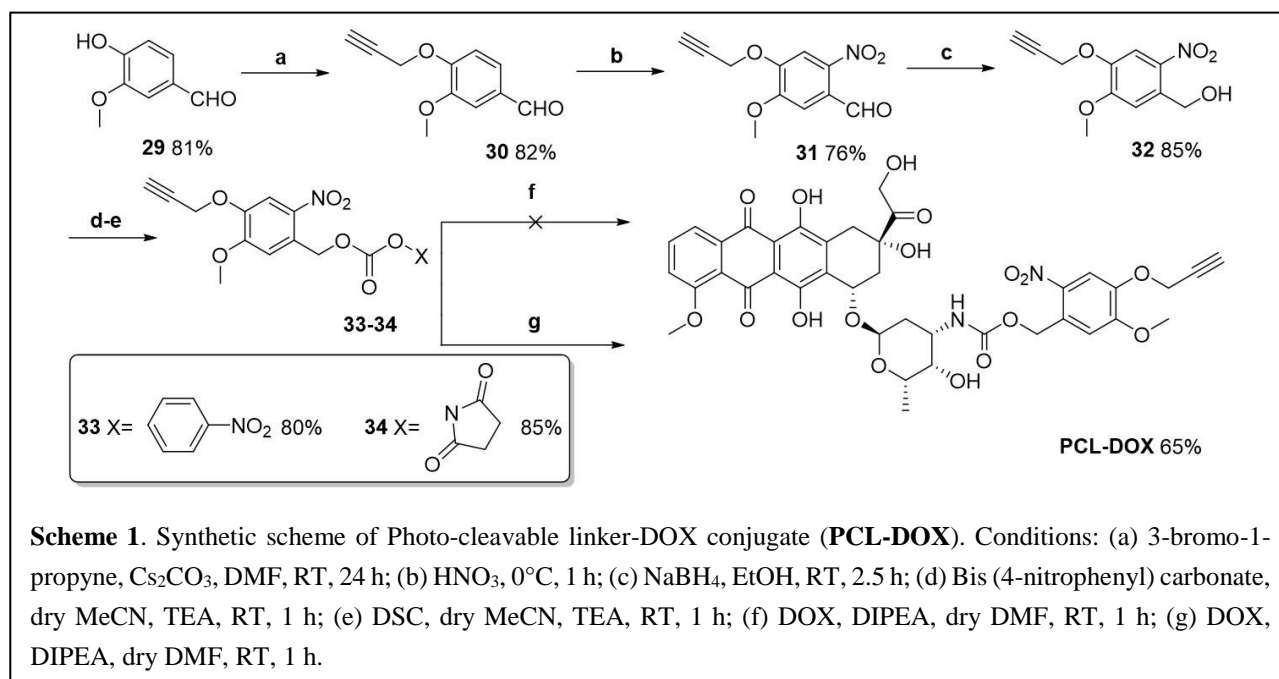
To accelerate the CuAAC process, numerous Cu(I) conjugating ligands, such as tris(benzimidazole) (BimC4A)<sub>3</sub> (**26**),<sup>219</sup> sulfonated bathrophenanthroline (BPDS) (**27**),<sup>220</sup> and tris(hydroxypropyltriazolylmethyl)amine (THPTA) (**28**)<sup>220</sup> (**Figure 13**) were introduced into the reaction to stabilise the oxidation state of CuI and thus increase its catalytic efficiency. As ‘click chemistry’ proceeds with a high yield and it can proceed under mild reaction conditions, we decided to choose this method to articulate our SCL-drug conjugates to pSiNPs.



This thesis will introduce the controlled release of a small molecule drug from pSiNPs *via* SCLs. DOX was used as a small molecule anti-cancer drug and conjugated to three different SCLs: (i) a PCL, (ii) an ACL, and (iii) an ECL. The successful covalent conjugation of the SCL-DOX conjugates and pSiNPs showed higher drug LC compared with the traditional drug loading method. The pSiNPs conjugated with the three different SCL-DOX conjugates were evaluated for their controlled release profile and further studied using *in vitro* and *in vivo* models of cancer.

## Chapter 2.0: Design and synthesis of SCL-DOX conjugates

### 2.1 Synthetic approach to Photo-cleavable linker (PCL)



The synthetic scheme to access the Photo-cleavable linker-DOX conjugate (**PCL-DOX**) is shown in **Scheme 1**, where Vanillin (**29**) was coupled with 3-Bromo-1-propyne, based on a nucleophilic substitution reaction, to form **30**. This was followed by a nitration reaction to establish the key structure for photo-hydrolysis. After the reduction of **31**, the resulting product was first activated by using N, N-disuccinimidyl carbonate (DSC), and then coupled with DOX based on known amide-bond forming chemistry.

#### Synthesis of 30

The first step in the synthesis of PCL was the formation of compound **30** through a nucleophilic substitution reaction between the commercially available **29** and 3-Bromo-1-propyne (**Scheme 1**). The formation of compound **30** was confirmed through <sup>1</sup>H NMR that displayed an upfield shift in aromatic protons (7.46 ppm, 7.43 ppm and 7.14 ppm) caused by increased shielding effects. Peak representing the propargyl group was also observed (2.56 ppm, 1H). LC-MS further displayed the formation of compound **30** with a MS peak at 191.0 [M + H]<sup>+</sup>.

### Synthesis of **31**

Succeeding this, compound **30** was then reacted with nitric acid through an electrophilic substitution reaction, resulting in a nitrate intermediate. Synthesis of compound **31** was confirmed through  $^1\text{H}$  NMR that displayed an upfield chemical shift in aromatic protons (7.79 ppm and 7.43 ppm) due to the nitro group's induction effect. Formation of the **31** was further confirmed through LC-MS that displayed a MS peak at 236.0  $[\text{M} + \text{H}]^+$ .

### Synthesis of **32**

The formation of compound **31** subsequently occurred in a reduction reaction to form compound **32**, a very critical intermediate in the synthesis of PCL (**Scheme 1**).  $^1\text{H}$  NMR verified the formation of compound **32** through the presence of a new methylene peak (4.84 ppm, 2H). LC-MS further showed the formation of the desired product with a peak at 259.9  $[\text{M} + \text{Na}]^+$ .

### Synthesis of **33** and **34**

The next step in the synthesis of PCL was to increase the reactivity of compound **32** for DOX attachment with two methods. Compound **32** was first attempted with Bis (4-nitrophenyl) carbonate to form compound **33**. Synthesis of compound **33** was verified through  $^1\text{H}$  NMR, which indicates two new peaks from the 4-nitrophenyl group (8.30 ppm and 7.42 ppm). LC-MS further shows the formation of compound **33** with a peak at 424.9  $[\text{M} + \text{Na}]^+$ . To investigate the coupling efficiency of the two different types of active esters with DOX in the final step, we also tried another method by using DSC to activate the hydroxyl group (**Scheme 1**).  $^1\text{H}$  NMR indicated the formation of compound **34** through a new peak (4.06 ppm, 4H) representing the two methylene groups from the NHS group. A MS peak at 400.9  $[\text{M} + \text{Na}]^+$  was further correlated to the desired product.

### Synthesis of PCL-DOX

The final step was to attach DOX to the PCL through an acylation reaction. In this step, the activated esters **33** and **34** were reacted with DOX, respectively, to form the final product **PCL-DOX** (**Scheme 1**).

In an initial attempt to form **PCL-DOX**, compound **33** was reacted with DOX while no product was identified after 3 h *via* LC-MS. Then, compound **34** was reacted with DOX, and LC-MS showed the desired product's peak at 828.9  $[\text{M} + \text{Na}]^+$ .

As the reaction proceeded, we can easily determine the quantity of unreacted DOX by performing micro-extraction work. After that, **PCL-DOX** was observed in the organic phase with a bright orange colour while DOX remained in the aqueous phase with a purple colour.

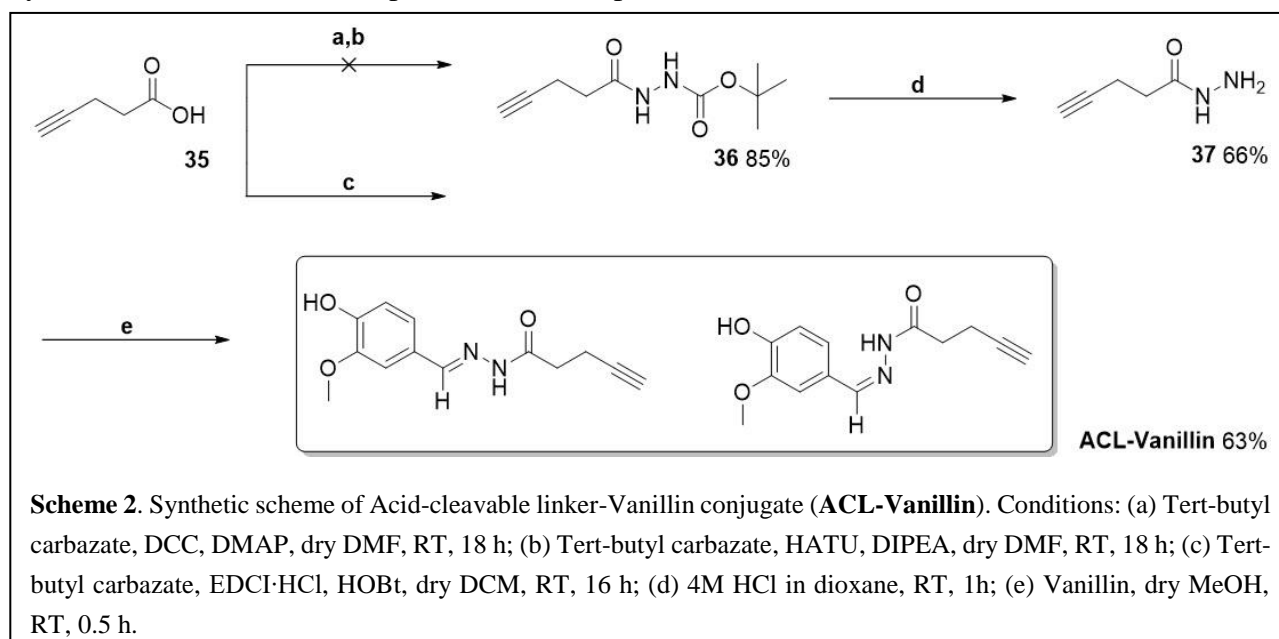
$^1\text{H}$  NMR further indicated the successful synthesis of **PCL-DOX** through three new aromatic protons (8.02 ppm, 7.80 ppm and 7.39 ppm) representative of D ring from DOX.

## 2.2 Synthetic approach to Acid-cleavable linker (ACL)

### 2.2.1 Synthetic approach to ACL-Vanillin

Due to the high cytotoxicity of DOX and regulation at Monash University, hydrazone linker was firstly conjugated to Vanillin that possesses the same functional group (aldehyde/ketone) as DOX does, to explore and optimise the synthetic route and release conditions.

The synthetic route of Acid-cleavable linker-Vanillin conjugate (**ACL-Vanillin**) is shown in **Scheme 2**. The synthesis of **ACL-Vanillin** was achieved through initial coupling of commercially available Tert-butyl carbazate with 4-Pentynoic acid **35**, where several coupling reagents were tried to produce **36**. The details will be provided in the following paragraphs. Hydrochloric acid (HCl) in dioxane (4M) was reacted with previously isolated **36** to form **37**, which was monitored by TLC. This was followed by the addition of Vanillin to produce the final product **ACL-Vanillin**.



### Synthesis of **36**

In an initial attempt to form **36**, an acylation reaction was performed with N, N'-dicyclohexylcarbodiimide (DCC) and 4-Dimethylaminopyridine (DMAP) as the coupling reagents (**Table 1**). However, these reaction conditions failed to produce the desired product, possibly because the Tert-butyl carbazate was not reactive enough to attack the activated starting material. The <sup>1</sup>H NMR for impurity in this reaction was verified to be the reactive intermediate derived from **35** and DCC. These reaction conditions can be improved by exploring different catalysts that activate carboxylic acid. An alternative approach by reacting **35** with 2-(7-Azabenzotriazol-1-yl)-N, N, N', N'-tetramethyluronium hexafluorophosphate (HATU) was performed (**Table 1**), resulting in the unreacted starting material.

Thus, N-ethyl-N'-(3-dimethylaminopropyl) carbodiimide hydrochloride (EDCI·HCl) and 1-Hydroxybenzotriazole (HOBt) were selected as activating agents (**Table 1**). This reaction condition

was successful and produced **36** with a yield of 85%. The successful synthesis of **36** was verified by  $^1\text{H}$  NMR through the presence of amide proton peaks at 7.75 ppm (s, 1H) and 6.68 ppm (s, 1H).

Reaction	Conditions	Temp	Time	Outcome
(a)	DCC, DMAP, dry DMF	RT	18 h	Impurity
(b)	HATU, DIPEA, dry DMF	0°C to RT	18 h	Unreacted starting material
(c)	EDCI·HCl, HOBt, dry DCM	RT	16 h	85% product isolated

**Table 1.** Reaction conditions undertaken in the synthesis of **36**.

### Synthesis of **37**

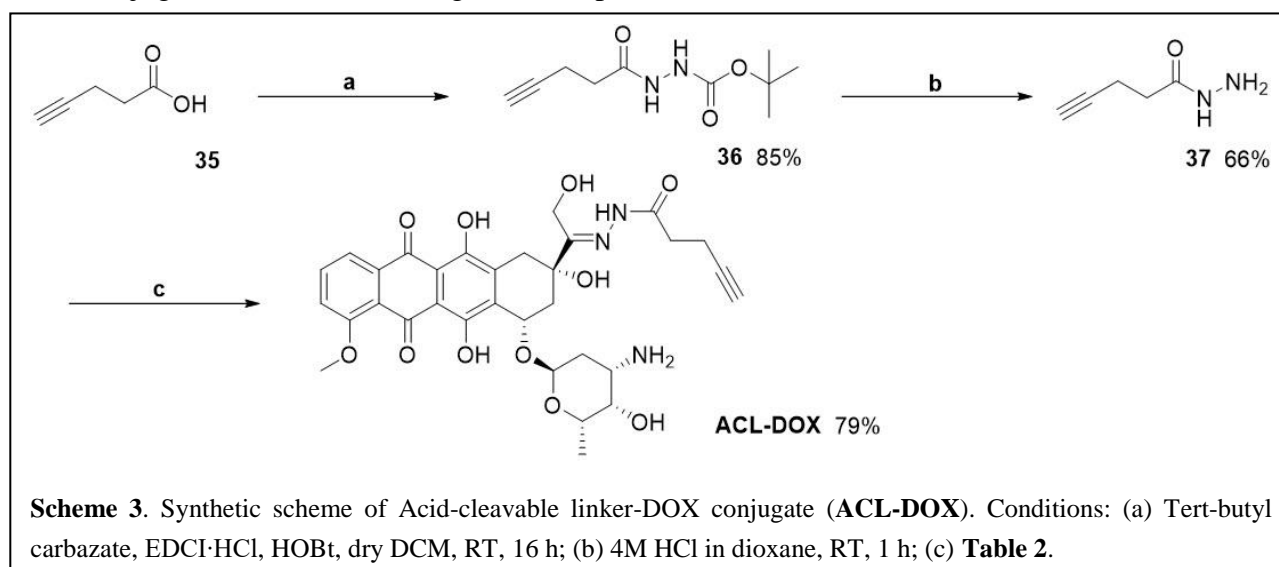
The pre-isolated **36** was treated with HCl to remove the tert-butoxycarbonyl (Boc) group (**Scheme 2**). The successful synthesis of **37** was confirmed by TLC with DCM and MeOH (20:1) as the mobile phase. The new point ( $R_f=0.1$ ) refers to **37** due to the high polarity of hydrazide, compared with **36** point ( $R_f=0.67$ ).

### Synthesis of ACL-Vanillin

Synthesis of **ACL-Vanillin** was achieved through reacting **37** with Vanillin in dry DCM at RT (**Scheme 2**), and the final product **ACL-Vanillin** was identified by  $^1\text{H}$  NMR through the aromatic proton peaks at 7.64 ppm (d, 1H), 7.0 ppm (dd, 1H) and 6.82 ppm (d, 1H). The LC-MS further indicated the formation of **ACL-Vanillin** with a peak at 247.0  $[\text{M} + \text{H}]^+$ .

### 2.2.2 Synthetic approach to ACL-DOX

The successful synthesis of the Vanillin-based model reaction indicates that our proposed synthetic route is approachable. Therefore, we conducted the synthesis of our target Acid-cleavable linker-DOX conjugate (**ACL-DOX**) using the same procedure (**Scheme 3**).



## Synthesis of ACL-DOX

In an initial attempt to synthesise **ACL-DOX** (Scheme 3), the intermediate **37** was reacted with DOX in the presence of 0.2 eq of acetic acid (AcOH) (Table 2a). These reaction conditions resulted in a crude product with a yield of 40%. This reaction was repeated with increased equivalence of AcOH and decreased reaction time (Table 2b) to finalise an appropriate catalytic amount of AcOH for this reaction. By reviewing the literature, we believe that the low yield might have been caused by the high sensitivity of hydrazone substrate to H<sub>2</sub>O in the system. Accordingly, a catalytic amount of sodium sulphate (Na<sub>2</sub>SO<sub>4</sub>) was added (Table 2c) to create the product with a significantly higher yield of 79%.

Reaction	Conditions	Temp	Time	Outcome
(a)	0.2 eq AcOH, dry MeOH	RT	24 h	40% yield
(b)	0.5 eq AcOH, dry MeOH	RT	20 h	50% yield
(c)	0.5 eq AcOH, Na <sub>2</sub> SO <sub>4</sub> , dry MeOH	RT	20 h	79% yield

**Table 2.** Experimental procedures used to synthesise **ACL-DOX**.

However, the purification of crude **ACL-DOX** faced great challenges due to its instability in an H<sub>2</sub>O-contained environment. In an initial effort to obtain pure **ACL-DOX**, the crude product was dissolved in MeOH and purified *via* prep-HPLC (phase A: H<sub>2</sub>O, phase B: MeCN), resulting in a mixture of **ACL-DOX** and DOX. This may be due to the degradation of **ACL-DOX** in the presence of H<sub>2</sub>O and formic acid (0.1%, v/v) from the mobile phase.

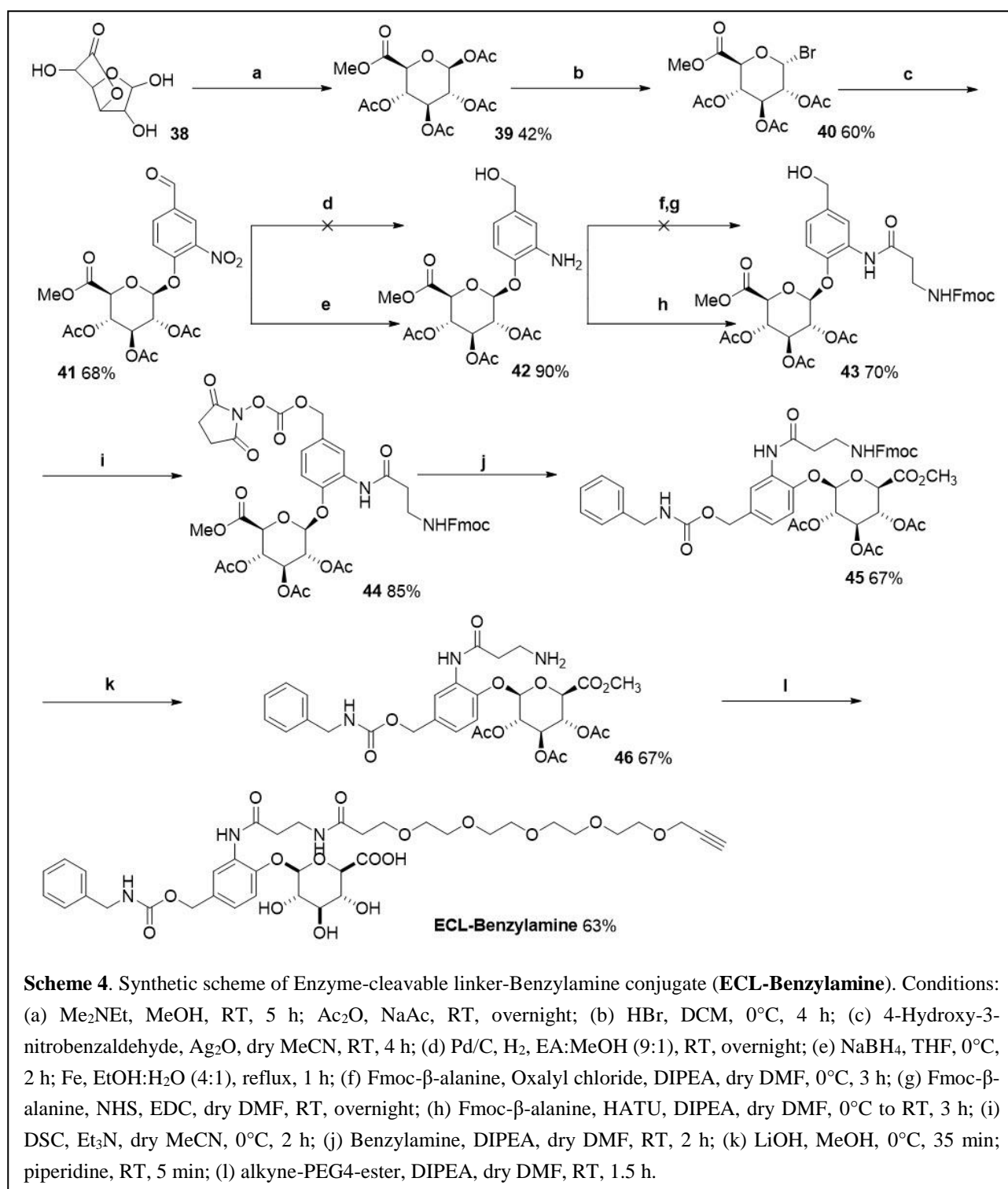
For this reason, H<sub>2</sub>O (phase A) was replaced with MeOH while formic acid was removed from the mobile phase. However, the modifications on the mobile phase predominantly resulted in DOX and a minor desired product. Moreover, there was only a slight difference in the retention time of **ACL-DOX** and DOX on the reverse phase column, suggesting that they can hardly be separated by prep-HPLC.

Recrystallisation was then pursued, including recrystallisation upon the addition of dry MeCN to the reaction mixture, followed by washing with dry MeCN three times and centrifugation to give the pure **ACL-DOX**.

## 2.3 Synthetic approach to Enzyme-cleavable linker (ECL)

### 2.3.1 Synthetic approach to ECL-Benzylamine

Owing to the cytotoxicity of DOX, an alternative (Benzylamine) compound featuring a free amine group was used to explore the synthetic route and evaluate the reactivity of ECL towards enzymatic cleavage.



The synthetic route of Enzyme-cleavable linker-Benzylamine conjugate (**ECL-Benzylamine**) is shown in **Scheme 4**. Compound **40** was prepared as previously reported.<sup>221</sup> Conjugation with 4-Hydroxy-3-nitrobenzaldehyde was then achieved in the presence of silver oxide (Ag<sub>2</sub>O) to form compound **41**. Furthermore, aldehyde and nitro group on **41** were reduced to form **42**, followed by coupling reaction with Fmoc-β-alanine to form **43**. Following the same procedure to introduce DOX into PCL, the benzyl alcohol site of **43** was activated and coupled with Benzylamine to form **45**. Considering that spacious reaction area will promote the enzymatic hydrolysis, the alkyne-PEG<sub>4</sub>-

NHS ester containing an alkyne end was attached to the deprotected linker **46** in one step, resulting in **ECL-Benzylamine**.

### Synthesis of **39**

The first step in the synthesis of the ECL was the formation of compound **39** (**Scheme 4**). Starting with the commercially available D-glucurono-6, 3-lactone **38**, N, N-dimethylethylamine (Me<sub>2</sub>NEt) was used as the catalyst for the hydrolysis reaction to form D-glucuronic acid, which was then reacted with acetic anhydride (Ac<sub>2</sub>O) to form compound **39**. After the reaction was completed, two methods were used to purify the crude product. First, flash column chromatography was used but it was time-consuming and resulted in some impurities. Then, an alternative approach was applied by performing recrystallisation to the crude product with absolute EtOH. Although recrystallisation led to a lower yield (42%), it resulted in much higher purity and corresponding physical character to published data. The formation of compound **39** was confirmed through <sup>1</sup>H NMR that displayed five protons (5.75 ppm, 5.26 ppm, 5.13 ppm and 4.17 ppm) from the hexatomic ring, as well as methyl peaks at 3.73 ppm, 2.10 ppm, and 2.02 ppm.

### Synthesis of **40**

Compound **39** was reacted with hydrobromic acid (HBr) in a nucleophilic substitution reaction to form compound **40** (**Scheme 4**). This halogenation reaction proceeded very quickly to form the desired product. <sup>1</sup>H NMR verified the formation of compound **40** through the presence of an upfield chemical shift in hexatomic ring protons (7.27 ppm, 6.24 ppm, 5.87 ppm, 5.48 ppm and 5.21 ppm) due to the bromine atom's induction effect.

### Synthesis of **41**

Compound **40** was then reacted with 4-Hydroxy-3-nitrobenzaldehyde to form compound **41** (**Scheme 4**). <sup>1</sup>H NMR verified the formation of compound **41** by presenting an aldehyde peak (9.98 ppm, 1H) and aromatic protons (8.31 ppm, 8.09 ppm and 7.50 ppm). LC-MS further displayed the formation of **41** with a MS peak at 505.9 [M + Na]<sup>+</sup>.

### Synthesis of **42**

The next step in the synthesis of ECL was the formation of compound **42** through a reduction reaction (**Scheme 4**), during which the aldehyde functional group was reduced to alcohol while the nitro group was converted into amine. We first chose hydrogen gas (H<sub>2</sub>) and palladium on charcoal (Pd/C) as the catalyst. For the quantity of catalyst, we started with 0.1 equivalent of starting material. However, the reaction proceeded so fast that a by-product showed up. The formation of by-product was confirmed through LC-MS with a peak at 440.0 [M + H]<sup>+</sup>, indicating that the benzyl alcohol was further reduced and formed methyl group.

Then, we decreased the amount of catalyst by 50% to prevent side reactions. After 3 h, TLC analysis exhibited that the starting material was completely consumed but there were still by-products

generated. To avoid the over reduction of the aldehyde group on **41**, we decided to proceed with a two-step reduction. Sodium borohydride ( $\text{NaBH}_4$ ) and iron powder (Fe) were utilised to reduce the aldehyde group and nitro group, respectively, and this method proceeded with a high yield to afford **42**.

The formation of compound **42** was verified through  $^1\text{H}$  NMR that displayed a new methylene peak at 4.55 ppm. Peaks representing the amine protons (3.85 ppm, 2H) also apparently indicated the formation of the desired product. Besides, LC-MS suggested the formation of the desired product with a peak at 456.0  $[\text{M} + \text{H}]^+$ .

### Synthesis of **43**

Fmoc- $\beta$ -alanine was initially tried with oxalyl chloride to form an acetic chloride, which was reacted with compound **42** without further purification due to the high reactivity of acetic chloride (**Scheme 4**). Nevertheless, this reaction was not satisfactory because of the impurity problem. TLC analysis showed eight points, which became an enormous challenge for purification works. Thus, the second method was applied to form an active ester by coupling the Fmoc- $\beta$ -alanine to the N-hydroxysuccinimide (NHS), followed by the acylation reaction between the NHS-activated Fmoc- $\beta$ -alanine and compound **42**. However, the main product for this reaction was not the desired product. Then, a general method to form the amide in peptide chemistry was adopted with HATU as the catalyst, resulting in the formation of **43**. The synthesis of compound **43** was confirmed with  $^1\text{H}$  NMR that indicated the formation of the amide (6.94 ppm, 1H). LC-MS further displayed the formation of compound **43** with a MS peak at 748.9  $[\text{M} + \text{H}]^+$ .

### Synthesis of **44**

Synthesis of **44** followed the way to form compound **34** in the synthesis of PCL, and compound **43** was reacted with DSC to increase the reactivity of benzyl alcohol (**Scheme 4**). The formation of compound **44** was confirmed through  $^1\text{H}$  NMR that indicated the two methylene peaks from the NHS. LC-MS further displayed the formation of compound **44** with a MS peak at 889.9  $[\text{M} + \text{H}]^+$ .

### Synthesis of **45**

Previously isolated **44** was then reacted with Benzylamine in the presence of DIPEA to produce **45** (**Scheme 4**) based on the same mechanism to afford **PCL-DOX**. The formation of **45** was confirmed by  $^1\text{H}$  NMR through an aromatic proton peak at 7.20 ppm (m, 7H). LC-MS further identified the formation of **45** with a peak at 904.4  $[\text{M} + \text{H}]^+$ .

### Synthesis of **46**

Following the synthesis of **45**, it was first treated with lithium hydroxide (LiOH) to remove the acetyl groups. The resulting intermediate was reacted with piperidine in DMF to remove the Fmoc group (**Scheme 4**). Crude **46** was purified through the prep-HPLC, eluting with 0.1% formic acid in an  $\text{H}_2\text{O}$  and MeCN gradient at a flow rate of 20 mL/min (gradient: 10% organic for 5 min followed by a ramp

up to 100% organic over 25 min). The fraction containing **46** was collected at the retention time of 6 min. The formation of **46** was verified by LC-MS through a peak at 520.0 [M + H]<sup>+</sup>.

### Synthesis of ECL-Benzylamine

In the final step, compound **46** was reacted with alkyne-PEG4-NHS ester to produce **ECL-Benzylamine** (Scheme 4). The formation of **ECL-Benzylamine** was confirmed through methylene proton peaks at 3.64 ppm (m, 6H), 3.60 ppm (d, 6H), and 3.55 ppm (s, 6H), as well as an alkyne peak at 2.84 ppm (t, 1H). LC-MS additionally displayed a MS peak at 806.3 [M + H]<sup>+</sup>.

### 2.3.2 Synthetic approach to ECL-DOX

As the synthetic route to afford ECL has been optimised, further conjugation of DOX with ECL was performed to form **ECL-DOX**. The synthetic route of **ECL-DOX** is shown in Scheme 5, where DOX was attached to the activated ECL, followed by deprotection reaction for further coupling reaction to form **ECL-DOX**.

### Synthesis of 47

Following the same procedure to introduce Benzylamine to ECL, DOX was attached to **44** (Scheme 5), and the coupling reaction proceeded well to give rise to **47**. The formation of **47** was confirmed by <sup>1</sup>H NMR through an amide proton peak at 7.75 ppm (dd, 1H). LC-MS also ascertained the successful synthesis of **47** with a MS peak at 1340.6 [M + Na]<sup>+</sup>.

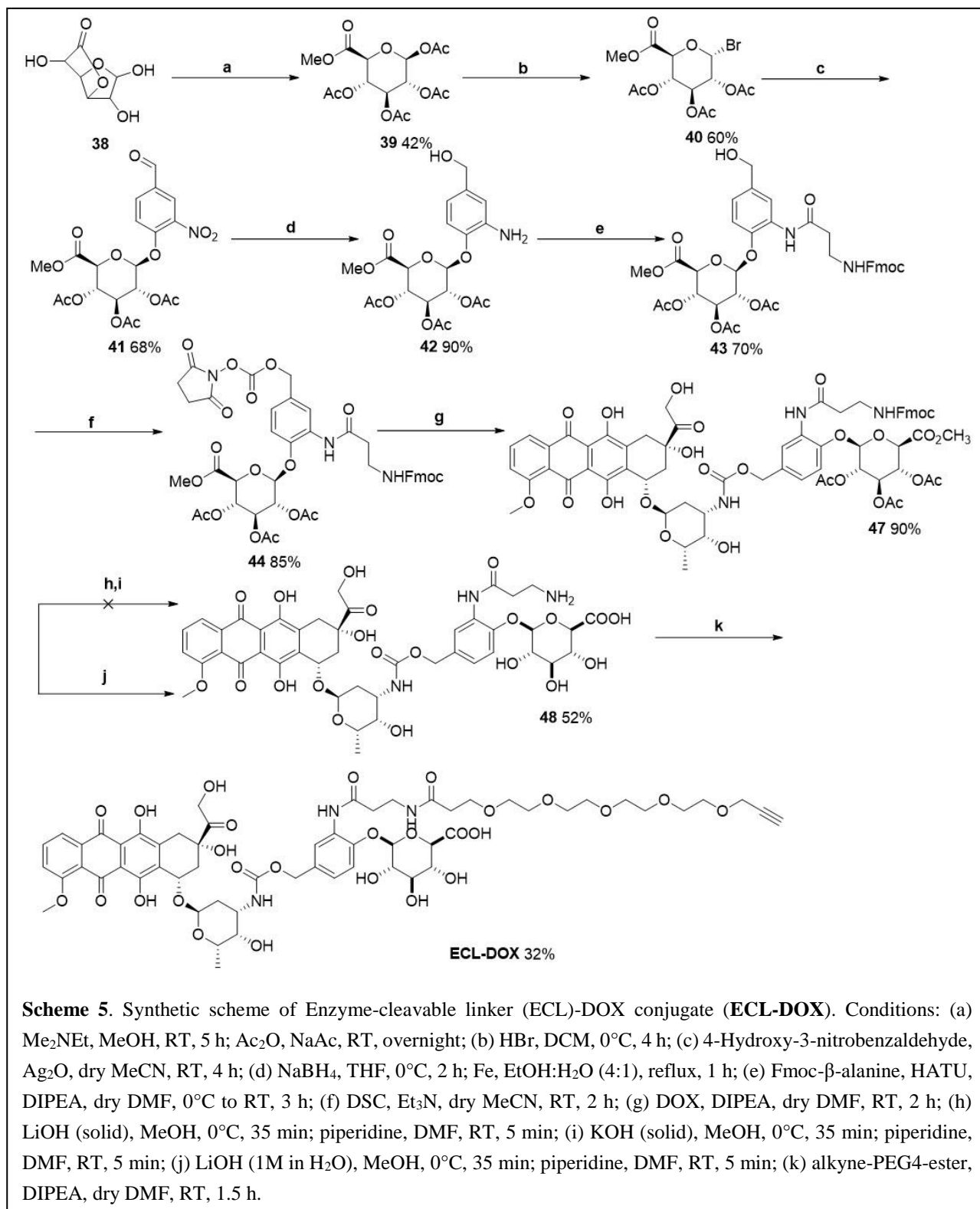
### Synthesis of 48

Reaction	Conditions	Temp	Time	Outcome
(a)	LiOH (Solid), piperidine	0 °C to rt	2h	90% by-product
(b)	KOH, piperidine	0 °C to rt	2h	unknown products
(c)	LiOH (1M in H <sub>2</sub> O), piperidine	0 °C to rt	2h	50% product isolated

**Table 3.** Reaction conditions undertaken in the synthesis of **48**.

The most challenging reaction in the synthesis of **ECL-DOX** was the deprotection of compound **47** to form **48** (Scheme 5). In an initial attempt to form compound **48**, previously synthesised **47** was first reacted with LiOH to remove the acetyl groups on the sugar ring. Upon the reaction with piperidine, the Fmoc group will detach from alanine to produce **48**. However, these reaction conditions failed to produce **48**, instead, predominantly resulting in a demethylated product. The structure of which was confirmed by LC-MS with a peak at 942.2. We hypothesised that LiOH might react with HCl from DOX hydrochloride to form lithium chloride (LiCl), which exists as Lewis acid and demethylated **48**. To avoid demethylation of **48**, an alternative method was performed by using potassium hydroxide (KOH) and piperidine. However, this resulted in unknown products. In another attempt to form **48**, LiOH was first dissolved in H<sub>2</sub>O to make a 1M LiOH stock, which was added to

compound **47** in MeOH. Additionally, piperidine was added to successfully produce **48** (Table 3). Synthesis of **48** was confirmed through LC-MS with a MS peak at 956.3 [M + H]<sup>+</sup>.



Another challenge refers to the purification of crude **48**, owing to the high hydrophilicity of glucuronide moiety. We used Prep-HPLC to purify the crude **48**, eluting with 0.1% formic acid in an H<sub>2</sub>O and MeCN gradient at a flow rate of 20 mL/min (gradient: 10% organic for 5 min followed by a ramp up to 100% organic over 25 min). However, the majority of product was carried away by

mobile phase within the first 5 min of purification, possibly because the crude product was injected into the prep-HPLC system with DMSO, a very polar solvent. Therefore, the crude product was dissolved in a mixture (10% of MeCN in H<sub>2</sub>O). Nonetheless, this modification turned out to be invalid with the same outcome gained by using DMSO as the solvent. Then, a new gradient (10% organic for 3 min followed by a ramp up to 50% over 25 min) was applied to purify the crude **48**, leading to a small amount of desired product that came off at the retention time of 10 min. The modification on gradient achieved a certain degree of success in separating crude **48**, demonstrating that extending the retention time of **48** might achieve better separation.

In this way, the flow rate was decreased from 20 mL/min to 0.5 mL/min while the modifications on the gradient were kept, contributing to the successful purification of **48**. Although the modified experimental conditions gave rise to compound **48**, the yield of the deprotection reaction was relatively low (52%). This is attributed to the low stability of DOX under basic conditions. Therefore, more efforts are required to improve the yield of this reaction.

### Synthesis of ECL-DOX

In the final step, **48** was reacted with commercially available alkyne-PEG4-NHS ester to produce our target product **ECL-DOX** (Scheme 5). After the purification through Prep-HPLC using the same eluting gradient to afford **48**, **ECL-DOX** was gained. The formation of **ECL-DOX** was confirmed by <sup>1</sup>H NMR through methylene proton peaks at 3.54 ppm (d, 3H), 3.52 ppm (s, 4H), 3.50 ppm (s, 3H), 3.48 ppm (s, 3H) and 3.46 ppm (s, 3H). High Resolution Mass Spectrometry (HRMS) further displayed an MS peak at 1264.4 [M + Na]<sup>+</sup>.

## Chapter 3.0: Fabrication and surface functionalisation of porous silicon nanoparticles

In this chapter, we will discuss the approaches to prepare the pSiNPs conjugated with pre-synthesised SCL-DOX conjugates.

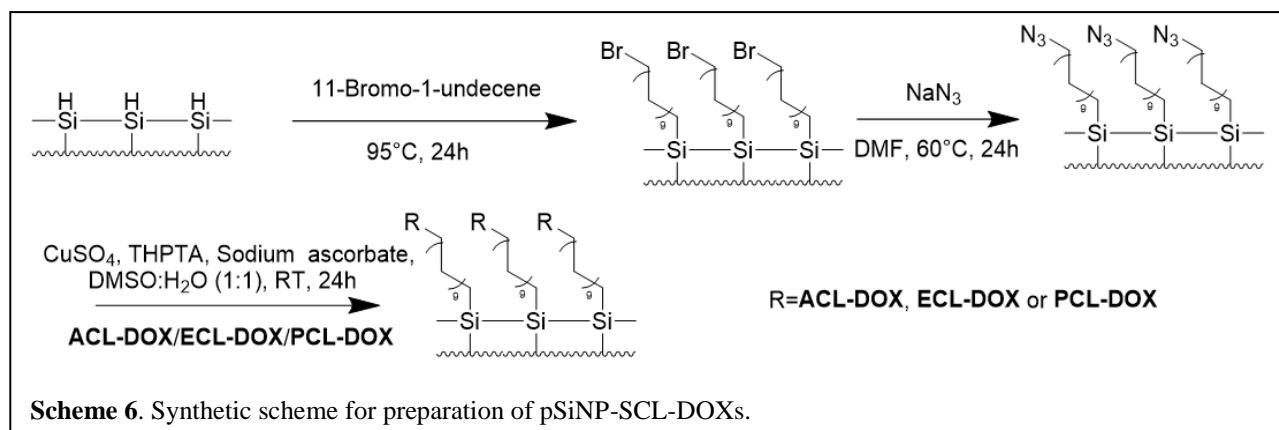
### 3.1 Preparation of freshly etched pSiNPs

pSi films were prepared by periodically etching p<sup>+</sup> type (0.0055-0.001 Ω cm) silicon wafers at 5 mA/cm<sup>2</sup> for 20 s and 139 mA/cm<sup>2</sup> for 1000 cycles in a 3:1 HF (49%): EtOH solution. Extra 60 s of etching at 139 mA/cm<sup>2</sup> in a solution of 1:1 HF (49%): EtOH lifted off the pSi films from the wafer.

Ultrasonication of pSi films was then performed in an ultrasonicator water bath for 24 h to produce the pSiNPs of approximately 180 nm in diameter, which were collected *via* ultracentrifugation (2000 xg for 6 min). The supernatant was also collected and then centrifuged at 20000 xg for 10 min to retrieve the desired particles.

### 3.2 Surface functionalisation of pSiNPs

As mentioned before, the freshly etched pSiNPs is highly reactive due to hydride-terminated surface. Therefore, surface modification is required to stabilise the surface of pSiNPs while providing chemical handles for further conjugation. The first step was the stabilisation of the pSiNPs surface based on a hydrosilylation reaction between freshly etched pSiNPs and 11-Bromo-undecene. After the hydrosilylation reaction, the surface of pSiNPs was modified with bromine handle (**pSiNP-Br**). This was followed by a nucleophilic substitution reaction by reacting the **pSiNP-Br** with sodium azide ( $\text{NaN}_3$ ) to form the **pSiNP-N<sub>3</sub>** (**Scheme 6**).



### 3.3 Preparation of pSiNP-SCL-DOX

The azide group on the surface of pSiNPs will serve as the attachment site for our SCL-DOX conjugates terminating with alkynes, which can be achieved by CuAAC reaction (**Scheme 6**). In this project, we chose the THPTA as the Cu(I) conjugating ligand to increase the catalytic efficiency. The **pSiNP-N<sub>3</sub>** was dispersed into a mixture of DMSO and H<sub>2</sub>O, since the three SCL-DOX conjugates have a promising solubility in this solvent system. The reaction proceeded for 24 h to afford **pSiNP-PCL-DOX** while the reaction time was extended to 48 h to obtain **pSiNP-ECL-DOX** with the highest yield. Different from the other two SCL-DOX conjugates, the hydrazone linkage in **ACL-DOX** is highly susceptible to aqueous solution, where it can be hydrolysed to form DOX and the linker residue. To avoid the hydrolysis of ACL, the reaction time was shortened to 30 min while a drop of DIPEA was added into the reaction mixture to provide a basic environment for ACL.

### 3.4 pSiNP-SCL-DOX Characterisation

#### 3.4.1 TEM and SEM result

Initial functionalisation with  $\text{NaN}_3$  was required to provide azide end, which will further react with the alkyne handle on SCL-DOX conjugates. Therefore, the SCL-DOX conjugates can be articulated to the surface of pSiNP. The **pSiNP-N<sub>3</sub>** were characterised by scanning electron microscopy (SEM) and transmission electron microscopy (TEM). The TEM and SEM images are shown in **Figure 14**. According to the SEM result, pores can be clearly seen on pSiNPs that had a horizontal orientation. pSiNPs vertically orientated were presented as a repeating column like structures. The average pore size of **pSiNP-N<sub>3</sub>** was measured to be  $22 \pm 5$  nm using ImageJ.

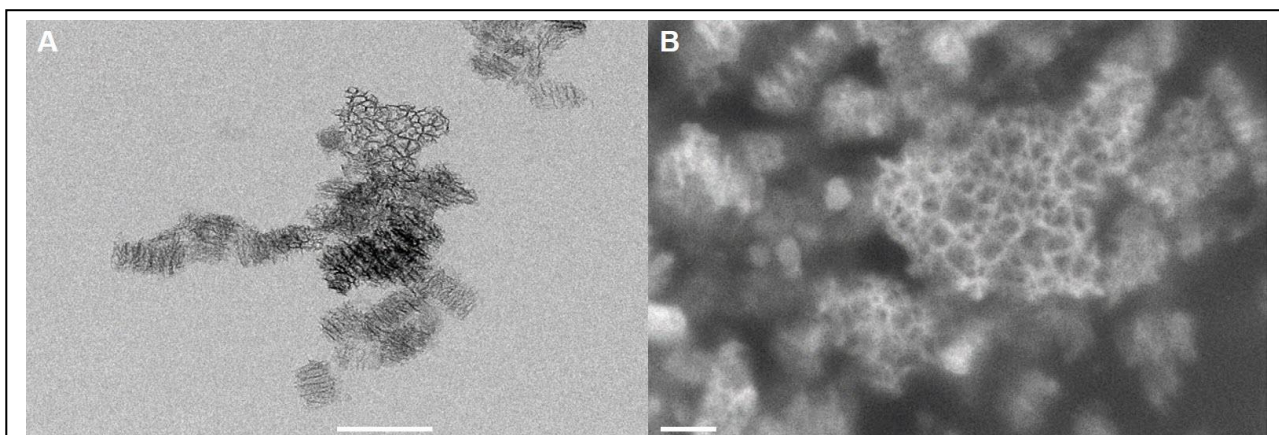


**Figure 14.** (A) TEM image of the **pSiNP-N<sub>3</sub>**. Scale bar= 200 nm. (B) SEM image of the **pSiNP-N<sub>3</sub>**. Scale bar= 100 nm.

**pSiNP-PCL-DOX** was prepared and characterised through SEM and TEM (**Figure 15**). Twenty random pores were averaged to determine the average pore size for the **pSiNP-PCL-DOX**. The average pore size of **pSiNP-PCL-DOX** was measured to be around  $24 \pm 7$  nm. Thus, it was expected that there was no structural change to pSiNPs during click reaction with **PCL-DOX**.

TEM and SEM images of **pSiNP-ACL-DOX** and **pSiNP-ECL-DOX** will be performed in the future.

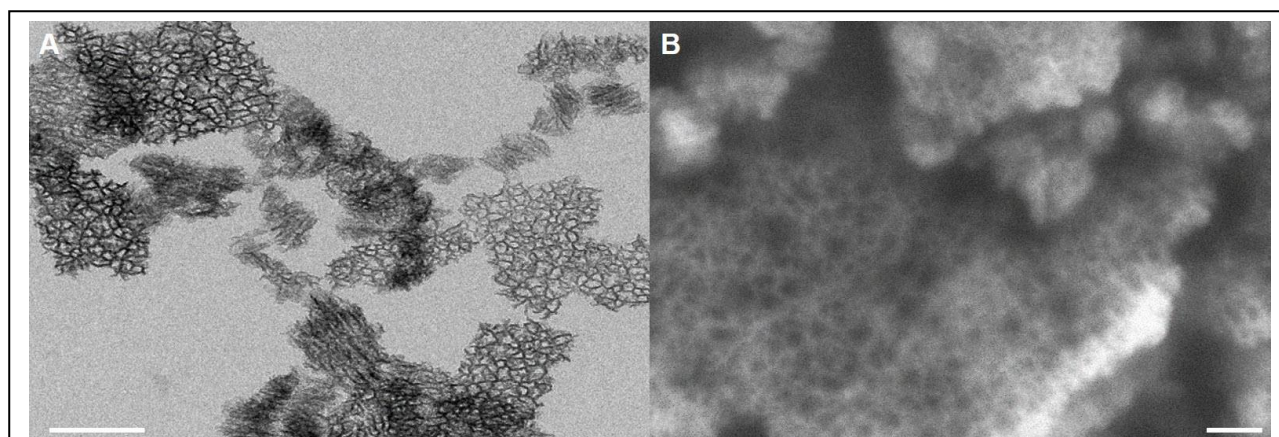
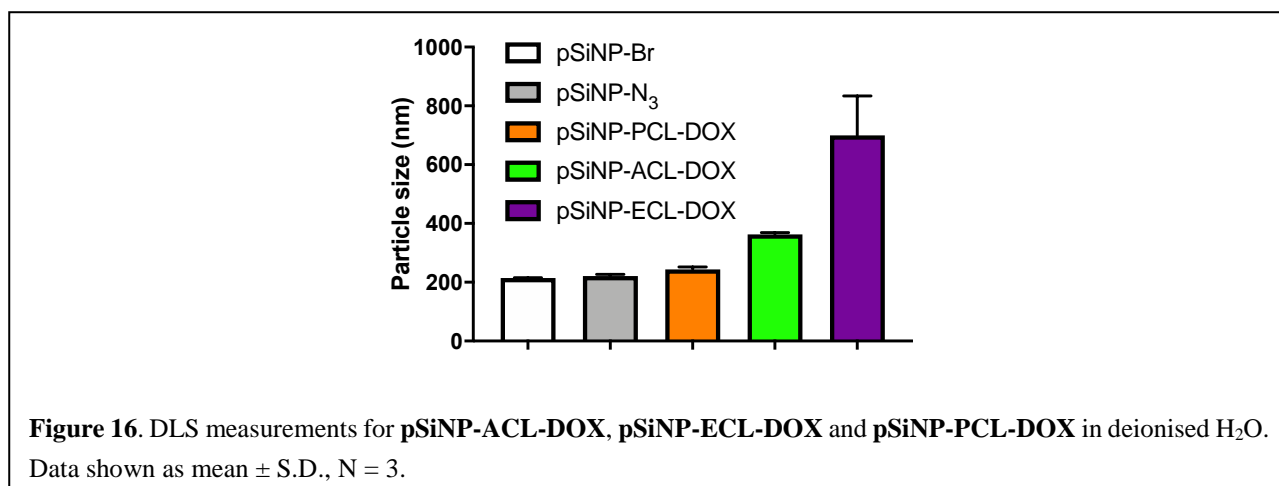


**Figure 15.** (A) TEM image of the **pSiNP-PCL-DOX**. Scale bar= 200 nm. (B) SEM image of the **pSiNP-PCL-DOX**. Scale bar= 100 nm.

### 3.4.2 DLS result

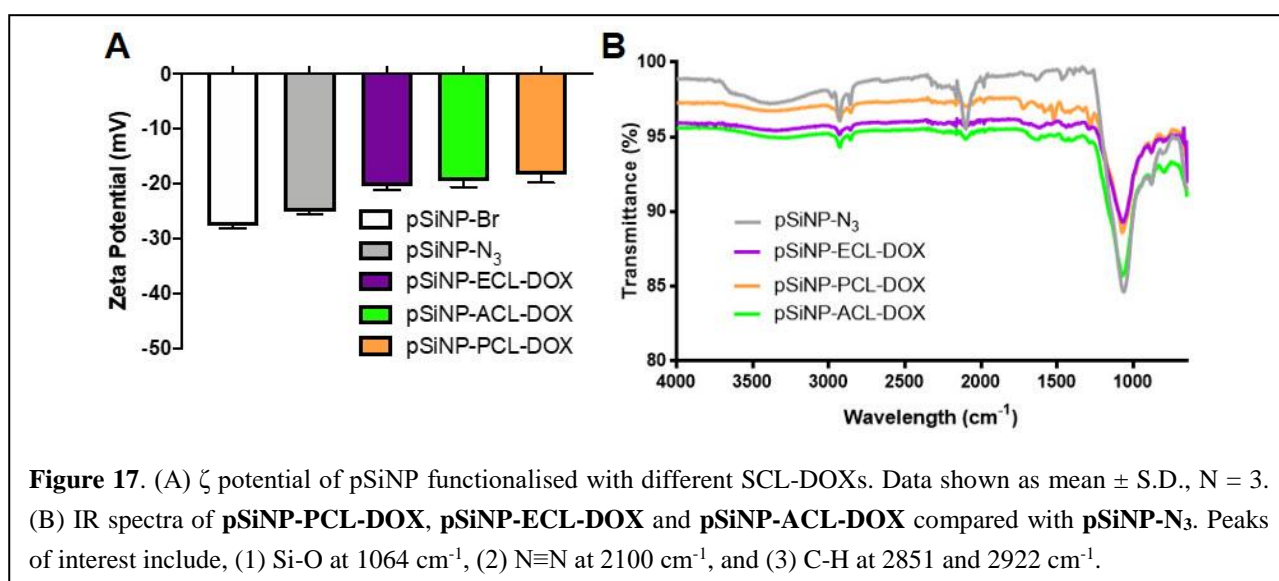
Furthermore, dynamic light scattering (DLS) exhibited the average size of **pSiNP-N<sub>3</sub>** to be approximately 205 nm in deionised H<sub>2</sub>O (PDI: 0.294).

Meanwhile, the average diameters of **pSiNP-ACL-DOX** (356 nm), **pSiNP-ECL-DOX** (746 nm), and **pSiNP-PCL-DOX** (215 nm) were confirmed, reflecting the changes in particle size after the click reaction (**Figure 16**). In comparison with **pSiNP-N<sub>3</sub>**, **pSiNP-ECL-DOX** showed great increase in particle size.



### 3.4.3 Surface chemistry characterisation

To further analyse the surface modification of pSiNP,  $\zeta$  potential and Fourier transform infrared spectroscopy (FTIR) measurements were performed. It is widely acknowledged that the  $\zeta$  potential exerts an important effect on various aspects of nanomaterial-based DDSs, including their circulation time in blood stream, macrophage uptake, and controlled drug release behaviour. Owing to their large surface area, pSiNPs tend to absorb proteins, and the macrophages can rapidly clear the protein-bonded pSiNPs before arriving at desired sites. Generally, NPs with a positive surface charge show good protein absorption due to the active electrostatic interaction between the NPs and protein.<sup>222</sup> In contrast, negatively charged NPs display poor protein absorption, which is preferable regarding the construction of DDSs. As illustrated in **Figure 17A**, the  $\zeta$  potential of all pSiNPs after click reaction is negative, indicating that these pSiNPs may possess prolonged circulation time. Furthermore, the  $\zeta$  potential of the pSiNP changed from -25 mV to -20.5 mV after the click reaction with **ECL-DOX**, while that of **pSiNP-ACL-DOX** and **pSiNP-PCL-DOX** also changed to -19.7 mV and -18 mV, respectively. The decreased surface charge of pSiNPs after the click reaction might originate from the positively charged DOX. Therefore, the decrease in the electrostatic repulsion between the pSiNPs can eventually cause the aggregation of pSiNPs,<sup>223</sup> corresponding to the DLS results.

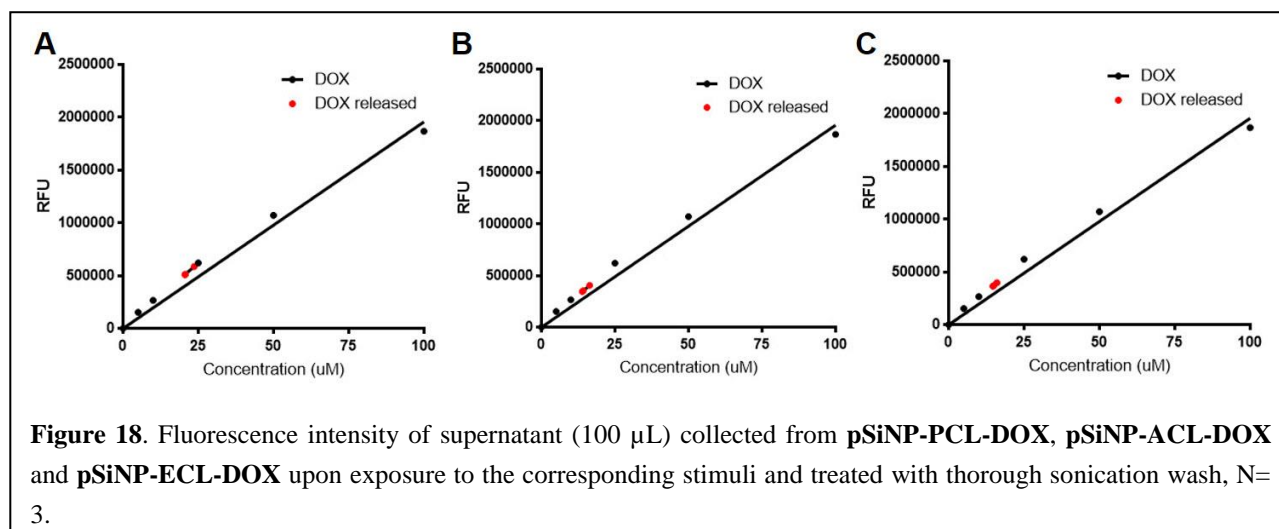


For the FTIR spectra, the C-H stretches at  $2940\text{ cm}^{-1}$  and  $2980\text{ cm}^{-1}$  appear on all the surface functionalised samples. The **pSiNP-N<sub>3</sub>** has a N=N=N stretch mode at  $2100\text{ cm}^{-1}$  (**Figure 17B**), and the signal is further demonstrated to be attenuated greatly in samples after click reaction, verifying the consumption of azide groups. Moreover, new IR peaks at  $1400\text{ cm}^{-1}$ ,  $1590\text{ cm}^{-1}$ , and  $1710\text{ cm}^{-1}$  are characteristics of O-H bending, N-H bending, and C=O stretching vibrations that indicates the successful installation of DOX onto the pSiNPs surface.

### 3.4.4 Drug loading capacity characterisation

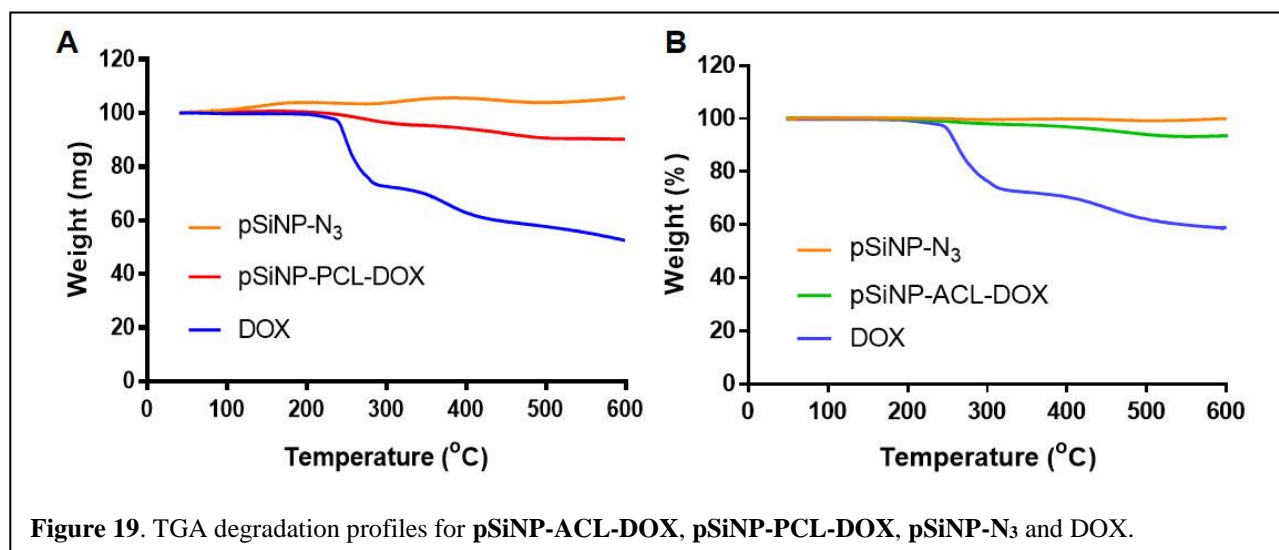
LC is considered one of the important parameters of nanomedicines, reflecting the mass ratio of drugs to the nanocarrier. Considering most of the concepts, drug LC is strongly related to drug metabolism and therapeutic effect of nanomedicines.<sup>224</sup> Basically, drug LC is determined by the physicochemical properties of carrier material. In most cases, drug molecules were loaded into the pSiNP through physical or electrostatic adsorption, resulting in a low controlled drug release profile and drug loading efficiency. Although pSiNP possess a large surface area, we speculated that the LC will be less than that of the traditional physical adsorption because physical adsorption would, in theory, utilize both the surface and porous void to accommodate drugs.

We first measured the drug LC of pSiNP-SCL-DOXs by performing fluorescence spectroscopy. **pSiNP-ACL-DOX**, **pSiNP-ECL-DOX** and **pSiNP-PCL-DOX** at the concentration of  $0.06\text{ mg/mL}$  were exposed to the corresponding stimuli, and the treated pSiNP solutions were sonicated thoroughly to burst the release of DOX contents from the pSiNPs. The amount of released DOX in the supernatant was collected and verified by fluorescence spectroscopy to provide the corresponding LC of each pSiNP-SCL-DOX (**Figure 18**). The LC of **pSiNP-PCL-DOX**, **pSiNP-ACL-DOX**, and **pSiNP-ECL-DOX** was calculated to be  $20.0 \pm 1.4\text{ wt\%}$ ,  $13.7 \pm 1.1\text{ wt\%}$ , and  $13.9 \pm 0.6\text{ wt\%}$ , respectively. Surprisingly, **pSiNP-PCL-DOX** possesses the highest LC of pSiNPs<sup>67</sup> reported to date.



Thermogravimetric analysis (TGA) was simultaneously conducted to further confirm the payload of DOX from the pSiNP-SCL-DOXs. Since TGA requires a certain mass of sample (more than  $0.8\text{ mg}$ ) but we only obtained a very limited amount of **ECL-DOX** at the end, we decided to accumulate more **ECL-DOX** in the future for TGA analysis while keeping the current batch for *in vitro* and *in vivo*

tests. We thoroughly sonicated and washed the **pSiNP-ACL-DOX** and **pSiNP-PCL-DOX** with DMSO to wash out the non-covalently loaded drugs prior to TGA.



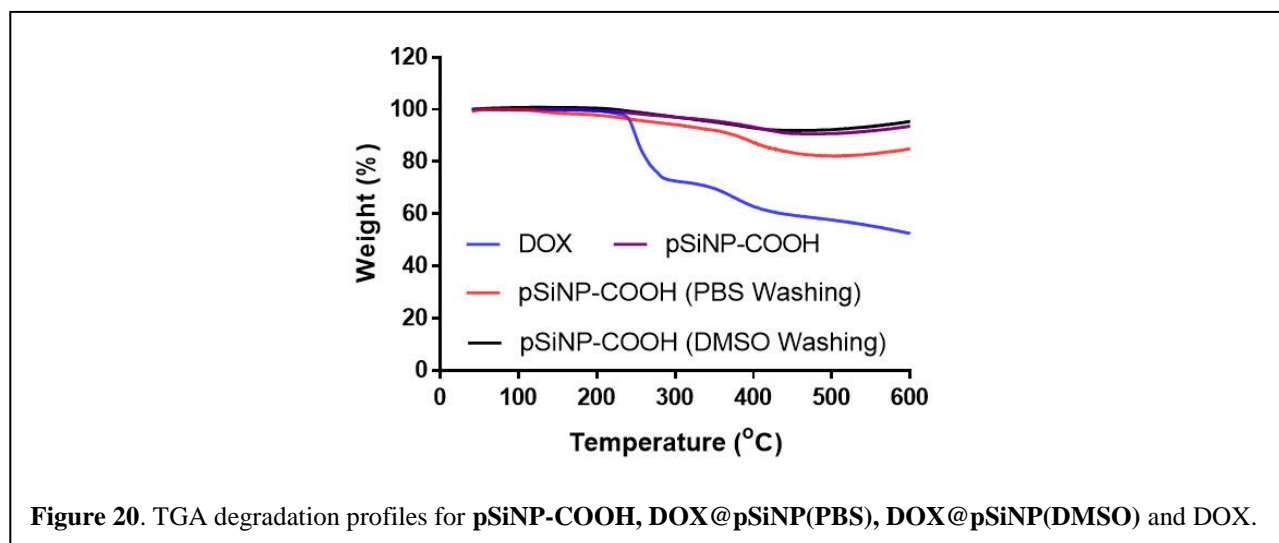
According to the TGA results in **Figure 19**, the minor mass loss up to 100°C is mostly due to the evaporation of moisture associated with hydrated DOX. Upon heating up to 600°C in a nitrogen (N<sub>2</sub>) atmosphere, **pSiNP-N<sub>3</sub>** experienced a 15% increase in weight ascribed to the partial oxidation of silicon. Besides, the weight of DOX decreased gradually as the heating continues, suggesting the decomposition of DOX (**Figure 19**). For **pSiNP-SCL-DOXs** comprising of **pSiNP-N<sub>3</sub>** and DOX, their mass change is affected by the thermal decomposition of DOX and oxidation of **pSiNPs** simultaneously. At 500 °C, the loading capacity of **pSiNP-SCL-DOX** can be calculated as follows:

$$LC (\%) = (\Delta W_2 + \Delta W_3) / (\Delta W_1 + \Delta W_2) \quad (3)$$

where  $\Delta W_1$  is the mass loss of drugs (wt%),  $\Delta W_2$  is the mass addition of **pSiNP-N<sub>3</sub>** (wt%) and  $\Delta W_3$  is the mass loss of **pSiNP-SCL-DOX** (wt%). By calculation, the LC of **pSiNP-PCL-DOX** and **pSiNP-ACL-DOX** is  $20.8 \pm 1.1$  wt% and  $16.0 \pm 1.5$  wt%, respectively. TGA results further demonstrated the high LC of our novel **pSiNP-SCL-DOX** system. Moreover, both fluorescence spectroscopy and TGA presented the consistent drug LC of our novel **pSiNP-SCL-DOXs** from different batches with a small standard deviation. This feature of our **pSiNP-SCL-DOX** system is imperative for biological applications, as the consistency and stability of drug LC of each batch will have a significant impact on the next stage biological experiments.

Lastly, to further confirm that a covalent bonding strategy can achieve higher drug LC in **pSiNP** as compared with physical adsorption, we also investigated the DOX LC of **pSiNP** through the physical adsorption process. Instead of **pSiNP-N<sub>3</sub>**, we chose carboxylic acid-functionalised **pSiNP** (**pSiNP-COOH**), considering that **pSiNP-COOH** has been reported to encapsulate DOX *via* the electrostatic forces between the carboxylic group from **pSiNP** and the primary amine from DOX,<sup>190</sup> while cases regarding **pSiNP-N<sub>3</sub>** were barely reported. After incubating the **pSiNP-COOH** with DOX in PBS buffer for 24 h, the **pSiNP** was divided into two groups for further wash process. One group applied the same wash method as **pSiNP-SCL-DOXs** using DMSO (**DOX@pSiNP(DMSO)**), and another

one only used PBS without sonication (**DOX@pSiNP(PBS)**). Then, both groups were analysed by TGA, and the results are illustrated in **Figure 20**.



Compared with **pSiNP-PCL-DOX**, the drug LC of **DOX@pSiNP(PBS)** is calculated to be  $12.0 \pm 1.0$  wt%, suggesting that covalent bonding strategy can indeed improve the drug loading efficiency. Meanwhile, the **DOX@pSiNP(DMSO)** only had less than 1.0 wt% LC, suggesting that thorough washing with DMSO can eliminate the majority of free SCL-DOX conjugates (**Figure 20**). This also highlights the advantage of our strategy that covalent encapsulation of drug results in significantly stable drug loading. As leaked drug in the circulation will cause side effect and low efficacy to target tissue, this property is imperative for *in vivo* applications.

In conclusion, our covalent drug encapsulation strategy basically outperforms the traditional physical adsorption method in all aspects. The TGA analysis of **pSiNP-ECL-DOX** will be performed once we accumulated enough **ECL-DOX**, and the result will be compared with fluorescence spectroscopy result.

## Chapter 4.0: Linker cleavage study

### 4.1 Study on the stimulus-responsive linker cleavage

#### 4.1.1 Cleavage of PCL-DOX

Following the synthesis of three SCL-DOX conjugates, we conducted a series of controlled drug release tests to study the responsiveness of each SCL to the corresponding stimuli.

Starting with **PCL-DOX**, the compound was dissolved in DMSO to make the concentration at 10 mM. Then, 100  $\mu$ L stock of **PCL-DOX** was diluted in 900  $\mu$ L PBS and exposed to different UV irradiation times ( $\lambda = 400$  nm). The process was monitored under analytical HPLC (**Figure 21**).

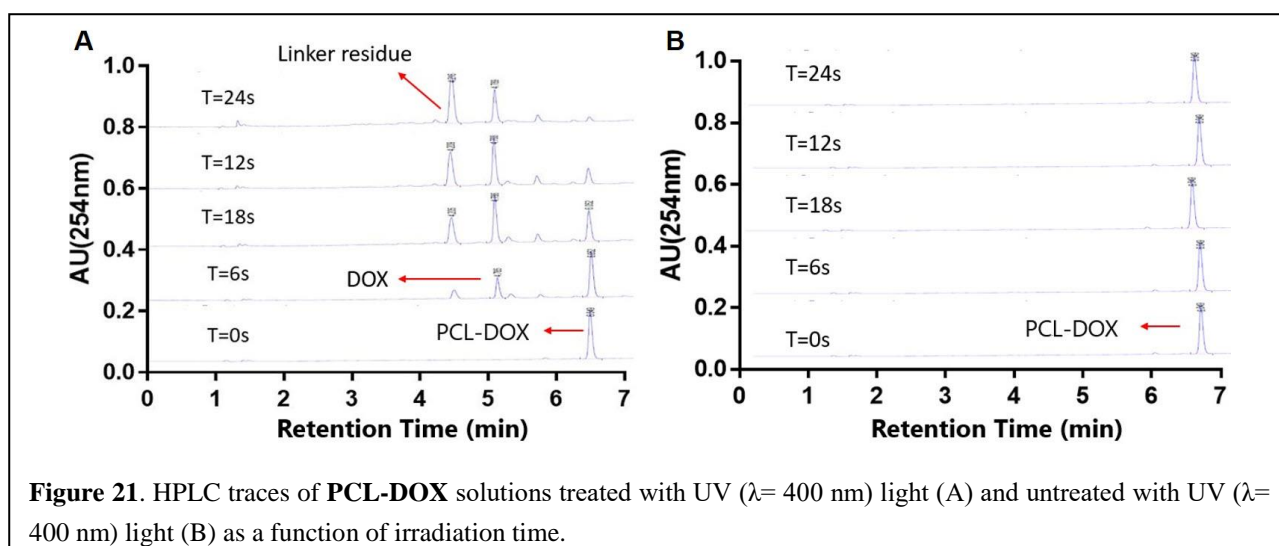


**Figure 21.** HPLC traces of **PCL-DOX** solutions treated with UV ( $\lambda = 400$  nm) light (A) and untreated with UV ( $\lambda = 400$  nm) light (B) as a function of irradiation time.

For a 24 s UV exposure (133 J), around 94% of **PCL-DOX** was cleaved to release DOX ( $T_r = 4.87$  min). Additionally, the stability of **PCL-DOX** in the absence of UV light was also confirmed through HPLC analysis. The results revealed no change in its peak area and retention time.

The rate of DOX release is presented in **Figure 22**, which further summarised the drug release occurred in a nonlinear manner.

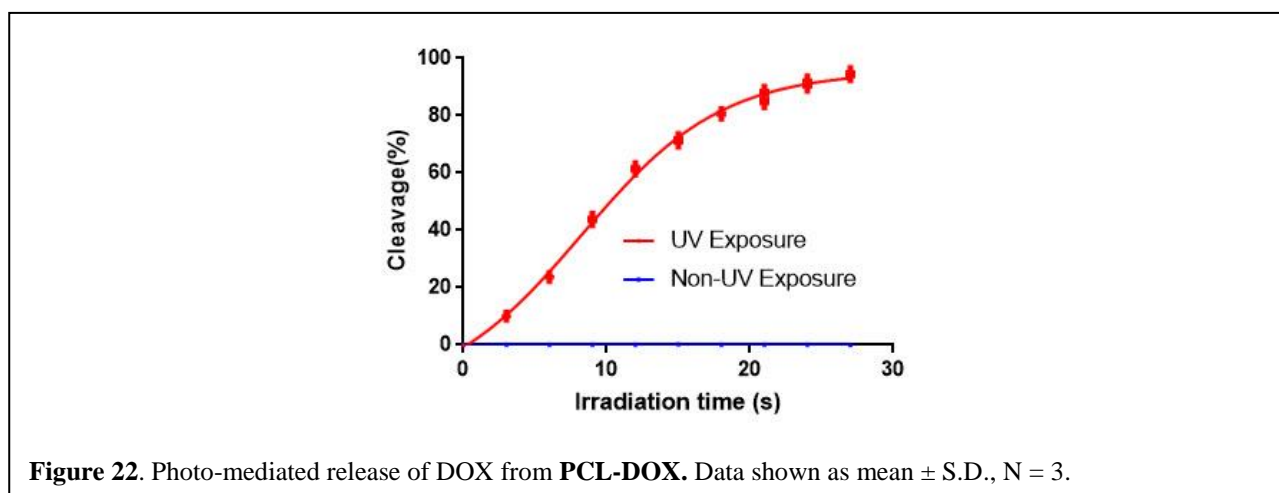
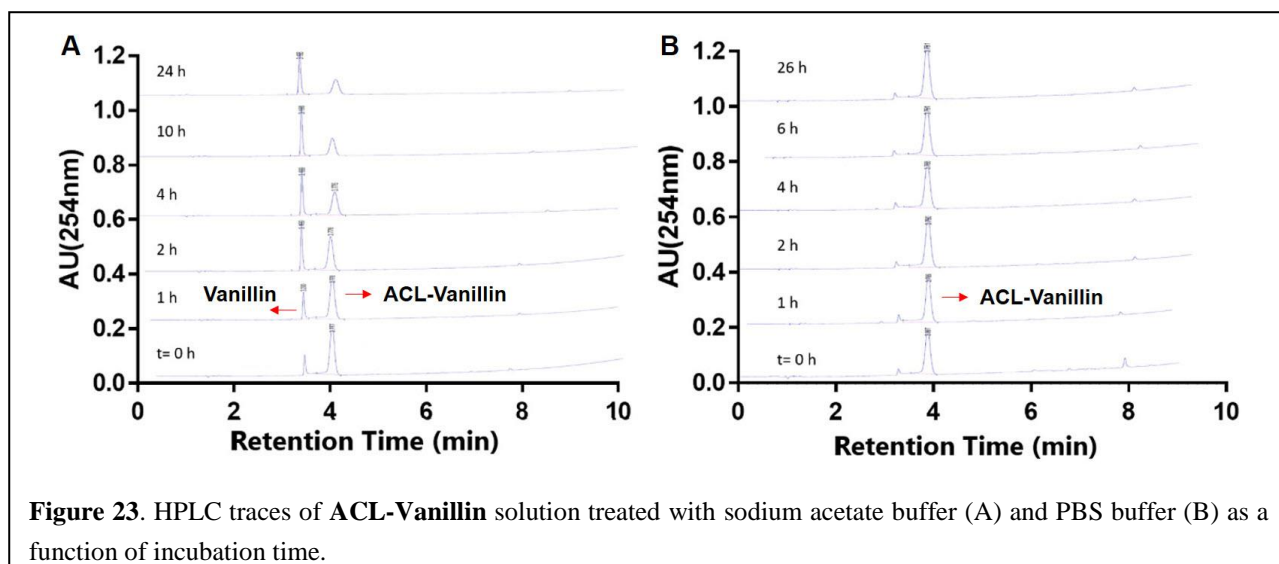


**Figure 22.** Photo-mediated release of DOX from **PCL-DOX**. Data shown as mean  $\pm$  S.D.,  $N = 3$ .

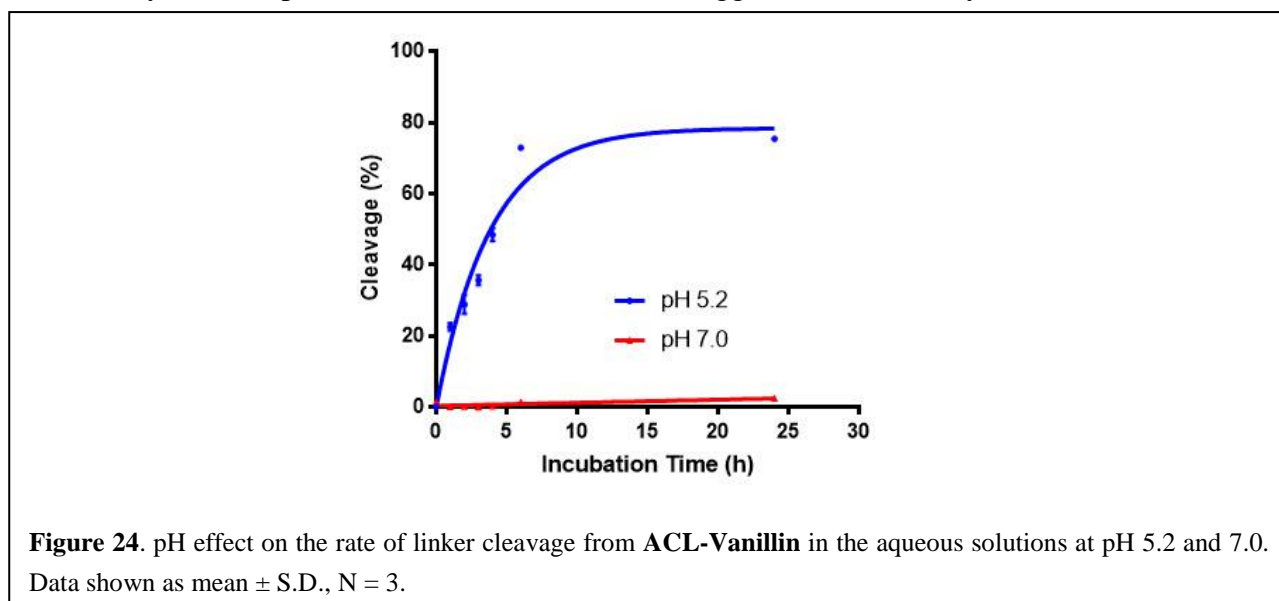
#### 4.1.2 Cleavage of ACL-Vanillin

Following the successful synthesis of **ACL-Vanillin**, the product was dissolved in DMSO to make the concentration at 10 mM. Afterwards, 100  $\mu$ L of **ACL-Vanillin** stock was diluted in 900  $\mu$ L sodium acetate buffer (pH 5.2) or PBS (pH 7.0). These conditions were chosen to mimic the pH of lysosomal and tumour microenvironments compared to the physiological pH.

At each time point, 100  $\mu$ L of reaction mixture was withdrawn and analysed by analytical HPLC. HPLC traces obtained after incubation with sodium acetate buffer (pH 5.2) showed an increase in a peak assigned to the free Vanillin ( $T_r = 3.5$  min) as a function of incubation time, as illustrated in **Figure 23**.



Release kinetics (**Figure 24**) exhibited an initial burst release of **Vanillin** for the first 4 h and then a slow release over the next 20 h. The cleavage of **ACL-Vanillin** was calculated to be at 78% after 24 h-incubation with sodium acetate buffer. Additionally, the stability of **ACL-Vanillin** in PBS was verified *via* analytical HPLC. The result indicated that **ACL-Vanillin** stayed stable in PBS for 26 h. In summary, the low pH value serves as an effective trigger to cleave the hydrazone linker.

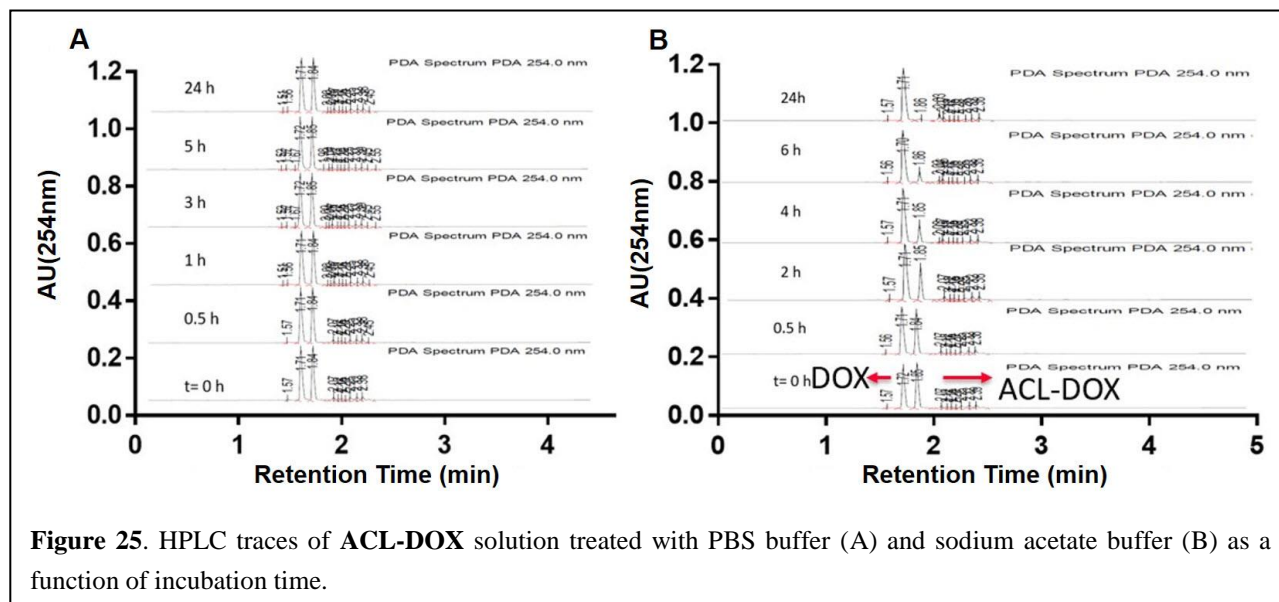


#### 4.1.3 Cleavage of **ACL-DOX**

After confirming that the majority of **ACL-Vanillin** can be hydrolysed in the sodium acetate buffer for 24 h while staying stable in PBS, we used the same buffer solutions to test the hydrolysis of **ACL-DOX**. **ACL-DOX** (100  $\mu$ L, 10 mM) was diluted in 900  $\mu$ L sodium acetate buffer (pH 5.2) or PBS (pH 7.0, negative control). At each time point, 100  $\mu$ L of reaction mixture was withdrawn and analysed by analytical HPLC.

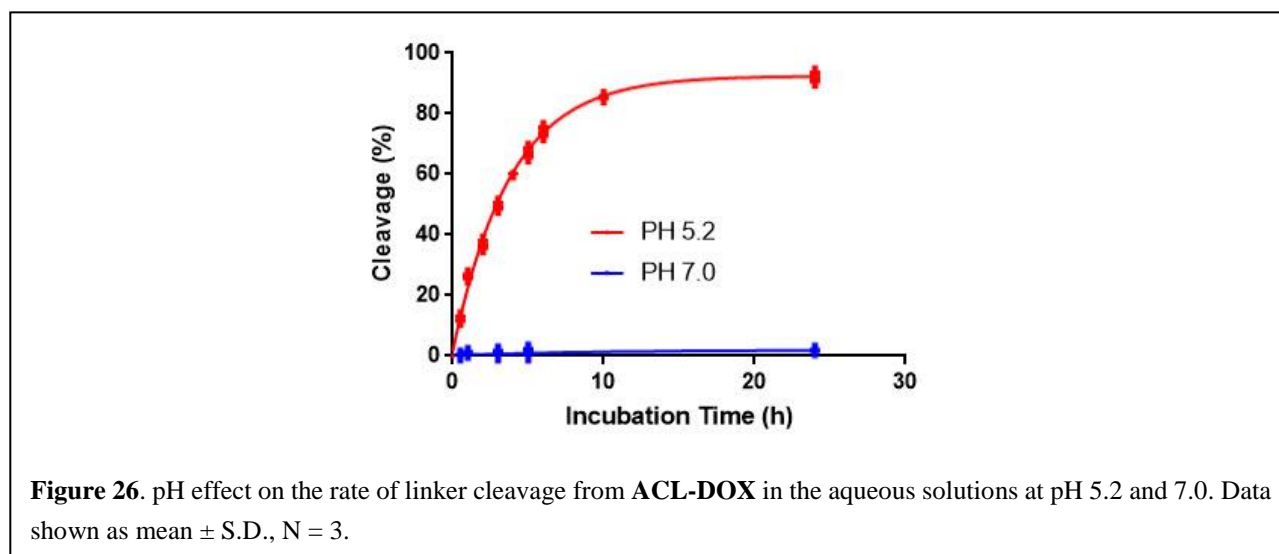
Notably, the HPLC traces (**Figure 25**) showed the peak assignable to **DOX** at T= 0 in both PBS and sodium acetate buffer, reflecting that part of **ACL-DOX** was hydrolysed at the beginning of

experiment. The HPLC analysis was performed in the presence of TFA, contributing to acidic environment. To acquire a better result, TFA was removed from the mobile phase, and the samples were re-analysed using the same gradient. However, the HPLC traces obtained in the absence of TFA presented overlapping double peaks assigned to DOX and **ACL-DOX**, supporting that the degradation of **ACL-DOX** on the reverse phase column was inevitable.



According to the hydrolysis experiment result of **ACL-Vanillin**, hydrazone linker can remain stable in PBS, Thus, we compared the peak area of **ACL-DOX** at each time point upon its exposure to PBS. The results suggested minor changes in the peak area of **ACL-DOX** over 24 h in PBS (**Figure 26**), demonstrating that the degradation of **ACL-DOX** occurred during the HPLC analysis.

From the perspective of chemical structure, Vanillin features a benzaldehyde group, and this aromatic functional group can contribute to the stabilisation of the hydrazone structure after reacting with hydrazide. However, DOX only bears a non-aromatic ketone, which forms a less stable hydrazone linker than Vanillin does.



Herein, the cleavage of **ACL-DOX** at T= 0 h was treated as 0% regardless of the DOX peak (to further support our assumption, please see **Section 4.2**). Consequently, the cumulative release of DOX from **ACL-DOX** in acidic buffer reached the peak at ~85% after 10 h-incubation while the linker remained stable in neutral medium (only 2% cleavage) (**Figure 26**). Another possible method to measure the hydrolysis rate is based on the NMR analysis, where the **ACL-DOX** is dissolved in PBS and sodium acetate buffer to be analysed, respectively. After a period of time, a fraction of the mixture was extracted and concentrated under vacuum prior to the analysis by  $^1\text{H}$  NMR. The change in the peak area of a specific functional group on DOX can be used to measure the hydrolysis rate of **ACL-DOX**.

#### 4.1.4 Cleavage of ECL-Benzylamine

To test the cleavage of ECL under the catalysis of  $\beta$ -glucuronidase, we first tested the previously synthesised **ECL-Benzylamine**. The susceptibility of ECL to enzymatic cleavage was determined by incubating the **ECL-Benzylamine** with *E. coli*  $\beta$ -glucuronidase (Sigma-Aldrich) at 37°C. The enzymatic hydrolysis progress was monitored by analytical HPLC (**Figure 27**).

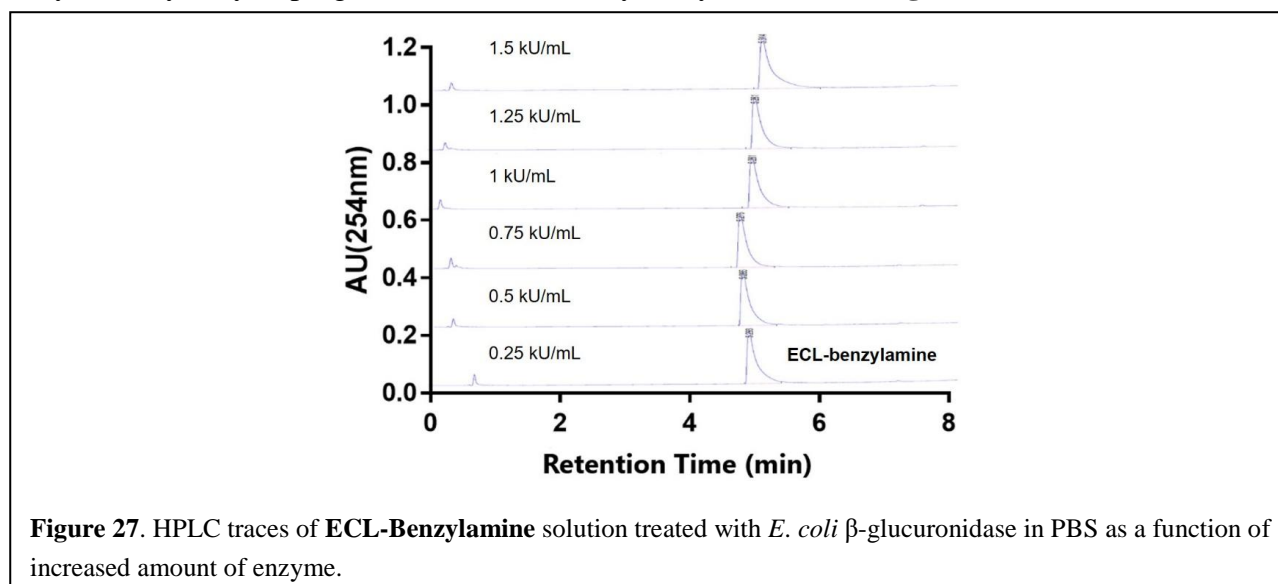


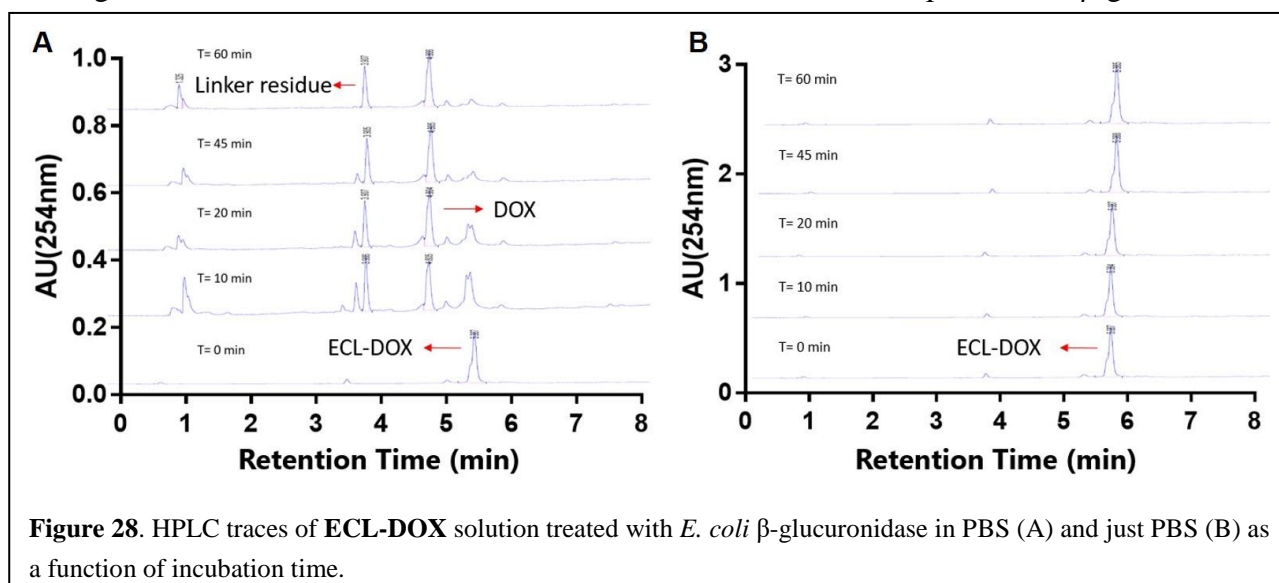
**Figure 27.** HPLC traces of **ECL-Benzylamine** solution treated with *E. coli*  $\beta$ -glucuronidase in PBS as a function of increased amount of enzyme.

**ECL-Benzylamine** was first dissolved in PBS with 3% BSA (w/v), followed by the addition of  $\beta$ -glucuronidase at the concentration of 0.25 kU/mL. After incubated at 37°C for 30 min, glycine buffer was added to the reaction mixture to quench the enzymatic reaction. Later, the reaction mixtures were analysed by analytical HPLC. However, HPLC results suggested that **ECL-Benzylamine** stayed unreacted in the presence of  $\beta$ -glucuronidase. The concentration of  $\beta$ -glucuronidase was increased gradually from 0.25 kU/mL to 1.5 kU/mL while no Benzylamine was released at any concentration of  $\beta$ -glucuronidase.

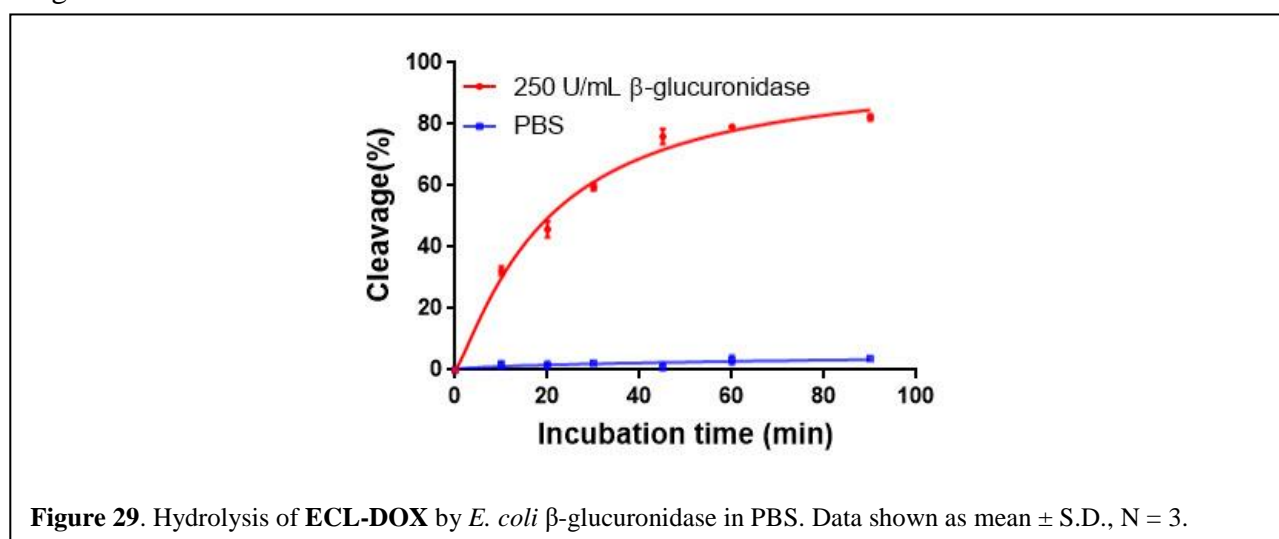
#### 4.1.5 Cleavage of ECL-DOX

We hypothesise that **ECL-Benzylamine** could not efficiently bind to  $\beta$ -glucuronidase, further resulting in the inability of cleavage of **ECL-Benzylamine**. As reported by Scott C. Jeffrey,<sup>225</sup> Monomethyl auristatin F (MMAF), MMAE, and DOX adopt a more favourable structure complementary to  $\beta$ -glucuronidase, supported by the facile release of the corresponding drug-linker

conjugate. Therefore, we proceeded the test of **ECL-DOX** with the same experimental conditions to investigate whether **ECL-DOX** could be cleaved to release DOX in the presence of  $\beta$ -glucuronidase.



Enzymatic cleavage of **ECL-DOX** was studied with the same experimental condition as aforementioned. For a 45 min-incubation with 0.25 kU/mL *E. coli*  $\beta$ -glucuronidase, HPLC traces (**Figure 28**) presented that  $\sim 79\%$  of **ECL-DOX** was cleaved and generated free DOX (Tr= 4.87 min) and linker residue (Tr= 2.97 min), indicating the high susceptibility of **ECL-DOX** to  $\beta$ -glucuronidase. Besides, HPLC traces (**Figure 28**) obtained after 90 min-incubation in PBS at 37°C demonstrated the stability of **ECL-DOX** in the absence of  $\beta$ -glucuronidase. As illustrated in **Figure 29**, **ECL-DOX** remained stable in PBS with no decomposition in comparison with  $\sim 82\%$  cleavage in the presence of  $\beta$ -glucuronidase in PBS, supporting this linker's excellent potential in the application of controlled drug release.

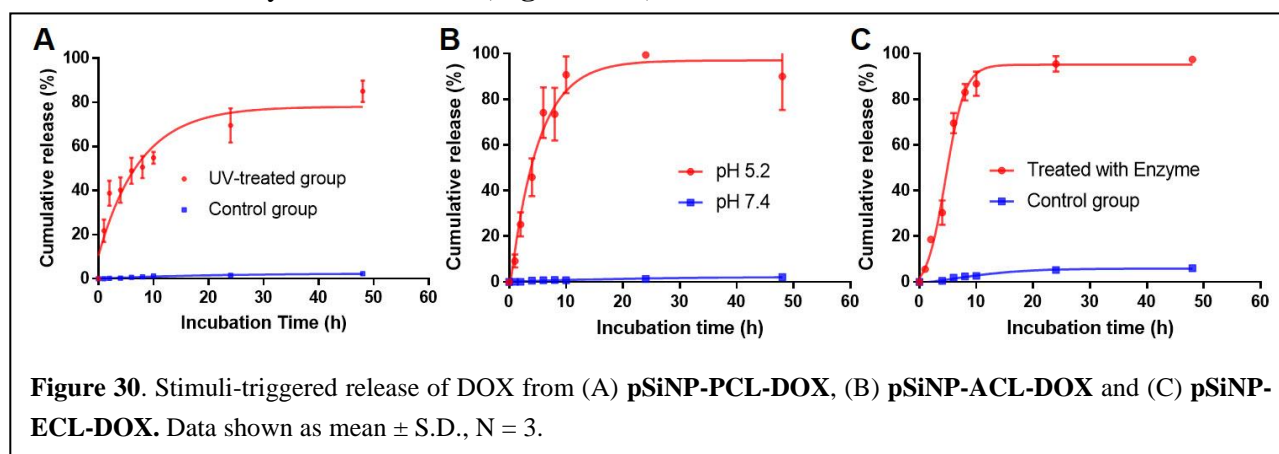


#### 4.2 DOX release from pSiNP-SCL-DOX upon exposure to corresponding stimuli

After confirming that all three SCLs showed high susceptibility to the corresponding stimuli, we further studied the DOX release from **pSiNP-PCL-DOX**, **pSiNP-ACL-DOX** and **pSiNP-ECL-DOX** through treatment with UV irradiation ( $\lambda = 400$  nm, 850 mW/cm<sup>2</sup>), sodium acetate buffer solution (pH

5.2), and  $\beta$ -glucuronidase solution (0.25 kU/mL) at the concentration of 1 mg/mL, respectively. The solution was incubated at a shaker incubator at 37°C. Samples (120  $\mu$ L) of reaction solution were taken at 0, 1, 2, 4, 6, 8, 10, 24 and 48 h post incubation and vortexed, followed by centrifugation at 27000 RCF for 10 min, to provide a supernatant, which was further analysed for the concentration of DOX in the supernatant by microplate reader ( $\lambda_{\text{ex}} = 470$  nm;  $\lambda_{\text{em}} = 595$  nm). The previously obtained drug LC from spectroscopy of each pSiNP-SCL-DOX was used as 100%.

As shown in **Figure 30A**, the release of DOX from **pSiNP-PCL-DOX** is UV dependent. Only 4% DOX was released over a 48 h-incubation in the dark. In contrast with the control group, more than 80% of DOX was released from the UV irradiated **pSiNP-PCL-DOX** during the incubation time. For **pSiNP-ACL-DOX**, the amount of released DOX reached significant levels (74%) within 8 h at pH 5.2, and gradually reached more than 90% with further incubation. While the cumulative release of DOX was only 0.8% at physiological pH, which further verified the stability of **ACL-DOX** in physiological pH and confirmed that the issue of the **ACL-DOX** release profile is caused by the HPLC column (**Figure 30B**). The release of DOX from **pSiNP-ECL-DOX** exhibited an enzyme-dependent profile, and a burst release of DOX (65%) was observed within the first 6 h of incubation with  $\beta$ -glucuronidase (0.25 kU/mL), followed by a slow but sustained release of DOX over the next 43 h (98% in total). From another perspective, only a small amount of DOX (around 6.5%) was detected in the supernatant after 48 h incubation in the absence of  $\beta$ -glucuronidase, related to the release kinetics study of **ECL-DOX** (**Figure 30C**).

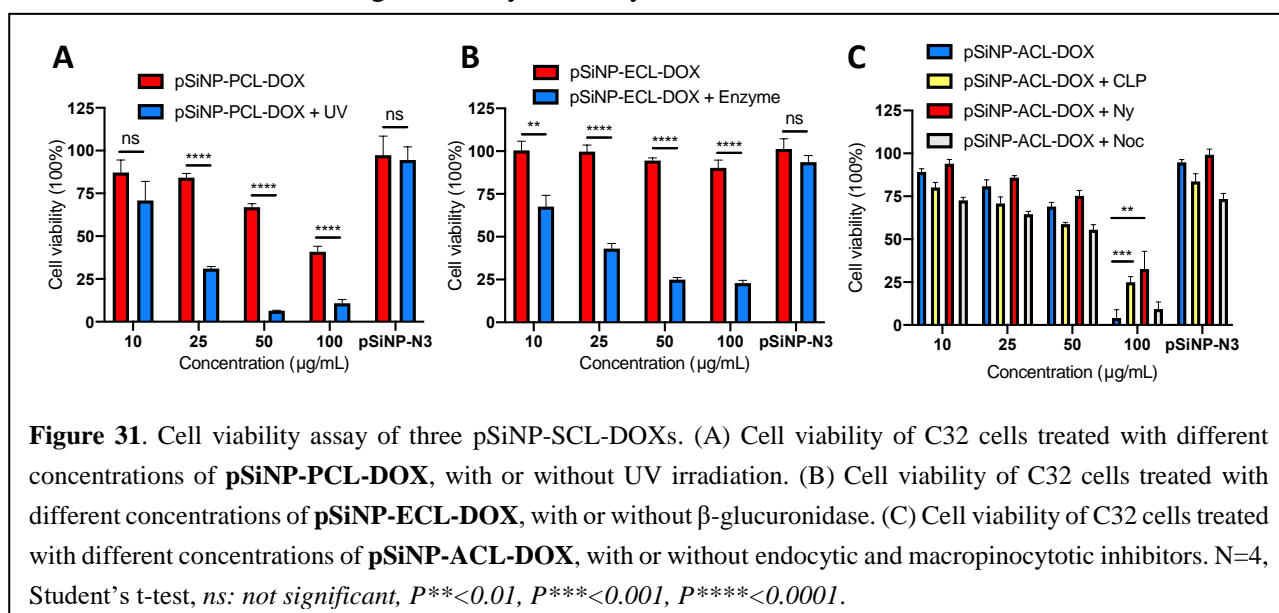


Of note, in our previous study with **pSiNP-PCL-DOX**, a certain amount of DOX (20%) was detected in the supernatant collected from the control group. After using the sterilised PBS buffer, the amount of released DOX dropped to 4%. We speculated that the old batch of PBS for experiment may be contaminated by bacteria. It contains nitroreductases capable of reducing the nitro group on the PCL to form hydroxylamine, and the latter functional group may induce the 1,4-elimination reaction to trigger the DOX release even in the absence of light.<sup>226</sup> Compared with **pSiNP-ACL-DOX** and **pSiNP-ECL-DOX**, only 80% of DOX was released from **pSiNP-PCL-DOX** after 48 h. This is probably because the poor solubility of DOX in PBS can further prevent them from escaping from the pores of pSiNPs.<sup>190</sup>

## Chapter 5.0: *In vitro* and *in vivo* test of pSiNP-SCL-DOX

### 5.1 Cytotoxicity test

We first evaluated the cytotoxicity of **pSiNP-PCL-DOX**, **pSiNP-ACL-DOX**, and **pSiNP-ECL-DOX** by employing the luminescence-based cell viability assay since pSiNP is known to interfere with the colourimetric assays such as 2,3-Bis-(2-methoxy-4-nitro-5-sulfophenyl)-2H-tetrazolium-5-carboxanilide (XTT) and Methylthiazolyldiphenyl-tetrazolium bromide (MTT) assays. Here we chose one cancer cell-line: melanoma cell-line C32, as our cell model. The viability assay showed that, without UV irradiation, **pSiNP-PCL-DOX** still induced minor cytotoxicity to this cell line. This is expected because the nitrobenzyl group in PCL is also known to be responsive to hypoxia.<sup>227</sup> However, upon the exposure of UV irradiation ( $\lambda = 400$  nm, 850 mW/cm<sup>2</sup>), the cytotoxicity of **pSiNP-PCL-DOX** increased significantly, reaching more than 90% cell killing at concentration of 50  $\mu$ g/mL. While under the same dosage of UV irradiation, **pSiNP-N<sub>3</sub>** (50  $\mu$ g/mL) did not exhibit any cytotoxicity (**Figure 31A**). Next, we evaluated the cytotoxicity of **pSiNP-ECL-DOX**. Since  $\beta$ -glucuronidase is not highly expressed in C32 cells, **pSiNP-ECL-DOX** did not induce much cell death at all concentrations (**Figure 31B**). However, the addition of exogenous  $\beta$ -glucuronidase (250 U/mL) to the cell culture induced significant cytotoxicity to C32 cells.

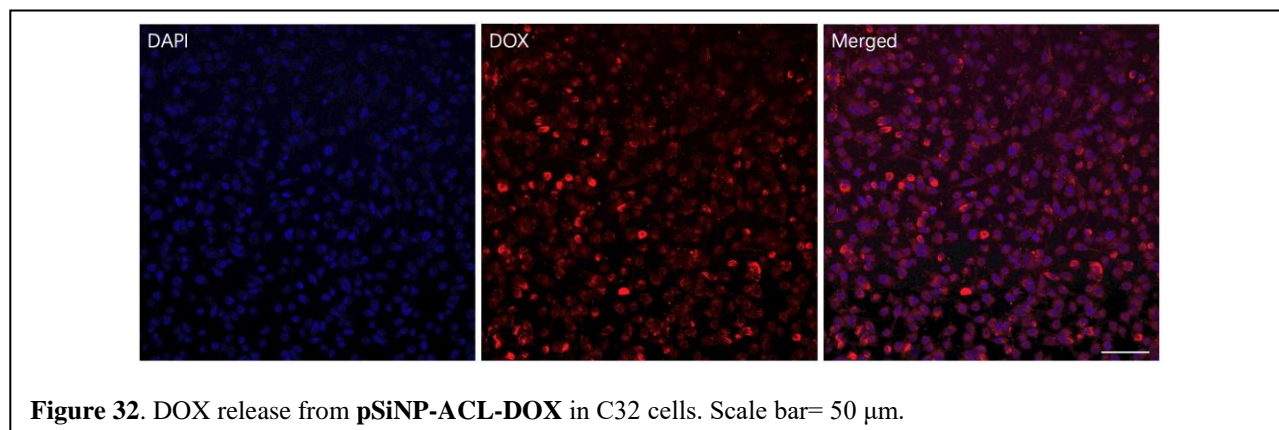


The last evaluated pSiNP-SCL-DOXs was **pSiNP-ACL-DOX**. We hypothesised that the pSiNP-SCL-DOXs entered the cells *via* the endocytosis pathway, and the pH of later endosome and lysosome is below 5.5, which will trigger the cleavage of ACL and release DOX. As expected, **pSiNP-ACL-DOX** showed high cytotoxicity to C32 and reached more than 95% cell killing at the concentration of 100  $\mu$ g/mL. To confirm the cytotoxicity was due to the cleavage of ACL during the endocytosis, we co-incubated the **pSiNP-ACL-DOX** with an array of endocytic and macropinocytotic inhibitors (**Figure 31C**). We observed that the cytotoxicity of **pSiNP-ACL-DOX** dropped significantly when co-incubated with nystatin (Ny), a caveolae-mediated endocytosis inhibitor. Chlorpromazine (CLP, clathrin-mediated endocytosis inhibitor), though not influence the activity of **pSiNP-ACL-DOX** at lower concentrations, significantly reversed the cytotoxicity of **pSiNP-ACL-DOX** at the concentration of 100  $\mu$ g/mL of the NPs. Meanwhile, nocodazole (Noc, micro-pinocytosis inhibitor)

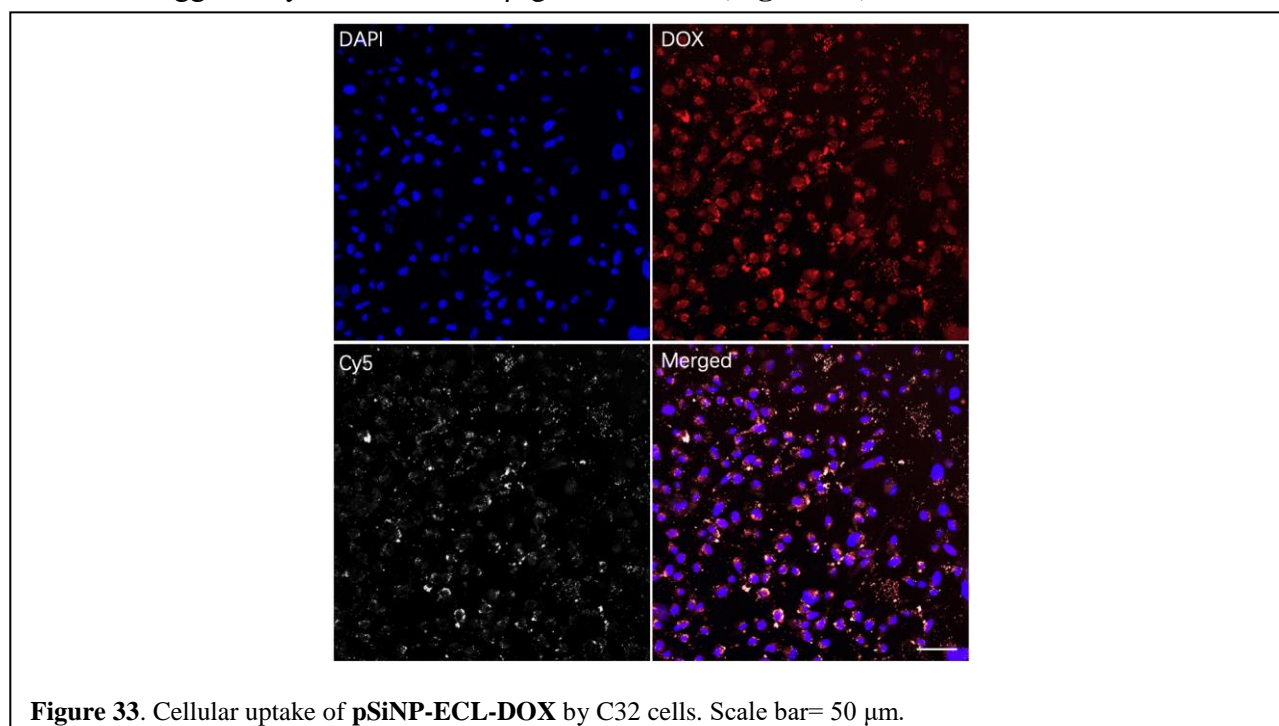
did not inhibit the activity of **pSiNP-ACL-DOX**. This result indicates that the release of DOX from **pSiNP-ACL-DOX** relied heavily on the caveolae-mediated endocytosis.

## 5.2 Cellular uptake study

To verify that the pSiNP-SCL-DOXs could enter the cells through endocytosis, accumulate and subsequently release DOX in the cells, we used confocal microscopy to monitor the cellular uptake and distribution of pSiNP. **pSiNP-ACL-DOX** was incubated for 24 h with C32 cells, followed by thorough wash of the pSiNPs. The content of released DOX in cells was virtualised *via* confocal microscopy (**Figure 32**).



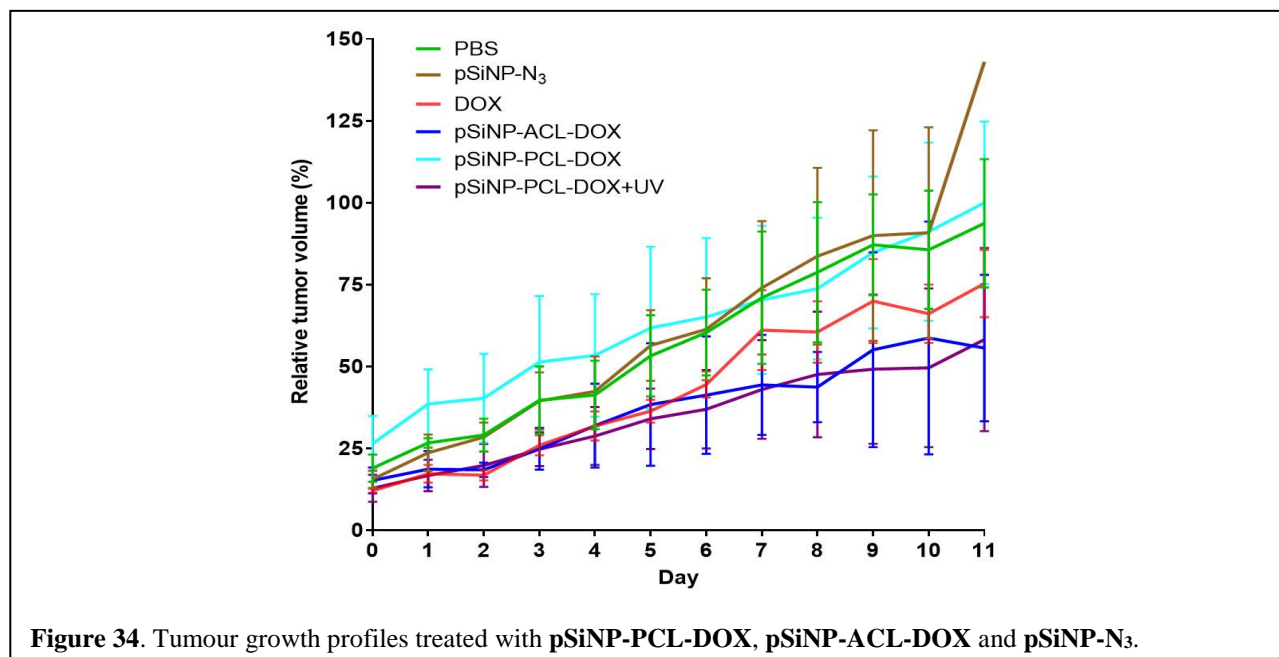
To visualise the pSiNPs under confocal microscopy, we co-labelled the **pSiNP-N<sub>3</sub>** with Cy5-alkyne and **ECL-DOX** (**Cy5-pSiNP-ECL-DOX**). After 24 h incubation of **Cy5-pSiNP-ECL-DOX** with C32, there is a considerable amount of pSiNPs observed in the cells (Cy5 channel, white). This result was closely related to above cytotoxicity assay. Besides, the release of DOX from **Cy5-pSiNP-ECL-DOX** was triggered by the addition of  $\beta$ -glucuronidase (**Figure 33**).



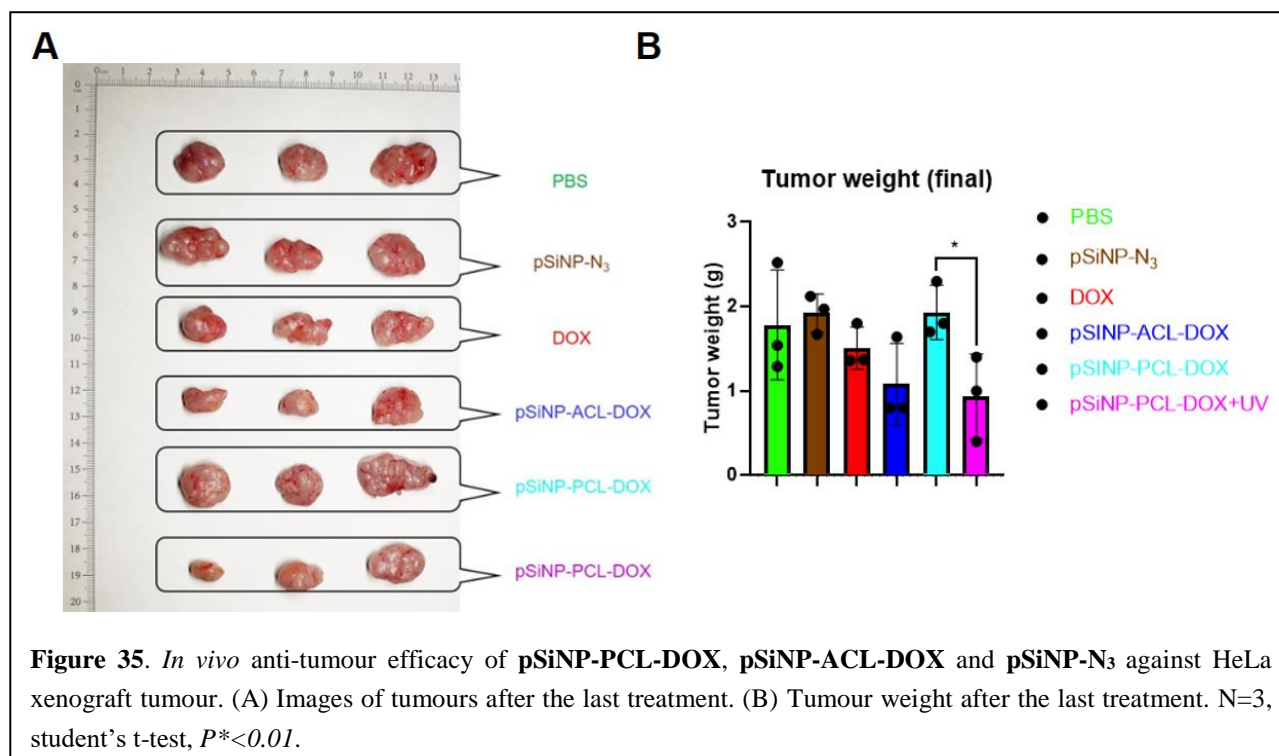
### 5.3 *In vivo* test

After the *in vitro* test using a cancer cell line, we used an *in vivo* tumour model to verify the impact of pSiNP-SCL-DOXs on inhibiting tumour growth. For the choice of tumour model, although the C32 cell line has been used for our *in vitro* test, the *in vivo* experiments were conducted by our collaborator at Northwestern Polytechnical University in China. They have successfully established mice xenograft model with HeLa cell line. Thus, the HeLa tumour model was utilised to examine the anti-tumour efficiency of **pSiNP-PCL-DOX** and **pSiNP-ACL-DOX** *in vivo*. The *in vitro* cytotoxic assay on HeLa cells is currently undergoing.

Considering that the amount of **pSiNP-ECL-DOX** is barely enough for *in vitro* test, the *in vivo* test only covered **pSiNP-PCL-DOX** and **pSiNP-ACL-DOX**. In the initial study, HeLa cell line was implanted into Balb/c nude mice, based on nude mouse tumourigenicity assay. The animals were then treated with doses of 1 mg/kg DOX or equimolar dose equivalents of **pSiNP-PCL-DOX**, **pSiNP-ACL-DOX**, **pSiNP-N<sub>3</sub>** or PBS as control. All the reagents were delivered *via* intravenous injection, and the group treated with **pSiNP-PCL-DOX** required further access to UV irradiation.



As exhibited in **Figure 34** and **Figure 35**, **pSiNP-ACL-DOX** and UV-irradiated **pSiNP-PCL-DOX** produced enhanced anti-tumour effects over DOX alone, with the 6.1 mg/kg and 7.3 mg/kg dose resulting in 50% complete responses (compared with 30% complete responses for mice treated with DOX at the same dose). The improved anti-tumour activity of these two pSiNP-SCL-DOXs should be attributed to multiple therapeutic advantages, including prolonged circulation time, enhanced tumour accumulation, improved drug LC, and efficient drug release at tumour site. The **pSiNP-ACL-DOX** and UV-irradiated **pSiNP-PCL-DOX** presented similar effects against tumour, and both of them are slightly higher than the DOX free drug, though additional data are required to confirm the significance. Notably, **pSiNP-N<sub>3</sub>** exhibited almost no tumour inhibition effect, demonstrating the excellent biocompatibility of pSiNPs.



## Chapter 6.0: Conclusion, supplementary experiment and future work

### 6.1 Conclusion

The integration of SCLs and pSiNPs has contributed to the development of pSiNP-based DDSs capable of highly controlled drug release, and this DDS had an overall higher drug LC than traditional pSiNPs. Regarding various options for SCLs, in this study, we chose UV irradiation (400 nm) as a remote trigger,  $\beta$ -glucuronidase and lower pH as cancer-related endogenous triggers. The novel pSiNP-SCL-DOXs exhibited outstanding controlled release ability both *in vitro* and *in vivo*, indicating that this SCL conjugation strategy might be amenable for the future development of pSiNP-based DDSs.

### 6.2 Supplementary experiment and future work

Since we used different cell lines for *in vitro* and *in vivo* experiments, the *in vitro* test needs to be repeated with HeLa cell line. To investigate the cellular uptake of pSiNP-SCL-DOXs in more detail, their localisation in cells was examined through confocal microscopy after incubating them with HeLa cells for 0 h, 1 h, 3 h, 6 h and 12 h. So far, the cellular uptake of pSiNP-ACL-DOX has been investigated and the result is shown in **Figure 36**. After 1 h of incubation, the faint red fluorescence from DOX was observed in the cytoplasm, indicating the primary uptake and release of DOX into cells. The fluorescence intensity of DOX increased with the incubation time, suggesting the sustained uptake of pSiNP-ACL-DOX as the time extended. With further 5 h of incubation, the fluorescence intensity further increased, indicating the consistent release of DOX from pSiNP-ACL-DOX. Due to the limited amount of time, the cellular uptake experiment of pSiNP-ECL-DOX and pSiNP-PCL-DOX is still in progress.

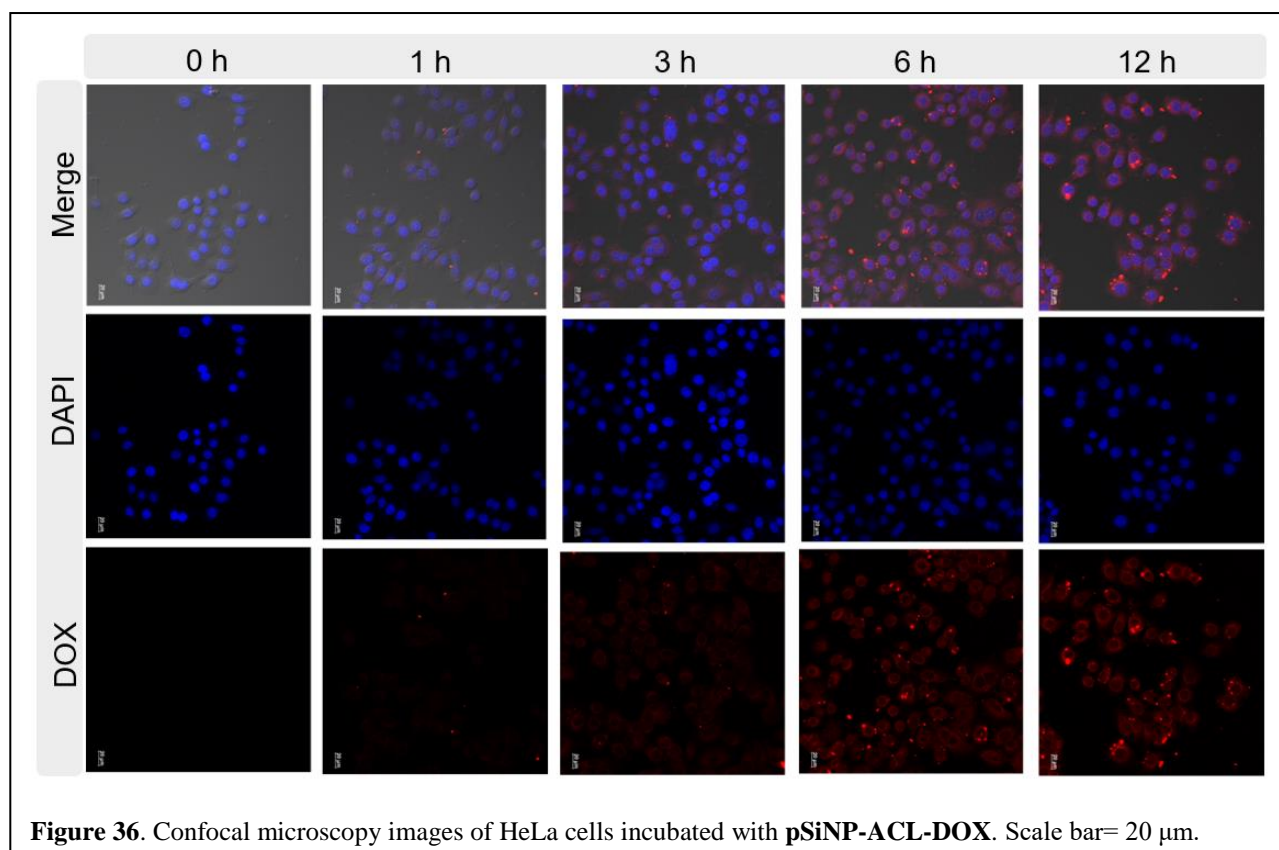
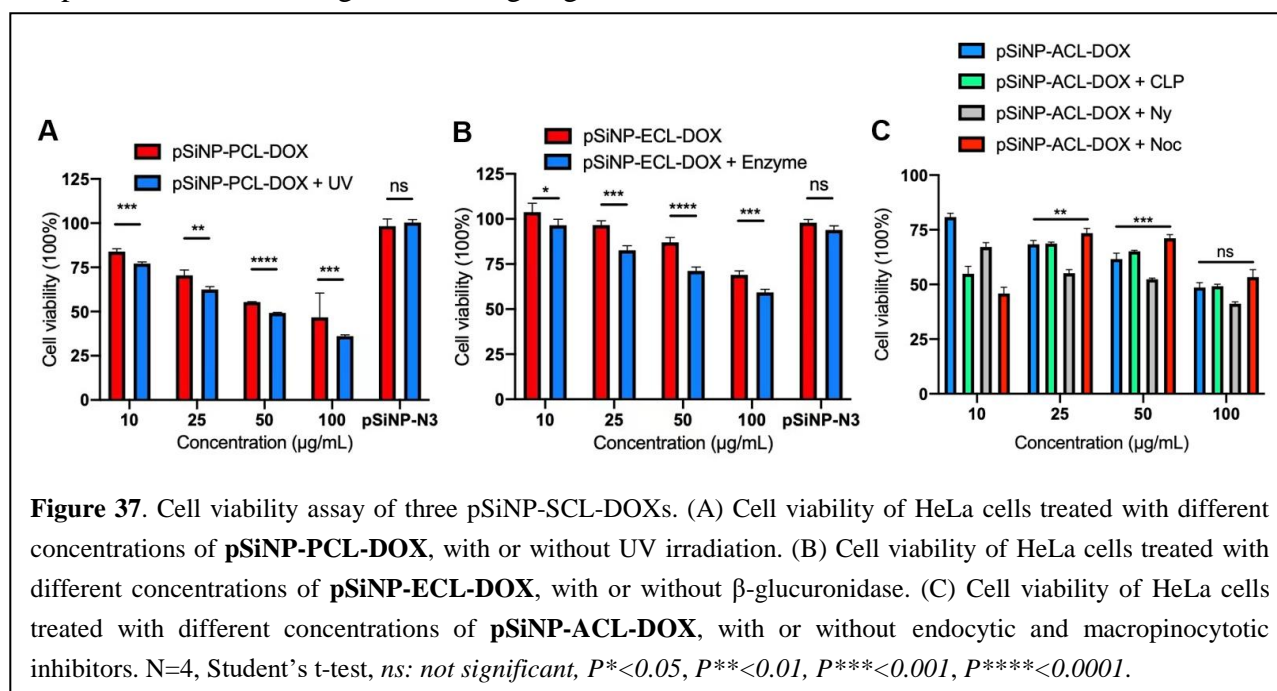


**Figure 36.** Confocal microscopy images of HeLa cells incubated with **pSiNP-ACL-DOX**. Scale bar= 20  $\mu\text{m}$ .

The cytotoxicity of pSiNP-SCL-DOXs against HeLa cells was then evaluated *via* a colorimetric assay using the CellTiter Glo<sup>®</sup> Luminescent Cell Viability Assay kit. We first investigated the influence of **pSiNP-N<sub>3</sub>** on the HeLa cell growth after incubating for 48 h. As shown in **Figure 37**, no significant cytotoxicity was found in **pSiNP-N<sub>3</sub>** at concentration of 50  $\mu\text{g}/\text{mL}$ . We next measured the cytotoxicity of **pSiNP-PCL-DOX** on the cells. As shown in **Figure 37A**, the UV-irradiated **pSiNP-PCL-DOX** exhibited significant cytotoxicity in a concentration-dependent manner. Although the **pSiNP-PCL-DOX** showed considerable cytotoxicity against HeLa cells in the absence of UV light, the UV-irradiated **pSiNP-PCL-DOX** still exhibited significantly higher cytotoxicity compared to the non-UV irradiated ones. This result corresponds to the result of our previous cytotoxicity experiment against C32 cells.

Next, we investigated the cytotoxicity of **pSiNP-ECL-DOX**. From **Figure 37B** we can see that **pSiNP-ECL-DOX** showed a moderate cytotoxicity at the concentration of 100  $\mu\text{g}/\text{mL}$ , indicating that the concentration of  $\beta$ -glucuronidase in HeLa cells was not enough to induce the DOX release. To ensure the sufficient cleavage of **ECL-DOX**, exogenous  $\beta$ -glucuronidase (250 U/mL) was added together with **pSiNP-ECL-DOX** to HeLa cells. Although the enzyme-treated **pSiNP-ECL-DOX** showed a significantly enhanced cytotoxicity compared to the non-treated ones, around 62% of the cells survived even at the concentration of 100  $\mu\text{g}/\text{mL}$ . Therefore, the limited *in vitro* efficacy of **pSiNP-ECL-DOX** prevented itself from moving to the *in vivo* test.

Finally, we examined the cytotoxicity of **pSiNP-ACL-DOX**. The cytotoxicity of **pSiNP-ACL-DOX** is also concentration-dependent, and reached 50% cell killing at the concentration of 100  $\mu\text{g/mL}$ . When incubated with Noc (micropinocytosis inhibitor), significantly lower cellular death was observed in **pSiNP-ACL-DOX** at concentrations of 25  $\mu\text{g/mL}$  and 50  $\mu\text{g/mL}$ , whereas at the concentration of 10  $\mu\text{g/mL}$  and 100  $\mu\text{g/mL}$  of **pSiNP-ACL-DOX**, Noc did not inhibit the cytotoxicity of **pSiNP-ACL-DOX**. Ny and CLP did not inhibit the activity of **pSiNP-ACL-DOX** (**Figure 37C**) at the all four concentration of NPs. Different from our previous work with C32 cells, the internalisation of **pSiNP-ACL-DOX** by HeLa cells seems to be more micropinocytosis-regulated. We plan to further investigate this intriguing effect.

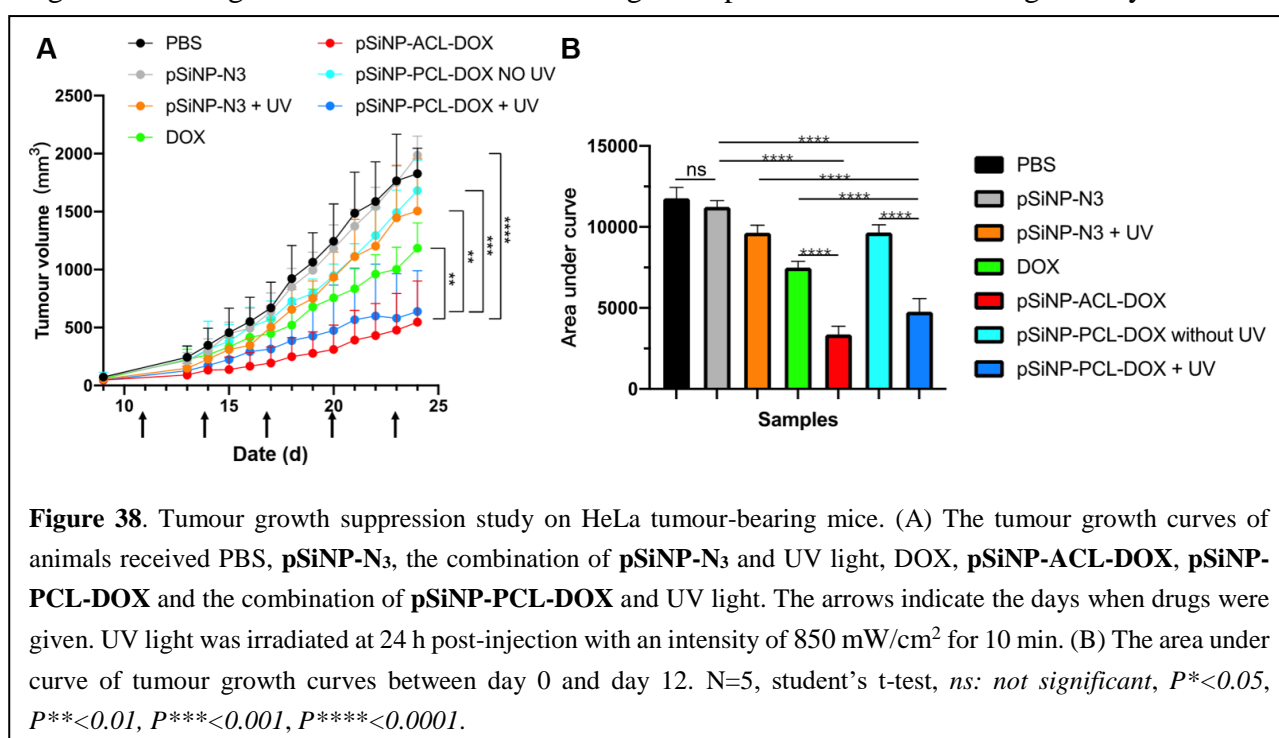


Meanwhile, the *in vivo* test was required to be repeated for several reasons. Firstly, in the initial experiment, the shape and volume gap of tumour among the mice were not well controlled. Secondly, the UV light showed certain toxicity to cancer cells, demonstrating that the anti-tumour effect of UV-irradiated **pSiNP-PCL-DOX** might take advantages of multiple therapeutic effects. In the repeated *in vivo* experiment, an extra control group was added where HeLa tumour-bearing mice were treated with **pSiNP-N<sub>3</sub>** and UV light to investigate the potential toxicity of UV light. Lastly, we increased the number of mice in each group to 5, therefore making the result more statistic sound.

As shown in **Figure 38 A and B**, DOX exhibited a moderate tumour growth inhibition compared to control groups (PBS). Notably, **pSiNP-N<sub>3</sub>** exhibited almost no tumour inhibition effect, further demonstrating that pSiNP is a biocompatible platform for drug delivery. The mice which were administrated with **pSiNP-PCL-DOX** but no UV irradiation only showed minor tumour growth inhibition, which correlated to the *in vitro* cytotoxicity. On the other hand, the group which were treated with **pSiNP-PCL-DOX** with the exposure of UV irradiation exhibited strong tumour growth inhibition, which is significantly higher than PBS, **pSiNP-N<sub>3</sub>**, as well as the UV irradiated **pSiNP-N<sub>3</sub>** control groups (**Figure 38B**). These results demonstrated that the tumour growth inhibitory activity

of **pSiNP-PCL-DOX** came from the UV triggered DOX release, rather than the photocytotoxicity from UV.

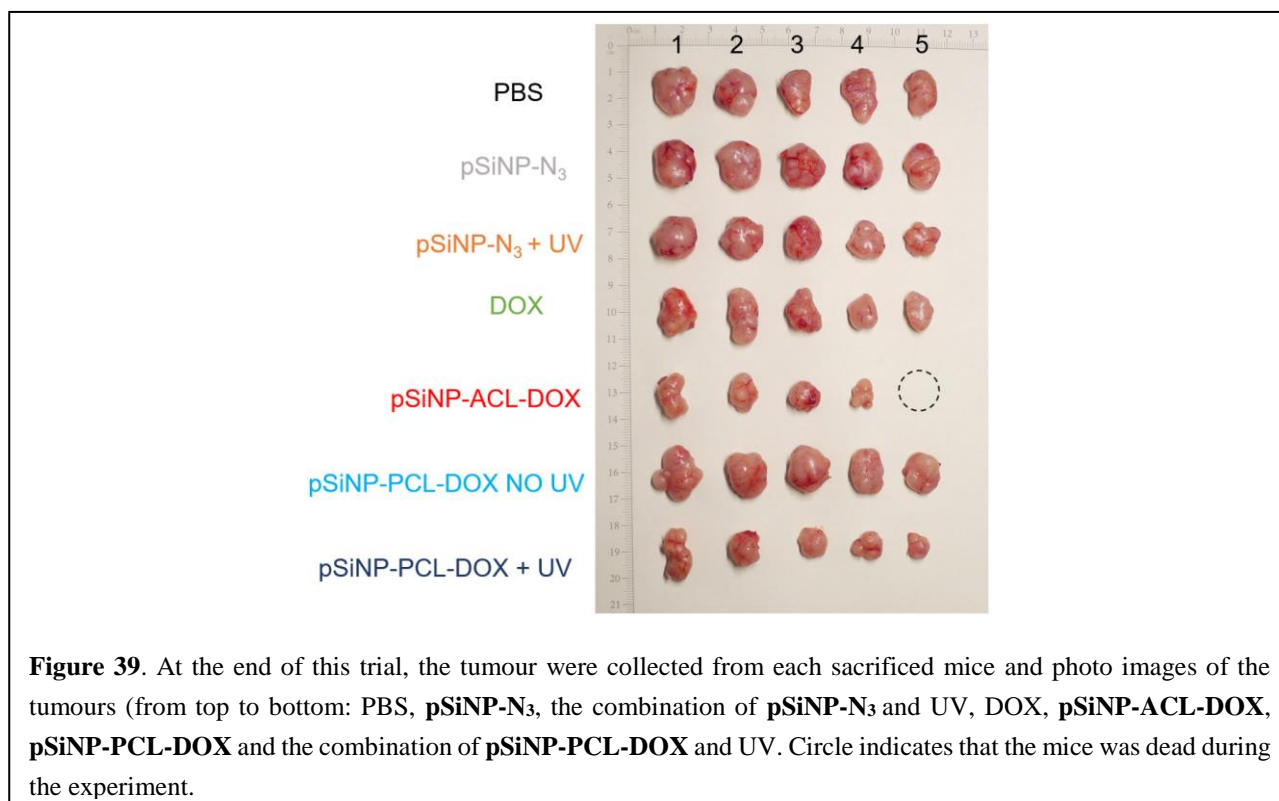
Similarly, **pSiNP-ACL-DOX** showed the strongest anti-tumour efficacy among all the formulations. The slightly higher activities of **pSiNP-ACL-DOX** over **pSiNP-PCL-DOX** may be due to the relatively low tissue penetration of UV irradiation, which resulted in non-full release of DOX. More importantly, both **pSiNP-ACL-DOX** and **pSiNP-PCL-DOX** exhibited significantly stronger tumour growth inhibitory activities than free DOX. We speculated that free DOX non-specifically distributed throughout the body due to the lack of tumour-targeting ability, leading to systemic cytotoxicity and reduced anti-tumour efficiency. While **pSiNP-PCL-DOX** and **pSiNP-ACL-DOX**, on the contrary, took advantages of the EPR effect and the highly controlled drug release ability, accumulating more cargoes to the targeted tumour site and exhibiting more potent tumour-inhibiting activity.



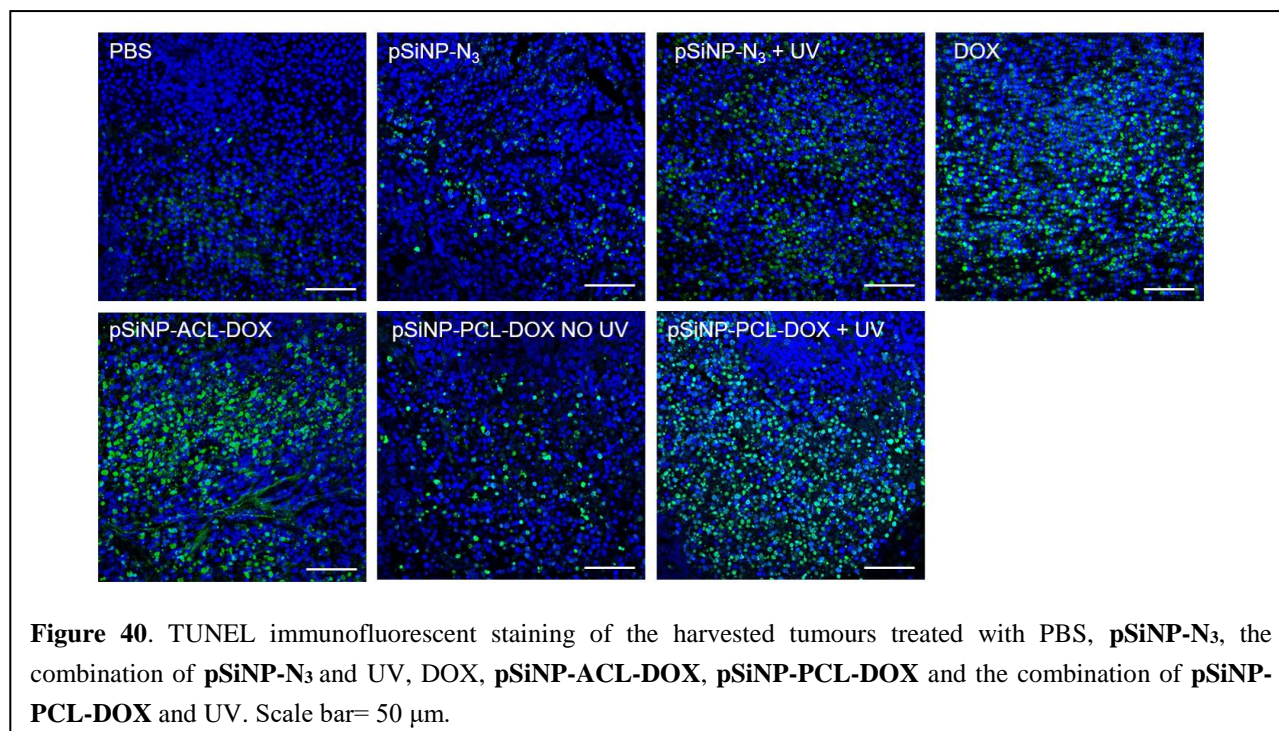
As shown in **Figure 39**, the size and shape of tumour was well controlled in the repeated *in vivo* experiment, and directly demonstrated the anti-tumour efficacy of UV-irradiated **pSiNP-PCL-DOX** and **pSiNP-ACL-DOX**.

For the histological analysis, the intravenous administration of **pSiNP-SCL-DOXs** and DOX to HeLa tumour-bearing mice at the dose of molar equivalent to 1 mg/kg of DOX was performed, and the apoptosis of tumour cells was examined by immunofluorescence staining of Terminal deoxynucleotidyl transferase dUTP nick end labeling (TUNEL), shown in **Figure 40**. TUNEL assay revealed that the highest cell apoptosis occurs in tumours from the **pSiNP-ACL-DOX** treated group, compared with PBS and **pSiNP-N<sub>3</sub>** groups where limited apoptotic cells were found. On the other hand, high levels of apoptosis was observed in the tumours harvested from mice treated with **pSiNP-PCL-DOX** + UV, while tumours in the **pSiNP-PCL-DOX** only group exhibited weak green

fluorescence, indicating slight apoptosis. Therefore, the comparison of with or without UV irradiation treatment groups verified the importance of UV light as the trigger for DOX release.

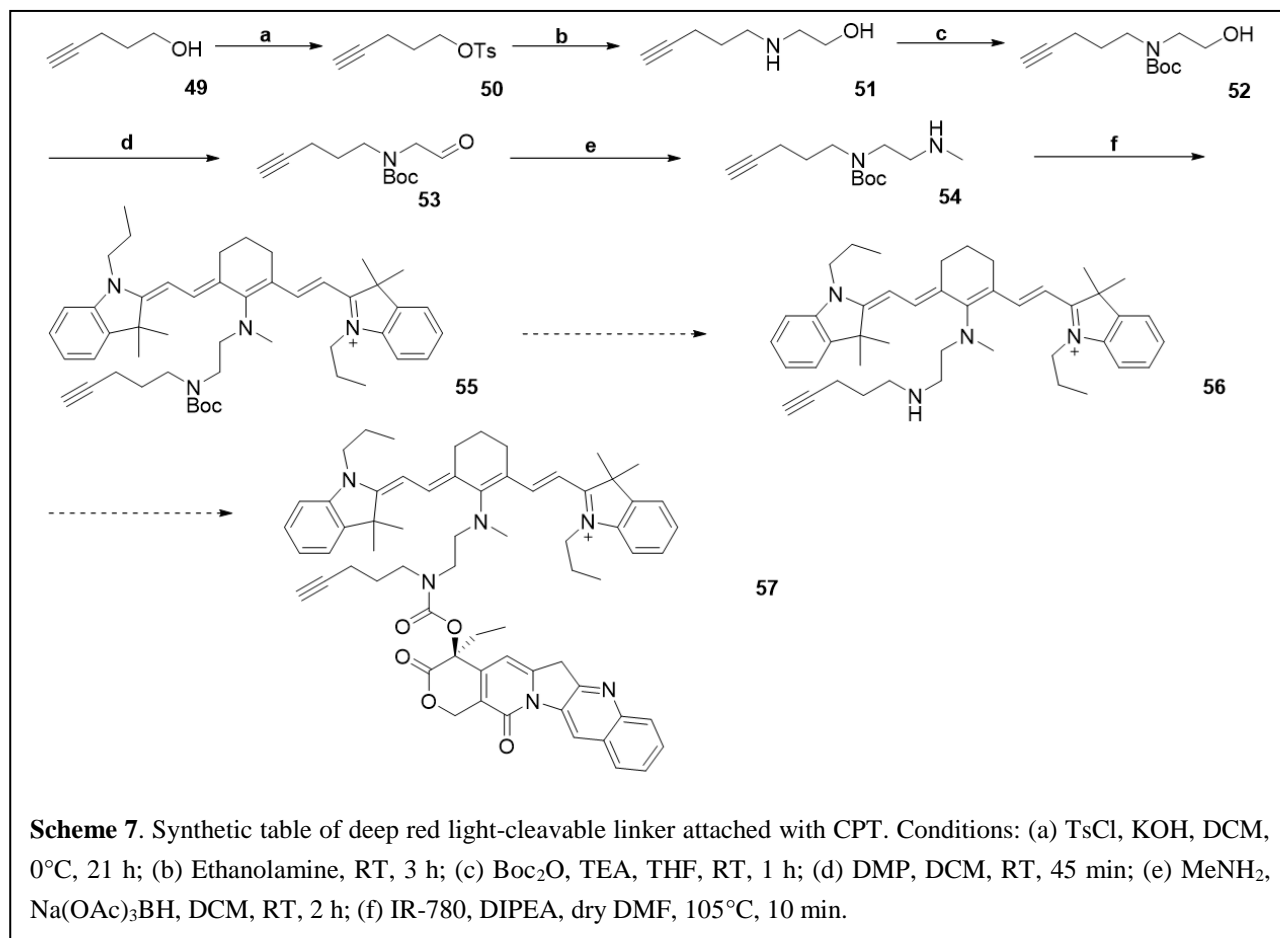


For future work, the covalent drug encapsulation strategy basically outperforms the traditional physical adsorption method in all aspects, which is based on our hypothesis. Therefore, all the three **pSiNP-SCL-DOXs** need to be analysed by TGA for their LC. As mentioned in the TGA part, the amount of **pSiNP-ECL-DOX** was only sufficient for the *in vitro* cytotoxicity test, leading to a requirement for more **ECL-DOX**. The accumulation of **ECL-DOX** is ongoing, and experiments including TGA will be performed.



Furthermore, the effect of the addition of pSiNP-SCL-DOXs can be further assessed at the gene and protein levels, and the PCR approach can be applied to study the expression of genes encoding anti-apoptotic proteins after the treatment with pSiNP-SCL-DOXs. Moreover, the proteomic analysis of HeLa cell line can reveal the expression of apoptosis-related proteins, which can be further analysed at the protein level by Western blotting.

Simultaneously, we planned to synthesise the Cy linker (**Scheme 7**) and attach a potent anti-cancer drug, CPT, to the linker. This deep red light-cleavable linker with an alkyne handle can be attached to the pSiNP-N<sub>3</sub> based on the ‘click chemistry’.



The synthesis of compound **57** started with reacting tosyl chloride with Pent-4-yn-1-ol **49**, resulting in the formation of **50**. Following the introduction of tosylate to **49**, further coupling reaction with ethanolamine was performed to afford **51**. Since the secondary amine on **51** serves as the drug attachment site, it was protected by reacting **51** with Di-tert-butyl carbonate to obtain **52**. After the protection reaction, the alcohol on **52** was oxidised to aldehyde, using Dess-Martin periodinane. The compound **53** was reacted with methanolamine to form **54**, based on a reductive amination reaction. Afterwards, the secondary amine on **54** was further reacted with commercially available IR-780 to form **55**. To date, **55** was obtained with high purity, as confirmed using LC-MS and <sup>1</sup>H NMR. Further efforts need to be made on removing the Boc group and attaching the CPT to the linker and installation of the drug-linker conjugate onto the surface of pSiNP-N<sub>3</sub>.

## Chapter 7.0: Experimental Section

### 7.1 Synthesis of test compounds general chemistry

All reactions were performed under an inert atmosphere of anhydrous N<sub>2</sub> using dry glassware. Toluene, dimethylformamide (DMF), dimethyl sulfoxide (DMSO) and dichloromethane (DCM) were obtained from a M-Braun Solvent Purification System (SPS-800 series). Starting materials used throughout this effort were purchased commercially from AK Scientific, Alfa-Aesar, Matrix Scientific, Merck and Sigma-Aldrich, unless otherwise indicated.

Thin layer chromatography (TLC) was performed using aluminium backed 0.2 mm silica gel 60 GF254 plates (Merck), and visualised by ultraviolet lamp at 254 nm. Flash column chromatography was conducted using Davisil silica gel 60 Å 40 - 63 µm. Products were either pre-adsorbed onto silica prior to column chromatography or dissolved in the appropriate solvent.

NMR spectra were routinely recorded using a Bruker Avance III Nanobay 400 MHz NMR spectrometer coupled to a BACS 60 automatic sample changer and equipped with a 5 mm PABBO BB-1H/D Z- GRD probe. NMR spectra were recorded at 401 MHz (<sup>1</sup>H NMR) and 101 MHz (<sup>13</sup>C NMR). Data acquisition and processing was managed using MestReNova v6.0.2. Chemical shifts (δ) for all <sup>1</sup>H NMR spectra were reported in parts per million (ppm) and referenced to an internal standard of residual proteo-solvents: δ 2.05 for acetone, δ 2.50 ppm for *d*<sub>6</sub>-dimethylsulfoxide (DMSO), and δ 7.26 ppm for d-chloroform (CDCl<sub>3</sub>).<sup>228</sup> The <sup>1</sup>H NMR spectra were reported as follows: chemical shift (δ), integration, multiplicity, and coupling constant (Hz). The following abbreviations were used to explain multiplicities: s= singlet, d= doublet, t= triplet, q= quartet, m= multiplet, br= broad, dd= doublet of doublets, dt= doublet of triplets. Chemical shifts (δ) for all <sup>13</sup>C NMR spectra were reported in parts per million (ppm) and referenced to an internal standard of residual proteo-solvents: δ 206.26 for acetone, δ 39.52 ppm for *d*<sub>6</sub>-dimethylsulfoxide (DMSO), and δ 77.16 ppm for d-chloroform (CDCl<sub>3</sub>).<sup>228</sup> <sup>13</sup>C NMR spectra were reported as chemical shift (δ), with signals assigned as: (CHO)= aldehyde carbon, (C=O)= carbonyl carbon, (C)= quaternary carbon, (CH)= methine carbon, (CH<sub>2</sub>)= methylene carbon and (CH<sub>3</sub>)= methyl carbon.

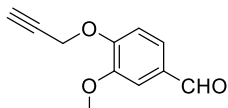
Liquid chromatography-Mass spectrometry (LC-MS) analysis was performed on an Agilent 1200 series separation module with an Agilent 6100 Quadrupole LC/MS. Reverse-phase HPLC analysis uses a Luna 5 µm C8(2) 100 Å 50 mm x 4.6 mm column. Solvent A: H<sub>2</sub>O 0.1% formic Acid; Solvent B: MeCN 0.1% formic Acid. Compounds were analysed using a gradient of 5-100% B over 10 min: 0-4 min gradient increase to 100% B, 4-7 min 100% B, 7-10 min gradient decrease to 95% A and 5% B, at a flow rate of 0.5 mL/min. Compounds were detected at 254 nm or 214 nm. System control and analysis was facilitated with Agilent Chemstation software coupled with Easy Access Software. Low Resolution Mass Spectrometry analyses were performed using a Multimode-ES and a quadrupole ion source. Acquisition and analysis were achieved using Masslynx v4.1 software. Using HPLC, compound purity was determined to be >95%.

High Resolution Mass Spectrometry analyses were performed on an Agilent 6224 time-of-flight LC-MS Mass Spectrometer coupled to an Agilent 1290 Infinity (Agilent, Palo Alto, CA). All data were acquired and reference mass corrected *via* a dual-spray electrospray ionisation (ESI) source using internal reference ions: Positive Ion Mode =  $m/z = 121.050873$  &  $922.009798$ . Each scan or data point on the Total Ion Chromatogram (TIC) is an average of 13,700 transients, producing a spectrum every second. Mass spectra were produced by averaging the scans across each peak and background subtracted against the first 10 seconds of the TIC. Acquisition was achieved using the Agilent Mass Hunter Data Acquisition software vB.05.00, and analysis performed using Mass Hunter Qualitative Analysis vB.05.00.

Analytical Reverse-Phase High Performance Liquid Chromatography was conducted on a Waters Millennium 2690 system fitted with a Phenomenex<sup>®</sup> Luna C8, 100 Å, 5 µm (50 x 4.60 mm I.D.) column. A binary solvent system was used (solvent A: 0.1% TFA, 99.9% H<sub>2</sub>O; solvent B: 0.1% TFA, 99.9% MeCN) over 10 min with a flow rate of 20 mL/min. Ultraviolet detection was at 254 nm.

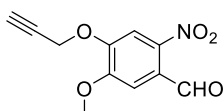
### 7.1.1 Synthesis of PCL-DOX

#### 3-methoxy-4-(prop-2-yn-1-yloxy)benzaldehyde (**30**)



Vanillin (**29**) (1.5 g, 9.86 mmol) was stirred with Cs<sub>2</sub>CO<sub>3</sub> (3.21 g, 9.86 mmol) for 5 min in dry DMF (25 mL). To the mixture was added propargyl bromide (3.74 mL, 49.3 mmol). The reaction was stirred at RT for 24 h. The reaction was then quenched with H<sub>2</sub>O (30 mL) and extracted with EA (3 x 30 mL) and back extracted with brine (3 x 80 mL). The organic layer was dried over MgSO<sub>4</sub>, filtered, and concentrated by rotatory evaporation. The resulting solution was purified *via* flash chromatography (EA: Hexane = 1:3), resulting in a white solid (1.521 g, 81%). <sup>1</sup>H NMR (400 MHz, CDCl<sub>3</sub>) δ 9.87 (s, 1H), 7.46 (dd, J = 8.2, 1.9 Hz, 1H), 7.43 (d, J = 1.8 Hz, 1H), 7.14 (d, J = 8.2 Hz, 1H), 4.86 (d, J = 2.4 Hz, 2H), 3.94 (s, 3H), 2.56 (t, J = 2.4 Hz, 1H). <sup>13</sup>C NMR (101 MHz, CDCl<sub>3</sub>) δ 190.84, 152.12, 150.05, 130.94, 126.18, 112.66, 109.54, 77.49, 76.67, 56.60, 56.01. LC-MS (ESI) calcd for [M+H]<sup>+</sup>: 191.06, found 191.0.

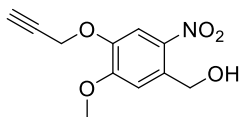
#### 5-methoxy-2-nitro-4-(prop-2-yn-1-yloxy)benzaldehyde (**31**)



A flask was charged with **30** (1.5 g, 8.00 mmol), wrapped in aluminum foil and incubated on ice. Chilled HNO<sub>3</sub> (50 mL, excess) was added to the flask and allowed to stir for 25 min at 0°C. The reaction was then warmed to RT for 2 h. The reaction was quenched with chilled H<sub>2</sub>O (100 mL) and the precipitate was collected by vacuum filtration and washed with ice H<sub>2</sub>O (3 x 30 mL). The resulting was a yellow solid (1.53 g, 82%) and required no further purification. <sup>1</sup>H NMR (400 MHz, CDCl<sub>3</sub>) δ 10.45 (s, 1H), 7.79 (s, 1H), 7.43 (s, 1H), 4.91 (d, J = 2.4 Hz, 2H), 4.02 (s, 3H), 2.63 (t, J = 2.4 Hz,

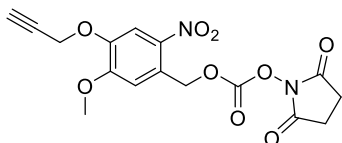
1H).  $^{13}\text{C}$  NMR (101 MHz,  $\text{CDCl}_3$ )  $\delta$  187.67, 153.75, 149.94, 143.41, 126.44, 110.28, 109.48, 76.72, 76.39, 57.25, 56.78. LC-MS (ESI) calcd for  $[\text{M}+\text{H}]^+$ : 236.05, found 236.0.

**(5-methoxy-2-nitro-4-(prop-2-yn-1-yloxy)phenyl)methanol (32)**



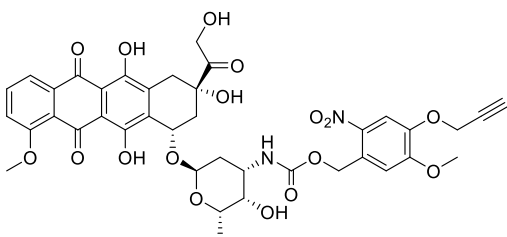
Compound **31** (1.53 g, 6.52 mmol) was dissolved in EtOH (120 mL) and wrapped in aluminum foil.  $\text{NaBH}_4$  (740 mg, 19.6 mmol) was dissolved in NaOH (50 mL, 1 M). The resulting solution was then added to **31** and allowed to stir at RT for 2.5 h. The reaction was neutralised by 1 M HCl and extracted with EA (3 x 30 mL) and back-extracted with brine (3 x 70 mL). The organic layer was dried with  $\text{MgSO}_4$  and concentrated using a rotary evaporator. The resulting compound was a pale-yellow solid (1.78 g, 76%) and required no further purification.  $^1\text{H}$  NMR (400 MHz,  $\text{CDCl}_3$ )  $\delta$  7.89 (s, 1H), 7.22 (s, 1H), 4.98 (s, 2H), 4.84 (d,  $J = 2.4$  Hz, 2H), 4.01 (s, 3H), 2.58 (t,  $J = 2.4$  Hz, 1H).  $^{13}\text{C}$  NMR (101 MHz,  $\text{CDCl}_3$ )  $\delta$  154.53, 133.36, 111.25, 76.98, 62.78, 57.11, 56.49. LC-MS (ESI) calcd for  $[\text{M}+\text{Na}]^+$ : 260.06, found 259.9.

**2,5-dioxopyrrolidin-1-yl (5-methoxy-2-nitro-4-(prop-2-yn-1-yloxy)benzyl) carbonate (34)**



To a solution of **32** (200 mg, 0.79 mmol) dissolved in MeCN (3 mL),  $\text{Et}_3\text{N}$  (151 mg, 1.5 mmol) and DSC (220 mg, 0.95 mmol) were added. After being stirred for 1.5 h under  $\text{N}_2$  at RT, TLC analysis showed that the starting material was consumed. The solvent was removed, and the residue was purified by flash column chromatography (EA: Hexane = 1:2) to provide the desired product as a light yellow solid (250 mg, 85%).  $^1\text{H}$  NMR (400 MHz,  $\text{CDCl}_3$ )  $\delta$  7.95 (s, 1H), 7.08 (s, 1H), 5.80 (d,  $J = 0.6$  Hz, 2H), 4.85 (d,  $J = 2.4$  Hz, 2H), 4.06 (s, 3H), 2.86 (s, 4H), 2.59 (s, 1H).  $^{13}\text{C}$  NMR (101 MHz,  $\text{CDCl}_3$ )  $\delta$  168.36, 154.81, 151.42, 146.11, 126.50, 111.13, 109.06, 69.09, 57.12, 56.69, 30.88, 25.46. LC-MS (ESI) calcd for  $[\text{M}+\text{Na}]^+$ : 401.07, found 400.9.

**PCL-DOX**

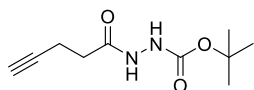


Compound **34** (10 mg, 0.026 mmol) in anhydrous DMF (3 mL), was added DOX (13 mg, 0.024 mmol) and DIPEA (6.72mg, 0.052 mmol) at RT. The reaction was stirred under an atmosphere of  $\text{N}_2$  for 1 h and LC-MS indicated full consumption of the **34** with the formation of the final product **PCL-DOX**.

Reaction mixture was diluted with EA (10 mL) and washed with H<sub>2</sub>O (3 x 10 mL) and brine (2 x 10 mL), followed by purification with silica gel flash column chromatography (DCM: MeOH = 20:1) to give the desired product as a red solid (13.6 mg, 65%). <sup>1</sup>H NMR (401 MHz, CDCl<sub>3</sub>) δ 8.02 (d, J = 7.1 Hz, 1H), 7.88-7.72 (m, 2H), 7.44-7.34 (m, 1H), 6.96 (s, 1H), 5.54-5.41 (m, 3H), 5.32-5.25 (m, 4H), 4.86-4.71 (m, 4H), 4.13 (dd, J = 14.5, 7.2 Hz, 1H), 4.07 (s, 2H), 3.94 (s, 2H), 3.69 (s, 1H), 3.48 (s, 1H), 3.25 (ddd, J = 18.6, 9.7, 1.8 Hz, 1H), 3.00 (d, J = 18.9 Hz, 1H), 2.55 (t, J = 2.3 Hz, 1H), 2.33 (d, J = 14.8 Hz, 1H), 2.17 (dd, J = 14.7, 4.0 Hz, 1H), 1.90 (dd, J = 13.3, 4.6 Hz, 1H), 1.84-1.75 (m, 1H), 1.29 (d, J = 6.6 Hz, 2H). <sup>13</sup>C NMR (101 MHz, CDCl<sub>3</sub>) δ 186.70, 161.08, 155.63, 145.67, 135.94, 135.81, 135.50, 133.58, 119.89, 118.49, 111.45, 110.97, 110.58, 100.64, 77.33, 76.61, 69.77, 69.57, 67.22, 65.55, 63.59, 62.19, 57.03, 56.68, 56.47, 53.41, 50.87, 35.63, 33.94, 30.21. HRMS (ESI) calcd for [M+Na]<sup>+</sup>: 829.22, found 829.2.

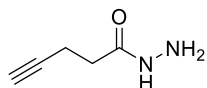
## 7.1.2 Synthesis of ACL-Vanillin and ACL-DOX

### tert-butyl 2-(pent-4-ynoyl)hydrazine-1-carboxylate (**36**)



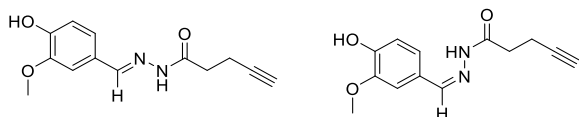
To a mixture of 4-Pentynoic acid (**35**) (49 mg, 0.5 mmol) and EDCI·HCl (115 mg, 0.6 mmol) in 5 mL of dry DCM was added HOBt (81 mg, 0.6 mmol) and the reaction was allowed to stir 30 min under N<sub>2</sub> atmosphere. Tert-butyl carbazate (66 mg, 0.5 mmol) was then added and the reaction vessel was stirred in a N<sub>2</sub> atmosphere for 18 h. The reaction was tracked *via* TLC using potassium permanganate as a TLC stain. The solvent was concentrated under vacuum to give a white solid which was purified using silica gel chromatography with a gradient of 1-5% in MeOH of a DCM: MeOH solution in increments of 100 mL to yield a pale white solid (90 mg, 85%). <sup>1</sup>H NMR (400 MHz, CDCl<sub>3</sub>) δ 7.75 (s, 1H), 6.68 (s, 1H), 2.65-2.38 (m, 5H), 1.99 (dt, J = 14.5, 2.6 Hz, 1H), 1.47 (s, 9H). <sup>13</sup>C NMR (101 MHz, CDCl<sub>3</sub>) δ 170.72 (s), 155.74 (s), 82.68 (s), 82.30 (s), 69.80 (s), 33.24 (s), 28.38 (s), 14.69 (s).

### pent-4-ynehydrazide (**37**)



To **36** (30 mg, 0.14 mmol) was added 1.5 mL of 4 N HCl in dioxane. After being stirred for 1 h at RT, TLC analysis showed the starting material was completely consumed. The solvent was removed under vacuum to yield a pale-yellow solid used without further purification. (10.5 mg, 66%).

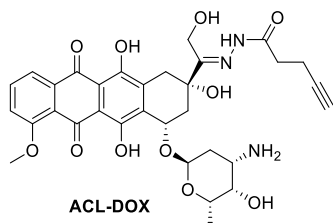
### ACL-Vanillin



Compound **37** (20 mg, 0.178 mmol) and Vanillin (27 mg, 0.178 mmol) were dissolved in 5 mL of dry EtOH in a round bottom flask at RT under N<sub>2</sub> atmosphere. The reaction was allowed to stir for 30 min, TLC analysis showed the starting material was consumed. The solvent was removed under

vacuum to form the crude product, followed by purification using prep-HPLC to yield 27 mg (62.8%) of **ACL-Vanillin**.  $^1\text{H NMR}$  (400 MHz, MeOD)  $\delta$  8.00 (s, 1H), 7.64 (d,  $J = 1.9$  Hz, 1H), 7.05 (dd,  $J = 8.2, 1.9$  Hz, 1H), 6.82 (d,  $J = 8.1$  Hz, 1H), 3.93 (s, 3H), 2.60-2.56 (m, 2H), 2.54-2.51 (m, 2H), 2.32 (t,  $J = 2.6$  Hz, 1H). LC-MS (ESI) calcd for  $[\text{M}+\text{H}]^+$ : 247.10, found 247.0.

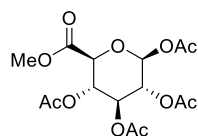
### ACL-DOX



Compound **37** (10 mg, 0.089 mmol) and  $\text{Na}_2\text{SO}_4$  (12.6 mg, 0.089 mmol) were dissolved in 5 mL of dry MeOH in a round bottom flask at RT under  $\text{N}_2$  atmosphere. To this was added DOX (48.5 mg, 0.089 mmol) and a drop of AcOH. The reaction was allowed to stir for 24 h. After the reaction was completed,  $\text{Na}_2\text{SO}_4$  was filtered out and the filtrate was concentrated under vacuum to form a red oily solid. The red solid was diluted in 5 mL of dry MeCN and the precipitate was collected by filtration and washed with dry MeCN ( $3 \times 5$  mL) to yield 45 mg (79.4%) **ACL-DOX** product.  $^1\text{H NMR}$  (400 MHz, DMSO)  $\delta$  5.86 (s, 1H), 5.51 (s, 1H), 5.43 (s, 2H), 5.33-5.25 (m, 1H), 4.95-4.90 (m, 1H), 4.59 (s, 1H), 4.43 (s, 1H), 4.13 (dd,  $J = 43.5, 6.8$  Hz, 1H), 3.97 (d,  $J = 2.6$  Hz, 3H), 3.61 (s, 1H), 3.36 (d,  $J = 11.3$  Hz, 2H), 3.03-2.88 (m, 1H), 2.80 (t,  $J = 2.4$  Hz, 1H), 2.43-2.35 (m, 4H), 2.29-2.06 (m, 2H), 1.89 (dd,  $J = 16.5, 7.9$  Hz, 1H), 1.70 (dd,  $J = 19.6, 7.7$  Hz, 1H), 1.16 (dd,  $J = 9.4, 6.6$  Hz, 3H).  $^{13}\text{C NMR}$  (101 MHz, DMSO)  $\delta$  186.97 (s), 172.65 (s), 170.31 (s), 161.24 (s), 156.88 (s), 154.74 (s), 153.88 (s), 136.71 (s), 135.26 (s), 120.51 (s), 119.46 (s), 111.11 (s), 99.48 (s), 83.98 (s), 72.60 (s), 72.26 (s), 72.12 (s), 71.38 (s), 66.76 (s), 66.46 (s), 57.08 (s), 56.55 (s), 47.06 (s), 32.29 (s), 31.18 (s), 17.30 (s), 14.16 (s), 13.45 (s). HRMS (ESI) calcd for  $[\text{M}+\text{H}]^+$ : 638.23, found 638.57.

### 7.1.3 Synthesis of ECL-Benzylamine and ECL-DOX

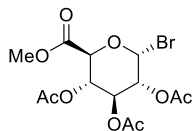
#### (2S,3R,4S,5S,6S)-6-(methoxycarbonyl)tetrahydro-2H-pyran-2,3,4,5-tetraol tetraacetate (**39**)



D-Glucurono-6,3-lactone (**38**) (5 g, 28.4 mmol) was suspended in dry MeOH (80 mL), to this  $\text{N,N}$ -dimethylethylamine (0.05 mL) was added. The reaction was stirred for 5 h until all the glucuronolactone was dissolved. The solvent was removed under reduced pressure, and the foam was used without purification. Acetic anhydride (25 mL) and pyridine (37 mL) were added and the suspension was stirred overnight. TLC indicated that the D-glucuronic acid was fully consumed and the solvent was removed under reduced pressure and recrystallised from absolute EtOH to give the title product as a white prism (3.40 g, 42%).  $^1\text{H NMR}$  (400 MHz,  $\text{CDCl}_3$ )  $\delta$  6.88 (d,  $J = 8.2$  Hz, 1H), 6.71 (d,  $J = 2.0$  Hz, 1H), 6.68-6.58 (m, 1H), 5.37-5.23 (m, 3H), 5.00 (d,  $J = 7.3$  Hz, 1H), 4.52 (s, 2H), 4.13 (dd,  $J = 14.7, 7.8$  Hz, 1H), 3.75 (d,  $J = 5.3$  Hz, 3H), 2.09-2.06 (m, 3H), 2.04 (d,  $J = 3.3$  Hz, 6H).

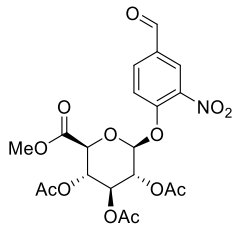
$^{13}\text{C}$  NMR (101 MHz,  $\text{CDCl}_3$ )  $\delta$  169.87, 169.38, 169.15, 168.80, 166.79, 91.36, 72.99, 71.82, 70.16, 68.91, 52.99, 20.74, 20.52, 20.44.

**(2R,3R,4S,5S,6S)-2-bromo-6-(methoxycarbonyl)tetrahydro-2H-pyran-3,4,5-triyl triacetate (40)**



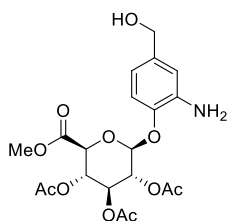
To **39** (2.0 g, 5.31 mmol) in DCM (5 mL), HBr (33% in AcOH, 8 mL) was added at  $0^\circ\text{C}$  and the reaction was stirred for additional 4 h (monitored by TLC). The reaction mixture was diluted with EA (15 mL), washed with  $\text{H}_2\text{O}$  (3 x 10 mL),  $\text{NaHCO}_3$  (2 x 10 mL),  $\text{H}_2\text{O}$  (2 x 10 mL), brine (2 x 10 mL), dried over  $\text{MgSO}_4$ , and the solvent was removed under reduced pressure. Recrystallisation of the residue from absolute EtOH gave the title compound (1.02 g, 60%) as a white solid.  $^1\text{H}$  NMR (400 MHz,  $\text{CDCl}_3$ )  $\delta$  7.27 (d,  $J = 4.0$  Hz, 1H), 6.24 (t,  $J = 9.7$  Hz, 1H), 5.87 (dd,  $J = 10.2, 9.6$  Hz, 1H), 5.48 (dd,  $J = 10.0, 4.1$  Hz, 1H), 5.21 (d,  $J = 10.3$  Hz, 1H), 4.39 (s, 3H), 2.72 (s, 3H), 2.68 (d,  $J = 2.5$  Hz, 6H).  $^{13}\text{C}$  NMR (101 MHz,  $\text{CDCl}_3$ )  $\delta$  169.38, 169.15, 168.80, 166.80, 91.38, 73.01, 71.84, 70.19, 68.93, 52.98, 20.73, 20.53, 20.43.

**(2S,3R,4S,5S,6S)-2-(4-formyl-2-nitrophenoxy)-6-(methoxycarbonyl)tetrahydro-2H-pyran-3,4,5-triyl triacetate (41)**



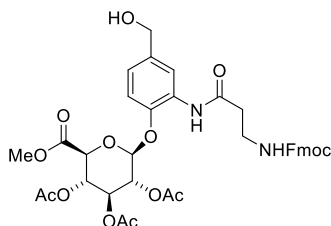
To a mixture of **40** (1.02 g, 2.57 mmol) in dry MeCN (25 mL) was added 4-Hydroxy-3-nitrobenzaldehyde (0.85 g, 5 mmol) followed by addition of  $\text{Ag}_2\text{O}$  (3.465 g, 15 mmol). The resulting slurry was stirred in the dark under  $\text{N}_2$  for 4 h. The solution passed through a pad of Celite to remove  $\text{Ag}_2\text{O}$  and the filtrate concentrated under reduced pressure. The residue was brought up in EA (20 mL) and washed with  $\text{NaHCO}_3$  (3 x 10 mL),  $\text{H}_2\text{O}$  (3 x 10 mL) and brine (2 x 10 mL). The organic layer was dried over  $\text{MgSO}_4$ , filtered and concentrated under reduced pressure to yield the title product (0.85 g, 68%).  $^1\text{H}$  NMR (400 MHz,  $\text{CDCl}_3$ )  $\delta$  9.98 (s, 1H), 8.31 (d,  $J = 2.0$  Hz, 1H), 8.09 (dd,  $J = 8.6, 2.1$  Hz, 1H), 7.50 (d,  $J = 8.6$  Hz, 1H), 5.47-5.39 (m, 2H), 5.36-5.26 (m, 2H), 4.32 (d,  $J = 8.4$  Hz, 1H), 3.71 (s, 3H), 2.13 (s, 3H), 2.08 (d,  $J = 4.0$  Hz, 6H).  $^{13}\text{C}$  NMR (101 MHz,  $\text{CDCl}_3$ )  $\delta$  188.55, 169.90, 169.23, 169.08, 166.64, 153.28, 134.23, 131.47, 126.69, 118.77, 98.56, 72.68, 70.18, 69.76, 68.12, 53.08, 20.54. LC-MS (ESI) calcd for  $[\text{M}+\text{Na}]^+$ : 506.10, found 505.9.

**(2S,3R,4S,5S,6S)-2-(2-amino-4-(hydroxymethyl)phenoxy)-6-(methoxycarbonyl)tetrahydro-2H-pyran-3,4,5-triyl triacetate (42)**



NaBH<sub>4</sub> (117.3 mg, 3.1 mmol) was added to a solution of **41** (500 mg, 1.05 mmol) in THF (20 mL) at 0°C and stirred for 2 h under N<sub>2</sub>. The solvent was removed under reduced pressure and saturated NH<sub>4</sub>Cl solution (10 mL) was added. The mixture was extracted with EA (3 x 10 mL) and the combined organic layer were washed with H<sub>2</sub>O (3 x 10 mL), brine (2 x 10 mL), and dried under reduced pressure to give the desired product as a white solid, which was subsequently re-dissolved in 12.5 mL of a mixed solution (EtOH: H<sub>2</sub>O = 4:1), followed by addition of Fe powder (1.13 g, 103.5 mmol) and HCl (3.77 mg, 0.10 mmol). The reaction was allowed to be refluxed under N<sub>2</sub> for 1 h. Removal of solvent gave a white crude product which was further purified through silica gel flash column chromatography (DCM: MeOH = 100:1) to provide the title compound (42.2 mg) in a yield of 90%. <sup>1</sup>H NMR (400 MHz, CDCl<sub>3</sub>) δ 6.90 (d, J = 8.2 Hz, 1H), 6.73 (d, J = 2.0 Hz, 1H), 6.65 (dd, J = 8.2, 2.0 Hz, 1H), 5.52 – 5.14 (m, 3H), 5.02 (d, J = 7.2 Hz, 1H), 4.55 (d, J = 5.5 Hz, 2H), 4.15 (d, J = 9.4 Hz, 1H), 3.85 (s, 2H), 3.75 (s, 3H), 2.08 (s, 3H), 2.05 (d, J = 4.2 Hz, 6H). <sup>13</sup>C NMR (101 MHz, CDCl<sub>3</sub>) δ 170.01, 169.65, 169.39, 166.83, 143.72, 137.89, 137.40, 116.66, 114.51, 100.60, 72.56, 71.68, 71.02, 69.29, 64.96, 52.98, 20.73, 20.58, 20.46. LC-MS (ESI) calcd for [M+H]<sup>+</sup>: 456.14, found 456.2.

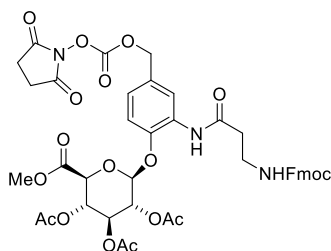
**(2S,3R,4S,5S,6S)-2-(2-(3-(((9H-fluoren-9-yl)methoxy)carbonyl)amino)propanamido)-4-(hydroxymethyl)phenoxy)-6-(methoxycarbonyl)tetrahydro-2H-pyran-3,4,5-triyl triacetate (43)**



The Fmoc-β-alanine (75 mg, 0.24 mmol) was dissolved in dry DMF (2 mL) in ice bath. To this was added HATU (92 mg, 0.24 mmol) in three times and the reaction was stirred for 0.5 h until a homogenous phase was formed. Then the mixture was added to a solution of **42** (74 mg, 0.163 mmol) in dry DMF (5 mL) dropwise at 0°C, followed by addition of DIPEA (7.37 mg, 0.33 mmol). After being stirred under N<sub>2</sub> for 2 h, the reaction mixture was diluted with EA (10 mL) and washed with H<sub>2</sub>O (2 x 10 mL) and brine (2 x 10 mL), followed by purification with silica gel flash column chromatography (DCM: MeOH = 50:1) to yield the as the title compound (85 mg, 70%). <sup>1</sup>H NMR (400 MHz, CDCl<sub>3</sub>) δ 8.35 (s, 1H), 8.07 (s, 1H), 7.75 (d, J = 7.5 Hz, 2H), 7.59 (d, J = 7.4 Hz, 2H), 7.38 (t, J = 7.4 Hz, 2H), 7.32 – 7.25 (m, 2H), 7.07 (dd, J = 8.3, 1.5 Hz, 1H), 6.94 (d, J = 8.3 Hz, 1H), 5.68 (s, 1H), 5.40 (t, J = 9.4 Hz, 1H), 5.35 – 5.23 (m, 3H), 5.04 (d, J = 7.5 Hz, 1H), 4.64 (s, 2H), 4.38

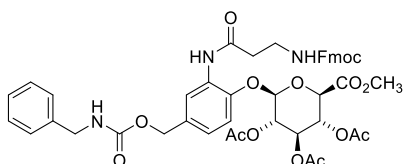
(dd,  $J = 16.2, 8.8$  Hz, 2H), 4.22 (t,  $J = 7.0$  Hz, 1H), 4.16 (d,  $J = 9.6$  Hz, 1H), 3.72 (s, 3H), 3.59 (d,  $J = 4.4$  Hz, 2H), 2.72 (s, 2H), 2.05 (t,  $J = 4.4$  Hz, 9H).  $^{13}\text{C}$  NMR (101 MHz,  $\text{CDCl}_3$ )  $\delta$  170.13, 169.81, 169.37, 166.72, 144.62, 144.03, 141.27, 137.40, 127.63, 127.04, 125.14, 122.59, 119.93, 119.56, 100.54, 72.48, 71.14, 69.21, 66.84, 64.86, 53.15, 47.24, 36.80, 20.75, 20.52, 20.43. LC-MS (ESI) calcd for  $[\text{M}+\text{Na}]^+$ : 749.25, found 748.9.

**(2S,3R,4S,5S,6S)-2-(2-(3-(((9H-fluoren-9-yl)methoxy)carbonyl)amino)propanamido)-4-(((2,5-dioxypyrrolidin-1-yl)oxy)carbonyl)oxy)methyl)phenoxy)-6-(methoxycarbonyl)tetrahydro-2H-pyran-3,4,5-triyl triacetate (44)**



Compound **43** was synthesised using the same reaction procedure of **34** using DSC (15.37 mg, 0.06 mmol),  $\text{Et}_3\text{N}$  (6.06 mg, 0.06 mmol) and dry MeCN (5 mL). The crude product **44** was purified by silica gel flash column chromatography (DCM: MeOH = 80:1). The title compound was isolated as a white solid (30.23 mg, 85%).  $^1\text{H}$  NMR (400 MHz,  $\text{CDCl}_3$ )  $\delta$  8.34 (s, 1H), 8.08 (s, 1H), 7.75 (d,  $J = 7.5$  Hz, 2H), 7.59 (d,  $J = 7.3$  Hz, 2H), 7.38 (t,  $J = 7.4$  Hz, 2H), 7.31 – 7.25 (m, 3H), 7.07 (dd,  $J = 8.3, 1.9$  Hz, 1H), 6.94 (d,  $J = 8.3$  Hz, 1H), 5.67 (s, 1H), 5.39 (d,  $J = 9.4$  Hz, 1H), 5.34 – 5.24 (m, 2H), 5.04 (d,  $J = 7.5$  Hz, 1H), 4.64 (s, 2H), 4.37 (t,  $J = 6.9$  Hz, 2H), 4.23 (d,  $J = 6.8$  Hz, 1H), 4.15 (d,  $J = 9.6$  Hz, 1H), 3.72 (s, 3H), 3.59 (d,  $J = 5.2$  Hz, 2H), 2.72 (s, 1H), 2.04 (dd,  $J = 5.8, 4.2$  Hz, 9H).  $^{13}\text{C}$  NMR (101 MHz,  $\text{CDCl}_3$ )  $\delta$  170.29 (s), 169.78 (s), 169.37 (s), 168.70 (s), 168.57 (s), 166.64 (s), 156.46 (s), 151.52 (s), 145.56 (s), 144.03 (d,  $J = 7.5$  Hz), 141.29 (s), 129.41 (d,  $J = 9.7$  Hz), 127.63 (s), 127.05 (s), 125.16 (d,  $J = 5.5$  Hz), 124.32 (s), 121.18 (s), 119.92 (s), 100.10 (s), 72.52 (s), 72.35 (s), 71.20 (s), 70.99 (s), 69.18 (s), 66.82 (s), 53.16 (s), 47.24 (s), 36.96 (s), 25.45 (s), 20.78 (s), 20.52 (s), 20.43 (s). LC-MS (ESI) calcd for  $[\text{M}+\text{H}]^+$ : 890.25, found 889.9.

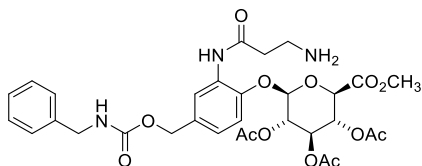
**(2R,3S,4R,5R,6R)-2-(2-(3-(((9H-fluoren-9-yl)methoxy)carbonyl)amino)propanamido)-4-(((benzylcarbamoyl)oxy)methyl)phenoxy)-6-(methoxycarbonyl)tetrahydro-2H-pyran-3,4,5-triyl triacetate (45)**



To a solution of **44** (60 mg, 0.067 mmol) in dry DMF (5 mL), benzylamine (7.3  $\mu\text{L}$ , 0.067 mmol) and DIPEA (17.5  $\mu\text{L}$ , 0.10 mmol) were added. After being stirred under  $\text{N}_2$  atmosphere, TLC analysis showed the starting material was consumed. Solvent was removed under vacuum to form a white residue which was brought up with EA (10 mL) and washed with  $\text{H}_2\text{O}$  ( $3 \times 10$  mL) and brine ( $3 \times 10$  mL). The organic layer was concentrated under vacuum to form 40 mg (67.8%) of title compound.

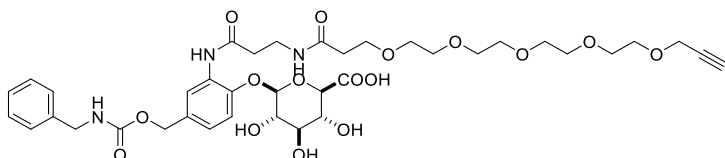
$^1\text{H}$  NMR (401 MHz,  $\text{CDCl}_3$ )  $\delta$  8.41 (s, 1H), 8.06 (s, 1H), 7.74 (d,  $J = 7.5$  Hz, 2H), 7.58 (d,  $J = 7.4$  Hz, 2H), 7.37 (t,  $J = 7.4$  Hz, 2H), 7.32 – 7.23 (m, 6H), 7.04 (d,  $J = 8.1$  Hz, 1H), 6.92 (d,  $J = 8.3$  Hz, 1H), 5.69 (s, 1H), 5.39 (d,  $J = 9.4$  Hz, 1H), 5.34 – 5.29 (m, 1H), 5.27 (d,  $J = 9.5$  Hz, 1H), 5.07 (s, 1H), 5.05 (d,  $J = 7.5$  Hz, 1H), 4.35 (d,  $J = 5.5$  Hz, 3H), 4.22 (d,  $J = 6.8$  Hz, 1H), 4.16 (d,  $J = 9.6$  Hz, 1H), 3.72 (d,  $J = 4.8$  Hz, 5H), 3.58 (d,  $J = 4.5$  Hz, 2H), 2.71 (s, 1H), 2.04 (t,  $J = 3.3$  Hz, 9H). LC-MS (ESI) calcd for  $[\text{M}+\text{Na}]^+$ : 904.3, found 904.5.

**(2R,3S,4R,5R,6R)-2-(2-(3-aminopropanamido)-4-(((benzylcarbamoyl)oxy)methyl)phenoxy)-6-(methoxycarbonyl)tetrahydro-2H-pyran-3,4,5-triyl triacetate (46)**



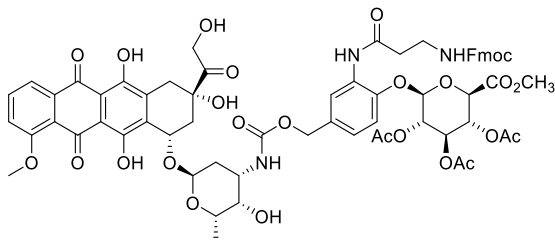
**45** (63 mg, 0.07 mmol) was dissolved in 5 mL MeOH at  $0^\circ\text{C}$ , to this reaction mixture was added a solution of LiOH (30 mg, 0.71 mmol) in  $\text{H}_2\text{O}$  (7 mL). The mixture was stirred for 35 min and neutralised with acetic acid (0.71 mmol) to pH 7. The solvent was removed to give a residue which was dissolved in DMF (5 mL) and treated with piperidine (1 mL). After being stirred for 5 min, the mixture was concentrated under vacuum to give the crude product which was purified using prep-HPLC to yield 25 mg (67.6%) of **46**, which required no further purification. LC-MS (ESI) calcd for  $[\text{M}+\text{H}]^+$ : 520.19, found 520.62.

**ECL-Benzylamine**



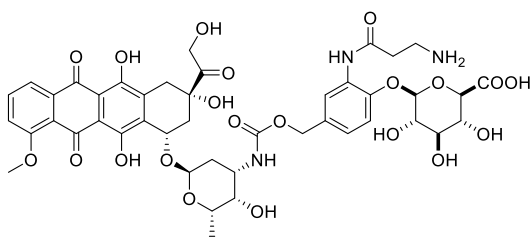
**46** (13.0 mg, 0.025 mmol) was dissolved in dry DMF (3 mL), to this was added Alkyne-PEG4-NHS ester (10 mg, 0.025 mmol) and DIPEA (8  $\mu\text{L}$ ). The reaction was allowed to stir for 1.5 h under  $\text{N}_2$  atmosphere. Removal of solvent was followed by purification on reverse phase column to form 12.65 mg (63.3%) of the **ECL-Benzylamine**.  $^1\text{H}$  NMR (400 MHz, MeOD)  $\delta$  8.21 (s, 1H), 7.46 (s, 1H), 7.34 – 7.19 (m, 6H), 7.10 (d,  $J = 8.1$  Hz, 1H), 5.05 (s, 2H), 4.30 (d,  $J = 4.5$  Hz, 2H), 4.17 (d,  $J = 2.4$  Hz, 2H), 3.70 (t,  $J = 6.0$  Hz, 3H), 3.67-3.61 (m, 6H), 3.60 (t,  $J = 2.5$  Hz, 6H), 3.58-3.56 (m, 4H), 3.55 (s, 6H), 2.84 (t,  $J = 2.4$  Hz, 1H), 2.66 (dd,  $J = 7.4, 5.3$  Hz, 2H), 2.45 (t,  $J = 5.9$  Hz, 2H). LC-MS (ESI) calcd for  $[\text{M}+\text{Na}]^+$ : 806.33, found 806.3.

**(2R,3S,4R,5R,6R)-2-(2-(3-(((9H-fluoren-9-yl)methoxy)carbonyl)amino)propanamido)-4-(((2S,3S,4S,6R)-3-hydroxy-2-methyl-6-(((1S,3S)-3,5,12-trihydroxy-3-(2-hydroxyacetyl)-10-methoxy-6,11-dioxo-1,2,3,4,6,11-hexahydrotetracen-1-yl)oxy)tetrahydro-2H-pyran-4-yl)carbamoyl)oxy)methyl)phenoxy)-6-(methoxycarbonyl)tetrahydro-2H-pyran-3,4,5-triyl triacetate (47)**

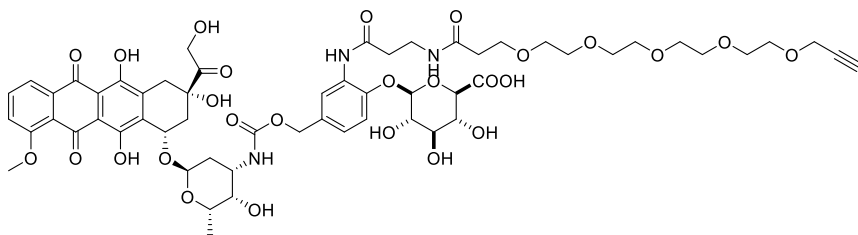


Compound **47** was synthesised using the same reaction procedure of **PCL-DOX** using DOX (23.60 mg, 0.04 mmol), DIPEA (3.30 mg, 0.05 mmol) and dry DMF (5 mL). The crude product was purified *via* prep-HPLC to give the title compound as a red solid (39.90 mg, 90%). <sup>1</sup>H NMR (400 MHz, MeOD)  $\delta$  8.14 (s, 1H), 7.99 (s, 1H), 7.86 (s, 1H), 7.72 (dd,  $J = 19.9, 7.7$  Hz, 2H), 7.57 (d,  $J = 7.1$  Hz, 1H), 7.43 (d,  $J = 8.6$  Hz, 1H), 7.31 (t,  $J = 7.4$  Hz, 1H), 7.25 – 7.18 (m, 1H), 7.03 (dd,  $J = 20.3, 8.2$  Hz, 1H), 6.80 (d,  $J = 8.0$  Hz, 1H), 5.43 (d,  $J = 7.0$  Hz, 1H), 5.31 (d,  $J = 7.5$  Hz, 1H), 5.24 – 5.11 (m, 2H), 4.76 (d,  $J = 1.8$  Hz, 1H), 4.45 – 4.24 (m, 2H), 4.15 (d,  $J = 6.6$  Hz, 1H), 3.97 (s, 1H), 3.65 (d,  $J = 9.2$  Hz, 2H), 3.54 – 3.43 (m, 1H), 3.19 – 3.00 (m, 2H), 2.62 (s, 1H), 2.39 (d,  $J = 13.2$  Hz, 1H), 2.19 (d,  $J = 9.4$  Hz, 1H), 2.00 (dd,  $J = 11.5, 4.1$  Hz, 9H), 1.79 (d,  $J = 8.9$  Hz, 1H), 1.28 (d,  $J = 6.5$  Hz, 1H). LC-MS (ESI) calcd for  $[M+Na]^+$ : 1340.40, found 1340.6.

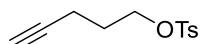
**(2R,3R,4R,5S,6R)-6-(2-(3-aminopropanamido)-4-(((2S,3S,4S,6R)-3-hydroxy-2-methyl-6-(((1S,3S)-3,5,12-trihydroxy-3-(2-hydroxyacetyl)-10-methoxy-6,11-dioxo-1,2,3,4,6,11-hexahydrotetracen-1-yl)oxy)tetrahydro-2H-pyran-4-yl)carbamoyl)oxy)methyl)phenoxy)-3,4,5-trihydroxytetrahydro-2H-pyran-2-carboxylic acid (48)**



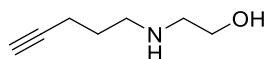
**47** (39.90 mg, 0.03 mmol) was dissolved in 5 mL MeOH at 0°C, to this reaction mixture was added a solution of LiOH (12.6 mg, 0.30 mmol) in H<sub>2</sub>O (3 mL). The mixture was stirred for 35 min and as neutralized with acetic acid (17.4  $\mu$ L, 0.3 mmol) to pH 7. The reaction mixture was concentrated under vacuum to give a residue which was dissolved in DMF (5 mL) and treated with piperidine (1 mL). After being stirred for 5 min, the mixture was concentrated under vacuum to give the crude product which was purified using prep-HPLC to yield 15 mg (52.4%) of **48** as a red solid. LC-MS (ESI) calcd for  $[M+H]^+$ : 956.29, found 956.3.

**ECL-DOX**

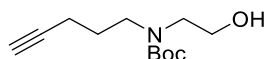
Alkyne-PEG4-NHS ester (6.5 mg, 0.016 mmol) and DIPEA (3  $\mu$ L) were added over 5 min to a solution of compound **48** (15 mg, 0.016 mmol) in dry DMF (3 mL) under  $N_2$  atmosphere. After 30 min, solvent was removed in vacuum to give out a crude product which was further purified *via* prep-HPLC, yielding 6.5 mg (32.7%) of compound **ECL-DOX** as a red solid.  $^1H$  NMR (400 MHz, DMSO)  $\delta$  9.14 (s, 1H), 8.12 (s, 1H), 8.01 (s, 1H), 7.94 (s, 1H), 7.70 (dd,  $J = 14.8, 3.5$  Hz, 1H), 7.07 (d,  $J = 8.1$  Hz, 1H), 6.99 (d,  $J = 8.0$  Hz, 1H), 6.83 (d,  $J = 7.9$  Hz, 1H), 5.73 (s, 1H), 5.49 (s, 1H), 5.36 -5.30 (m, 1H), 5.20 (d,  $J = 24.5$  Hz, 1H), 4.97 (s, 1H), 4.86 (d,  $J = 11.4$  Hz, 1H), 4.74-4.65 (m, 1H), 4.58 (d,  $J = 4.7$  Hz, 1H), 4.24 (dd,  $J = 20.8, 4.2$  Hz, 1H), 4.14 (d,  $J = 2.4$  Hz, 2H), 4.00 (s, 2H), 3.71 (d,  $J = 13.1$  Hz, 1H), 3.64 (d,  $J = 4.2$  Hz, 1H), 3.58 (d,  $J = 4.4$  Hz, 2H), 3.57 – 3.44 (m, 14H), 3.18 (s, 1H), 3.00 (s, 1H), 2.47-2.39 (m, 1H), 2.30 (t,  $J = 6.4$  Hz, 2H), 2.21-2.09 (m, 1H), 1.99 (d,  $J = 6.2$  Hz, 1H), 1.84 (dd,  $J = 12.8, 9.0$  Hz, 1H), 1.13 (d,  $J = 6.5$  Hz, 2H). HRMS (ESI) calcd for  $[M+Na]^+$ : 1264.43, found 1264.4.

**7.1.4 Synthesis of deep red light-cleavable linker****pent-4-yn-1-yl 4-methylbenzenesulfonate (50)**

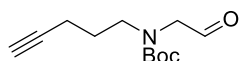
To a solution of 4-Pentyn-1-ol (**49**) (0.421 g, 5.0 mmol) and TsCl (1.14 g, 6.0 mmol) in DCM at 0°C was added KOH (1.12 g, 20 mmol) as a solid portionwise. The reaction was stirred, allowing to warm to RT, for 21 h. DCM (20 mL) and  $H_2O$  (30 mL) were added. After separation of the organic phase, the aqueous phase was further extracted with DCM ( $2 \times 15$  mL). The combined organic phases were washed with brine (20 mL), dried over  $MgSO_4$  and the solvent removed in vacuum to give the title compound as a colourless oil (1.15 g, 97%).  $^1H$  NMR (400 MHz,  $CDCl_3$ )  $\delta$ : 7.80 (d,  $J = 8.3$ , 2H), 7.35 (d,  $J = 8.0$ , 2H), 4.15 (t,  $J = 6.1$ , 2H), 2.45 (s, 3H), 2.26 (td,  $J = 6.9, 2.7$  Hz, 2H), 1.89-1.83 (m, 3H).  $^{13}C$  NMR (101 MHz,  $CDCl_3$ )  $\delta$ : 144.9, 133.2, 130.0, 128.1, 82.3, 69.6, 68.9, 27.9, 21.8, 14.9.

**2-(pent-4-yn-1-ylamino)ethan-1-ol (51)**

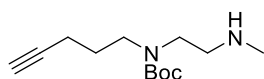
A round bottom flask was charged with **50** (10 g, 42 mmol) and immersed in a RT water bath. Ethanolamine (15 mL, 248 mmol) was added slowly in one portion and the reaction was stirred neat for 3 h at RT. The reaction was then diluted with  $H_2O$  (100 mL) and brine (100 mL) and extracted with diethyl ether (10 x 75 mL). The combined organic layers were dried over  $MgSO_4$ , filtered, and concentrated to afford 5 g of crude **51** (80%), which was used directly in the next step.

**tert-butyl (2-hydroxyethyl)(pent-4-yn-1-yl)carbamate (52)**

To a solution of crude **51** (5 g, 35 mmol) in THF (10 mL) under N<sub>2</sub> was added TEA (9.7 mL, 70 mmol) and di-*t*-butyl dicarbonate (8.4 g, 39 mmol) in succession. Vigorous gas evolution occurred for 10 s immediately after Boc<sub>2</sub>O addition, and the resulting clear yellow solution was stirred for 1 h at RT thereafter. After concentration of the solvent in vacuum, the crude oil was purified by silica gel chromatography with a gradient of 0-10% in MeOH of a DCM: MeOH solution in increments of 100 mL to afford **52** (3.0 g, 32%) as a colorless oil. <sup>1</sup>H NMR (CDCl<sub>3</sub>, 400 MHz) δ 3.74 (q, J = 5.0 Hz, 2H), 3.46-3.36 (m, 2H), 3.33 (t, J = 7.2 Hz, 2H), 3.17 (s, 1H), 2.20 (td, J = 7.0, 2.7 Hz, 2H), 1.96 (t, J = 2.7 Hz, 1H), 1.83 – 1.69 (m, 2H), 1.46 (s, 9H); <sup>13</sup>C NMR (CDCl<sub>3</sub>, 100 MHz) δ 157.4, 83.5, 80.3, 68.8, 62.6, 50.4, 47.7, 28.4, 27.4, 15.9.

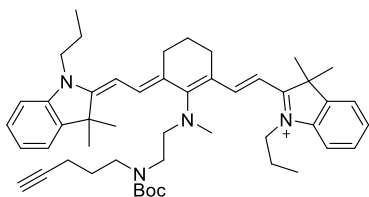
**tert-butyl (2-oxoethyl)(pent-4-yn-1-yl)carbamate (53)**

To a solution of **52** (400 mg, 1.76 mmol) in DCM (9 mL) was added Dess-Martin periodinane (780 mg, 1.85 mmol). The hazy light yellow solution was stirred at RT for 45 min. The reaction was diluted with EA (50 mL), and the organic layer was washed with saturated aqueous Na<sub>2</sub>S<sub>2</sub>O<sub>3</sub> (2 x 5 mL), saturated aqueous NaHCO<sub>3</sub>, and brine. The organic layer was dried over MgSO<sub>4</sub>, filtered, and concentrated in vacuo to afford (370 mg, 93%) as a colorless oil. <sup>1</sup>H NMR (CDCl<sub>3</sub>, 400 MHz) δ 9.59 (s, 1H), 4.04-3.82 (m, 2H), 3.46-3.31 (m, 2H), 2.30-2.16 (m, 2H), 1.97 (t, J = 2.7 Hz, 1H), 1.82 -1.68 (m, 2H), 1.52-1.39 (m, 9H); <sup>13</sup>C NMR (CDCl<sub>3</sub>, 100 MHz) δ 198.8, 155.4, 83.3, 80.8, 69.0, 57.8, 47.8, 28.3, 27.4, 15.8.

**tert-butyl (2-(methylamino)ethyl)(pent-4-yn-1-yl)carbamate (54)**

To a solution of **53** (190 mg, 0.84 mmol) in DCM (10 mL) was added methylamine (420 μL, 3.38 mmol, 33 wt% in EtOH) in one portion at rt. The orange/brown solution was stirred at RT for 10 min. Sodium triacetoxyborohydride (267 mg, 1.27 mmol) solid was charged in one portion, and the hazy brown mixture was stirred for 2 h. The mixture was diluted with DCM (100 mL) and washed with 1 M NaOH (30 mL). The organic layer was washed with brine, dried over MgSO<sub>4</sub>, and filtered. The volatiles were concentrated in vacuo and the brown residue was purified by silica gel chromatography (0-20% MeOH/DCM with 1% Et<sub>3</sub>N) to afford the title compound (101 mg, 50%) as a colorless oil. <sup>1</sup>H NMR (CDCl<sub>3</sub>, 500 MHz) δ 3.43-3.19 (m, 4H), 2.83-2.65 (m, 2H), 2.45 (s, 3H), 2.18 (td, J = 7.0, 2.7 Hz, 2H), 1.95 (t, J = 2.7 Hz, 1H), 1.79-1.66 (m, 2H), 1.44 (s, 9H); <sup>13</sup>C NMR (CDCl<sub>3</sub>, 125 MHz) δ 155.7, 83.6, 79.7, 68.8, 50.2, 46.9, 46.8, 36.1, 28.4, 27.4, 15.9.

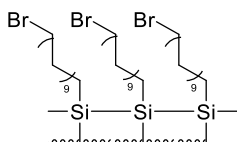
**2-((E)-2-((E)-2-((2-((tert-butoxycarbonyl)(pent-4-yn-1-yl)amino)ethyl)(methyl)amino)-3-(2-((E)-3,3-dimethyl-1-propylindolin-2-ylidene)ethylidene)cyclohex-1-en-1-yl)vinyl)-3,3-dimethyl-1-propyl-3H-indol-1-ium (55)**



To a solution of IR-780 (81 mg, 0.097 mmol) in DMF (0.9 mL) was added **54** (70 mg, 0.29 mmol) and DIPEA (67  $\mu$ L, 0.39 mmol). The green solution was sparged with N<sub>2</sub> for 5 min, then heated to 105 °C in a sealed vial for 50 min. LC-MS analysis of the dark blue reaction showed complete consumption of IR-780. The reaction was cooled to 30°C and charged with 4-(trifluoromethyl)-benzyl bromide (45  $\mu$ L, 0.29 mmol) and DIPEA (33  $\mu$ L, 0.19 mmol). After 2 h, LC-MS analysis showed complete consumption of the remaining portion of **54**. The reaction was diluted with saturated aqueous NaHCO<sub>3</sub> (10 mL), H<sub>2</sub>O (5 mL), and MeCN (0.5 mL), and stirred for 20 min at RT. The entire mixture was loaded directly onto a pre-packed 50 g C18 column and purified by reversed-phase chromatography (5-45% MeCN/H<sub>2</sub>O). The solvent was removed in vacuo to afford **55** (76 mg, 81% yield) as a dark blue solid. <sup>1</sup>H NMR (CD<sub>3</sub>OD, 400 MHz)  $\delta$  7.71 (d, J = 13.4 Hz, 2H), 7.44-7.28 (m, 4H), 7.23-7.09 (m, 4H), 6.00 (d, J = 13.4 Hz, 2H), 4.15-3.96 (m, 4H), 3.92- 3.81 (m, 2H), 3.60-3.51 (m, 2H), 3.45 (s, 3H), 3.37-3.32 (m, 2H), 2.93-2.83 (m, 4H), 2.65-2.50 (m, 4H), 2.26-2.14 (m, 3H), 2.04-1.90 (m, 8H), 1.91-1.83 (m, 2H), 1.80-1.71 (m, 2H), 1.68 (s, 12H), 1.43 (s, 9H). LC-MS (ESI) calcd for [M]<sup>+</sup>: 743.53, found 743.5.

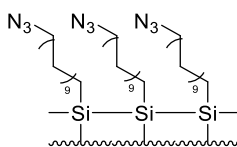
## 7.2 Surface functionalisation of pSiNPs

### pSiNP-Br



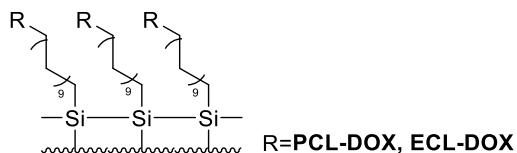
N<sub>2</sub> was bubbled through 11-Bromo-1-undecene (5 mL) for 20 min to remove all trace oxygen and H<sub>2</sub>O from the system. Freshly etched pSiNP (4 mg) was then added to the solution and the reaction mixture was allowed to be refluxed at 95°C under N<sub>2</sub>. After 24 h, the pSiNPs were collected by centrifugation, and washed with DMF twice in order to afford **pSiNP-Br**.

### pSiNP-N<sub>3</sub>



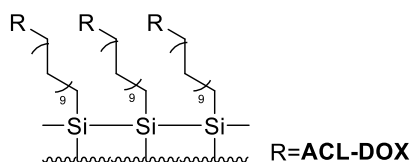
To the **pSiNP-Br** (4 mg) in DMF (5 mL) was added NaN<sub>3</sub> (30 mg, 10% in DMF, excess) and the resulting slurry was allowed to stir for 24 h at 60°C. After 24 h, the pSiNPs were washed with deionised H<sub>2</sub>O three times to eliminate the excess NaN<sub>3</sub>, affording **pSiNP-N<sub>3</sub>**.

## pSiNP-PCL-DOX and pSiNP-ECL-DOX



2.4 mg of **pSiNP-N<sub>3</sub>** was dispersed in 1.5 mL of a 1:1 DMSO: H<sub>2</sub>O solution, followed by addition of a premixed solution of CuSO<sub>4</sub> (50 μL, 1 mM), THPTA (5 μL, 60 mM) and sodium ascorbate solution (25 μL, 100 mM). **PCL-DOX** (62 μL, 10 mg/mL in DMSO) or **ECL-DOX** (95 μL, 10 mg/mL in DMSO) was added to the reaction mixture and the reaction proceeded for 24 h or 48 h. The pSiNPs were collected by centrifugation and washed with H<sub>2</sub>O (1.5 mL × 1) and DMSO (1.5 mL × 2) to eliminate the catalysts and unreacted **PCL-DOX/ECL-DOX**, and afford the product **pSiNP-PCL-DOX/pSiNP-ECL-DOX**.

## pSiNP-ACL-DOX



CuSO<sub>4</sub> (50 μL, 1 mM), THPTA (5 μL, 60 mM) and sodium ascorbate solution (50 μL, 100 mM) was mixed, the mixture and a drop of DIPEA was then added to **ACL-DOX** (49 μL, 10 mg/mL in DMSO) and **pSiNP-N<sub>3</sub>** (2.8 mg) in 1.5 mL of a 1:1 DMSO: H<sub>2</sub>O solution. After 15 min, a fresh solution of sodium ascorbate (50 μL, 100 mM) was added to the reaction mixture and the reaction proceeded for another 15 min. The pSiNPs were centrifuged and washed immediately with DMSO twice to afford the product **pSiNP-ACL-DOX**.

## 7.3 Biological assays

### 7.3.1 C32 cell viability assays

#### *Routine cell culture.*

C32 melanoma cell lines were cultured in DMEM (containing 10% fetal calf serum and penicillin–streptomycin). A frozen aliquot of cells was resuspended in 5 mL of warm media and centrifuged for 5 min at 200 xg. The supernatant was aspirated and the cell pellet resuspended in 5 mL media. Cells were then grown in tissue culture flasks at 37°C with 5% CO<sub>2</sub> and passaged with 80–90% confluent four times before use.

#### *Plating.*

Cells were then incubated for 5 min with Trypsin to separate from cell culture flasks, and enzymatic activity quenched using an equal volume of serum containing media. The cell suspension was then centrifuged at 200 xg for 5 min and the pellet resuspended in 5 mL of media. Cells were exposed to Trypan blue (excludes dead cells) and counted with a hemocytometer. Before treatment with drug compounds, cells were plated at 2,500 cells/well in 96-well plates and incubated at 37°C with 5% CO<sub>2</sub> in a humidified incubator for 24 h. Cells were only plated in columns 3-10 and rows C-F to

ensure uniform humidity and warmth across all wells. The remaining wells were filled with 100  $\mu$ L of phosphate buffered saline.

#### *Nanoparticle treatment.*

pSiNP-SCL-DOX stock solutions (50 mg/mL) were diluted  $\times$  1000 in media to a final concentration of 100  $\mu$ g/mL with an EtOH vehicle concentration of 0.2%. Compounds were then serially diluted in media (containing 0.2% EtOH) to give 4 final concentrations. Cell culture supernatants were aspirated and replaced with pSiNP-SCL-DOX containing media. Nanoparticle treatments were performed in quadruplicate wells, while potential plate layout-specific variation in cell growth was accounted for by addition of a vehicle control (0.2% EtOH). An untreated control (media only) was included in each assay. Cells were then incubated with drug compounds at 37°C with 5% CO<sub>2</sub> in a humidified incubator for 48 h prior to the viability assay.

#### *Cell viability assay.*

Cell media was diluted with CellTiter Glo® Luminescent Cell Viability Assay kit (Promega, Cat # G7570) according to manufacturer's instructions. 25  $\mu$ L of CellTiter-Glo® Reagent was directly added to each well of a 384-well plate. The contents were mixed for 2 minutes on an orbital shaker to induce cell lysis. The luminescence was read *via* a microplate reader after a 10-min stabilisation of signal in dark.

#### *Data analysis.*

When analysing data, background absorbance (taken from cell-free control wells) was subtracted from each reading. To determine percentage inhibition of cell viability, absorbance readings for each drug treatment were expressed as a fraction of the vehicle control (0.2% EtOH) readings. For each drug concentration, the mean ( $\pm$  SEM) was calculated and graphed using GraphPad Prism (Version 5). A sigmoidal curve was then fitted to the data and used to calculate the IC<sub>50</sub> of each compound.

### **7.3.2 *In vivo* test**

The HeLa xenograft tumour was allowed to grow on bilateral scapular region of Balb/c nude mice, when the tumour sizes reached about 250-300 mm<sup>3</sup>, the mice were divided into 5 groups and treated with **pSiNP-ACL-DOX** (6.1 mg/kg), **pSiNP-PCL-DOX** (7.3 mg/kg), DOX (1 mg/kg), **pSiNP-N<sub>3</sub>** (4 mg/kg) and PBS respectively through intravenous injection. Treatments were performed on day 0, 3, 6 and 9. For mice treated with **pSiNP-PCL-DOX**, the HeLa xenograft tumour on the right side of each mice was exposed to UV light for 10 min, while the tumour on the left was protected from UV light. The UV irradiation was performed two days after each **pSiNP-PCL-DOX** treatment. The tumour size was measured every day and the mice were sacrificed on day 12 to obtain the HeLa xenograft tumour for weighing test.

## Chapter 8.0: References

1. A. P. Gorka, R. R. Nani, J. Zhu, S. Mackem and M. J. Schnermann, *J Am Chem Soc*, 2014, **136**, 14153-14159.
2. Y. Zhao, X. Mu and G. Du, *Pharmacol Ther*, 2016, **162**, 134-143.
3. M. P. Pollastri, *Trends Parasitol*, 2018, **34**, 178-179.
4. J. F. Rossignol, *J Infect Public Health*, 2016, **9**, 227-230.
5. Y. Arbel, W. Abuzeid, R. S. Rosenson, A. Weisman and M. E. Farkouh, *Cardiovasc Drugs Ther*, 2018, **32**, 223-232.
6. N. Sattar, M. C. Petrie, B. Zinman and J. L. Januzzi, Jr., *J Am Coll Cardiol*, 2017, **69**, 2646-2656.
7. G. Srivastava and C. Apovian, *Curr Obes Rep*, 2018, **7**, 147-161.
8. A. A. Robitzki and R. Kurz, *Handb Exp Pharmacol*, 2010, DOI: 10.1007/978-3-642-00477-3\_3, 87-112.
9. W. H. Lee, C. Y. Loo, M. Bebawy, F. Luk, R. S. Mason and R. Rohanizadeh, *Curr Neuropharmacol*, 2013, **11**, 338-378.
10. A. K. Singla, A. Garg and D. Aggarwal, *Int J Pharm*, 2002, **235**, 179-192.
11. C. Wischke and S. P. Schwendeman, *Int J Pharm*, 2008, **364**, 298-327.
12. V. R. Patel and Y. K. Agrawal, *J Adv Pharm Technol Res*, 2011, **2**, 81-87.
13. E. A. Dubikovskaya, S. H. Thorne, T. H. Pillow, C. H. Contag and P. A. Wender, *Proc Natl Acad Sci U S A*, 2008, **105**, 12128-12133.
14. S. Kunjachan, B. Rychlik, G. Storm, F. Kiessling and T. Lammers, *Adv Drug Deliv Rev*, 2013, **65**, 1852-1865.
15. P. Wang, H. L. Yang, Y. J. Yang, L. Wang and S. C. Lee, *Evid Based Complement Alternat Med*, 2015, **2015**, 767136.
16. L. J. Goldstein, H. Galski, A. Fojo, M. Willingham, S. L. Lai, A. Gazdar, R. Pirker, A. Green, W. Crist, G. M. Brodeur and et al., *J Natl Cancer Inst*, 1989, **81**, 116-124.
17. S. Senapati, A. K. Mahanta, S. Kumar and P. Maiti, *Signal Transduct Target Ther*, 2018, **3**, 7.
18. T. G. Burish and D. M. Tope, *J Pain Symptom Manage*, 1992, **7**, 287-301.
19. R. Oun, Y. E. Moussa and N. J. Wheate, *Dalton Trans*, 2018, **47**, 6645-6653.
20. J. A. Johnson, Y. Y. Lu, A. O. Burts, Y. H. Lim, M. G. Finn, J. T. Koberstein, N. J. Turro, D. A. Tirrell and R. H. Grubbs, *J Am Chem Soc*, 2011, **133**, 559-566.
21. J. F. Coelho, P. C. Ferreira, P. Alves, R. Cordeiro, A. C. Fonseca, J. R. Gois and M. H. Gil, *EPMA J*, 2010, **1**, 164-209.
22. D. J. Crommelin and A. T. Florence, *Int J Pharm*, 2013, **454**, 496-511.
23. C. X. He, Z. G. He and J. Q. Gao, *Expert Opin Drug Deliv*, 2010, **7**, 445-460.
24. B. Tang, G. Cheng, J. C. Gu and C. H. Xu, *Drug Discov Today*, 2008, **13**, 606-612.
25. P. Milla, F. Dosio and L. Cattel, *Curr Drug Metab*, 2012, **13**, 105-119.
26. X. Xu, W. Ho, X. Zhang, N. Bertrand and O. Farokhzad, *Trends Mol Med*, 2015, **21**, 223-232.
27. P. Chytil, E. Koziolova, T. Etrych and K. Ulbrich, *Macromol Biosci*, 2018, **18**.
28. T. Miller, S. Breyer, G. van Colen, W. Mier, U. Haberkorn, S. Geissler, S. Voss, M. Weigandt and A. Goepferich, *Int J Pharm*, 2013, **445**, 117-124.
29. Y. H. Yun, B. K. Lee and K. Park, *J Control Release*, 2015, **219**, 2-7.
30. A. Baeza, D. Ruiz-Molina and M. Vallet-Regi, *Expert Opin Drug Deliv*, 2017, **14**, 783-796.
31. E. J. Anglin, L. Cheng, W. R. Freeman and M. J. Sailor, *Adv Drug Deliv Rev*, 2008, **60**, 1266-1277.
32. T. M. Allen and P. R. Cullis, *Adv Drug Deliv Rev*, 2013, **65**, 36-48.
33. C. Zylberberg and S. Matosevic, *Drug Deliv*, 2016, **23**, 3319-3329.
34. J. Rip, *Drug Discov Today Technol*, 2016, **20**, 53-58.
35. Y. Qiu and K. Park, *Adv Drug Deliv Rev*, 2001, **53**, 321-339.
36. J. C. Imperiale, G. B. Acosta and A. Sosnik, *J Control Release*, 2018, **285**, 106-141.
37. L. Jaimes-Aguirre, B. V. Gibbens-Bandala, E. Morales-Avila, B. E. Ocampo-Garcia, M. Seyedeh-Fatemeh and A. Amirhosein, *Curr Pharm Des*, 2016, **22**, 2886-2903.
38. A. J. Halliday and M. J. Cook, *CNS Neurol Disord Drug Targets*, 2009, **8**, 205-221.
39. Y. Cao, C. Zhang, W. Shen, Z. Cheng, L. L. Yu and Q. Ping, *J Control Release*, 2007, **120**, 186-194.

40. N. L. Fry, G. R. Boss and M. J. Sailor, *Chem Mater*, 2014, **26**, 2758-2764.
41. J. W. Park, *Breast Cancer Res*, 2002, **4**, 95-99.
42. L. M. Bimbo, M. Sarparanta, H. A. Santos, A. J. Airaksinen, E. Makila, T. Laaksonen, L. Peltonen, V. P. Lehto, J. Hirvonen and J. Salonen, *ACS Nano*, 2010, **4**, 3023-3032.
43. C. Chiappini, E. Tasciotti, J. R. Fakhoury, D. Fine, L. Pullan, Y. C. Wang, L. Fu, X. Liu and M. Ferrari, *Chemphyschem*, 2010, **11**, 1029-1035.
44. J. Riikonen, A. Correia, M. Kovalainen, S. Nakki, M. Lehtonen, J. Leppanen, J. Rantanen, W. Xu, F. Araujo, J. Hirvonen, K. Jarvinen, H. A. Santos and V. P. Lehto, *Biomaterials*, 2015, **52**, 44-55.
45. J. L. Heinrich, C. L. Curtis, G. M. Credo, M. J. Sailor and K. L. Kavanagh, *Science*, 1992, **255**, 66-68.
46. J. Salonen, L. Laitinen, A. M. Kaukonen, J. Tuura, M. Bjorkqvist, T. Heikkila, K. Vaha-Heikkila, J. Hirvonen and V. P. Lehto, *J Control Release*, 2005, **108**, 362-374.
47. K. L. Jarvis, T. J. Barnes and C. A. Prestidge, *Adv Colloid Interface Sci*, 2012, **175**, 25-38.
48. K. L. Jarvis, T. J. Barnes and C. A. Prestidge, *J Colloid Interface Sci*, 2011, **363**, 327-333.
49. J. H. Song and M. J. Sailor, *Inorganic Chemistry*, 1998, **37**, 3355-3360.
50. G. Mattei, E. V. Alieva, J. E. Petrov and V. A. Yakovlev, *physica status solidi (a)*, 2000, **182**, 139-143.
51. U. Frotscher, U. Rossow, M. Ebert, C. Pietryga, W. Richter, M. G. Berger, R. Arens-Fischer and H. Münder, *Thin Solid Films*, 1996, **276**, 36-39.
52. F. Wang, T. J. Barnes and C. A. Prestidge, *Pharmaceutics*, 2019, **11**.
53. A. S. Anderson, A. M. Dattelbaum, G. A. Montano, D. N. Price, J. G. Schmidt, J. S. Martinez, W. K. Grace, K. M. Grace and B. I. Swanson, *Langmuir*, 2008, **24**, 2240-2247.
54. A. J. Nijdam, M. Ming-Cheng Cheng, D. H. Geho, R. Fedele, P. Herrmann, K. Killian, V. Espina, E. F. Petricoin, L. A. Liotta and M. Ferrari, *Biomaterials*, 2007, **28**, 550-558.
55. E. Valeur and M. Bradley, *Chem Soc Rev*, 2009, **38**, 606-631.
56. M. D. Perretti, L. A. Perez-Marquez, R. Garcia-Rodriguez and R. Carrillo, *J Org Chem*, 2019, **84**, 840-850.
57. S. Ciampi, J. B. Harper and J. J. Gooding, *Chem Soc Rev*, 2010, **39**, 2158-2183.
58. J. M. Buriak, *Chem Rev*, 2002, **102**, 1271-1308.
59. D. Dattilo, L. Armelao, G. Fois, G. Mistura and M. Maggini, *Langmuir*, 2007, **23**, 12945-12950.
60. J. M. Buriak and M. D. Sikder, *J Am Chem Soc*, 2015, **137**, 9730-9738.
61. D. Kim, J. Joo, Y. Pan, A. Boarino, Y. W. Jun, K. H. Ahn, B. Arkles and M. J. Sailor, *Angew Chem Int Ed Engl*, 2016, **55**, 6423-6427.
62. R. G. Acres, A. V. Ellis, J. Alvino, C. E. Lenahan, D. A. Khodakov, G. F. Metha and G. G. Andersson, *The Journal of Physical Chemistry C*, 2012, **116**, 6289-6297.
63. D. Kim, J. M. Zuidema, J. Kang, Y. Pan, L. Wu, D. Warther, B. Arkles and M. J. Sailor, *J Am Chem Soc*, 2016, **138**, 15106-15109.
64. Y. Pan, A. Maddox, T. Min, F. Gonzaga, J. Goff and B. Arkles, *Chem Asian J*, 2017, **12**, 1198-1203.
65. S. P. Low, N. H. Voelcker, L. T. Canham and K. A. Williams, *Biomaterials*, 2009, **30**, 2873-2880.
66. M. Wang, P. S. Hartman, A. Loni, L. T. Canham, N. Bodiford and J. L. Coffey, *Langmuir*, 2015, **31**, 6179-6185.
67. W. Li, Z. Liu, F. Fontana, Y. Ding, D. Liu, J. T. Hirvonen and H. A. Santos, *Adv Mater*, 2018, **30**, e1703740.
68. E. Makila, M. P. Ferreira, H. Kivela, S. M. Niemi, A. Correia, M. A. Shahbazi, J. Kauppila, J. Hirvonen, H. A. Santos and J. Salonen, *Langmuir*, 2014, **30**, 2196-2205.
69. J. R. McCombs and S. C. Owen, *AAPS J*, 2015, **17**, 339-351.
70. T. Solomek, S. Mercier, T. Bally and C. G. Bochet, *Photochem Photobiol Sci*, 2012, **11**, 548-555.
71. M. Karimi, P. Sahandi Zangabad, A. Ghasemi, M. Amiri, M. Bahrami, H. Malekzad, H. Ghahramanzadeh Asl, Z. Mahdieh, M. Bozorgomid, A. Ghasemi, M. R. Rahmani Taji Boyuk and M. R. Hamblin, *ACS Appl Mater Interfaces*, 2016, **8**, 21107-21133.
72. J. H. Lee, Q. Lu, J. Y. Lee and H. J. Choi, *Polymers (Basel)*, 2019, **11**.
73. G. Hariri, H. Yan, H. Wang, Z. Han and D. E. Hallahan, *Clin Cancer Res*, 2010, **16**, 4968-4977.
74. Y. Z. Zhao, L. N. Du, C. T. Lu, Y. G. Jin and S. P. Ge, *Int J Nanomedicine*, 2013, **8**, 1621-1633.
75. H. Yonezawa, Y. Nishiyama, K. Takeo, T. Iwatsubo, T. Tomita, S. Yokoshima and T. Fukuyama, *Bioorg Med Chem Lett*, 2014, **24**, 2831-2833.
76. A. Raza, T. Rasheed, F. Nabeel, U. Hayat, M. Bilal and H. M. N. Iqbal, *Molecules*, 2019, **24**.

77. W. B. Bair, 3rd, C. M. Cabello, K. Uchida, A. S. Bause and G. T. Wondrak, *Melanoma Res*, 2010, **20**, 85-96.
78. X. Zhang, Y. Lin and R. J. Gillies, *J Nucl Med*, 2010, **51**, 1167-1170.
79. J. Mu, J. Lin, P. Huang and X. Chen, *Chem Soc Rev*, 2018, **47**, 5554-5573.
80. W. Wu, L. Luo, Y. Wang, Q. Wu, H. B. Dai, J. S. Li, C. Durkan, N. Wang and G. X. Wang, *Theranostics*, 2018, **8**, 3038-3058.
81. Y. Zeng, J. Ma, Y. Zhan, X. Xu, Q. Zeng, J. Liang and X. Chen, *Int J Nanomedicine*, 2018, **13**, 6551-6574.
82. J. W. Walker, J. A. McCray and G. P. Hess, *Biochemistry*, 1986, **25**, 1799-1805.
83. X. Tan, B. B. Li, X. Lu, F. Jia, C. Santori, P. Menon, H. Li, B. Zhang, J. J. Zhao and K. Zhang, *J Am Chem Soc*, 2015, **137**, 6112-6115.
84. J. Olejniczak, C. J. Carling and A. Almutairi, *J Control Release*, 2015, **219**, 18-30.
85. E. Maverakis, Y. Miyamura, M. P. Bowen, G. Correa, Y. Ono and H. Goodarzi, *J Autoimmun*, 2010, **34**, J247-257.
86. G. Mayer and A. Heckel, *Angew Chem Int Ed Engl*, 2006, **45**, 4900-4921.
87. C. Park, K. Lee and C. Kim, *Angew Chem Int Ed Engl*, 2009, **48**, 1275-1278.
88. B. Peng, C. Yu, S. Du, S. S. Liew, X. Mao, P. Yuan, Z. Na and S. Q. Yao, *Chembiochem*, 2018, **19**, 986-996.
89. S. K. Choi, T. Thomas, M. H. Li, A. Kotlyar, A. Desai and J. R. Baker, Jr., *Chem Commun (Camb)*, 2010, **46**, 2632-2634.
90. S. K. Choi, T. P. Thomas, M. H. Li, A. Desai, A. Kotlyar and J. R. Baker, Jr., *Photochem Photobiol Sci*, 2012, **11**, 653-660.
91. X. Hu, J. Tian, T. Liu, G. Zhang and S. Liu, *Macromolecules*, 2013, **46**, 6243-6256.
92. S. S. Agasti, A. Chompoosor, C. C. You, P. Ghosh, C. K. Kim and V. M. Rotello, *J Am Chem Soc*, 2009, **131**, 5728-5729.
93. L. Kammari, T. Solomek, B. P. Ngoy, D. Heger and P. Klan, *J Am Chem Soc*, 2010, **132**, 11431-11433.
94. A. Momotake, N. Lindegger, E. Niggli, R. J. Barsotti and G. C. Ellis-Davies, *Nat Methods*, 2006, **3**, 35-40.
95. P. Neveu, I. Aujard, C. Benbrahim, T. Le Saux, J. F. Allemand, S. Vriz, D. Bensimon and L. Jullien, *Angew Chem Int Ed Engl*, 2008, **47**, 3744-3746.
96. I. Aujard, C. Benbrahim, M. Gouget, O. Ruel, J. B. Baudin, P. Neveu and L. Jullien, *Chemistry*, 2006, **12**, 6865-6879.
97. P. Klan, T. Solomek, C. G. Bochet, A. Blanc, R. Givens, M. Rubina, V. Popik, A. Kostikov and J. Wirz, *Chem Rev*, 2013, **113**, 119-191.
98. J. Engels and E. J. Schlaeger, *J Med Chem*, 1977, **20**, 907-911.
99. J. A. Johnson, Y. Y. Lu, A. O. Burts, Y. Xia, A. C. Durrell, D. A. Tirrell and R. H. Grubbs, *Macromolecules*, 2010, **43**, 10326-10335.
100. M. Meinhardt, R. Krebs, A. Anders, U. Heinrich and H. Tronnier, *J Biomed Opt*, 2008, **13**, 044030.
101. P. P. Goswami, A. Syed, C. L. Beck, T. R. Albright, K. M. Mahoney, R. Unash, E. A. Smith and A. H. Winter, *J Am Chem Soc*, 2015, **137**, 3783-3786.
102. M. M. Alam, F. Bolze, C. Daniel, L. Flamigni, C. Gourlaouen, V. Heitz, S. Jenni, J. Schmitt, A. Sour and B. Ventura, *Phys Chem Chem Phys*, 2016, **18**, 21954-21965.
103. W. Lv, Y. Li, F. Li, X. Lan, Y. Zhang, L. Du, Q. Zhao, D. L. Phillips and W. Wang, *J Am Chem Soc*, 2019, **141**, 17482-17486.
104. D. Kand, P. Liu, M. X. Navarro, L. J. Fischer, L. Rousso-Noori, D. Friedmann-Morvinski, A. H. Winter, E. W. Miller and R. Weinstain, *J Am Chem Soc*, 2020, **142**, 4970-4974.
105. R. R. Nani, A. P. Gorka, T. Nagaya, H. Kobayashi and M. J. Schnermann, *Angew Chem Int Ed Engl*, 2015, **54**, 13635-13638.
106. R. R. Nani, A. P. Gorka, T. Nagaya, T. Yamamoto, J. Ivanic, H. Kobayashi and M. J. Schnermann, *ACS Cent Sci*, 2017, **3**, 329-337.
107. P. Swietach, R. D. Vaughan-Jones, A. L. Harris and A. Hulikova, *Philos Trans R Soc Lond B Biol Sci*, 2014, **369**, 20130099.
108. A. J. Thistlethwaite, D. B. Leeper, D. J. Moylan, 3rd and R. E. Nerlinger, *Int J Radiat Oncol Biol Phys*, 1985, **11**, 1647-1652.

109. G. J. Casimir, N. Lefevre, F. Corazza, J. Duchateau and M. Chamekh, *Front Immunol*, 2018, **9**, 475.
110. R. A. Gatenby and R. J. Gillies, *Nat Rev Cancer*, 2004, **4**, 891-899.
111. J. Mauro and E. C. Kulakowski, *Biochem Pharmacol*, 1988, **37**, 3755-3760.
112. S. Aryal, C. M. Hu and L. Zhang, *ACS Nano*, 2010, **4**, 251-258.
113. L. M. Kaminskis, B. D. Kelly, V. M. McLeod, G. Sberna, D. J. Owen, B. J. Boyd and C. J. Porter, *J Control Release*, 2011, **152**, 241-248.
114. T. Yoshida, T. C. Lai, G. S. Kwon and K. Sako, *Expert Opin Drug Deliv*, 2013, **10**, 1497-1513.
115. K. Kono, C. Kojima, N. Hayashi, E. Nishisaka, K. Kiura, S. Watarai and A. Harada, *Biomaterials*, 2008, **29**, 1664-1675.
116. W. She, D. Pan, K. Luo, B. He, G. Cheng, C. Zhang and Z. Gu, *J Biomed Nanotechnol*, 2015, **11**, 964-978.
117. Y. Bae, N. Nishiyama and K. Kataoka, *Bioconjug Chem*, 2007, **18**, 1131-1139.
118. Y. Bae, W. D. Jang, N. Nishiyama, S. Fukushima and K. Kataoka, *Mol Biosyst*, 2005, **1**, 242-250.
119. Y. Ding, D. Sun, G. L. Wang, H. G. Yang, H. F. Xu, J. H. Chen, Y. Xie and Z. Q. Wang, *Int J Nanomedicine*, 2015, **10**, 6199-6214.
120. R. M. Sawant, J. P. Hurley, S. Salmaso, A. Kale, E. Tolcheva, T. S. Levchenko and V. P. Torchilin, *Bioconjug Chem*, 2006, **17**, 943-949.
121. F. Wang, Y. C. Wang, S. Dou, M. H. Xiong, T. M. Sun and J. Wang, *ACS Nano*, 2011, **5**, 3679-3692.
122. C. H. Lee, S. H. Cheng, I. P. Huang, J. S. Souris, C. S. Yang, C. Y. Mou and L. W. Lo, *Angew Chem Int Ed Engl*, 2010, **49**, 8214-8219.
123. P. A. Trail, D. Willner, S. J. Lasch, A. J. Henderson, S. Hofstead, A. M. Casazza, R. A. Firestone, I. Hellstrom and K. E. Hellstrom, *Science*, 1993, **261**, 212-215.
124. N. K. Damle, *Expert Opin Biol Ther*, 2004, **4**, 1445-1452.
125. J. Kalia and R. T. Raines, *Angew Chem Int Ed Engl*, 2008, **47**, 7523-7526.
126. L. Pes, S. D. Koester, J. P. Magnusson, S. Chercheja, F. Medda, K. Abu Ajaj, D. Rognan, S. Daum, F. I. Nollmann, J. Garcia Fernandez, P. Perez Galan, H.-K. Walter, A. Warnecke and F. Kratz, *Journal of Controlled Release*, 2019, **296**, 81-92.
127. Y. Zhang, W. Wang, Y. Zhang, M. Cheng, Q. Wu and Z. Yuan, *ACS Applied Bio Materials*, 2018, **1**, 572-580.
128. H. Wang, L. Wang, Y. Gao and Y. Ding, *Chinese Chemical Letters*, 2020, DOI: <https://doi.org/10.1016/j.ccl.2020.08.044>.
129. Y. Zhang, M. Gao, C. Chen, Z. Wang and Y. Zhao, *RSC Advances*, 2015, **5**, 34800-34802.
130. A. Warshel, *Proc Natl Acad Sci U S A*, 1984, **81**, 444-448.
131. M. Beigi, E. Gauchenova, L. Walter, S. Waltzer, F. Bonina, T. Stillger, D. Rother, M. Pohl and M. Muller, *Chemistry*, 2016, **22**, 13999-14005.
132. R. Roy, J. Yang and M. A. Moses, *J Clin Oncol*, 2009, **27**, 5287-5297.
133. P. Vadas, J. Browning, J. Edelson and W. Pruzanski, *J Lipid Mediat*, 1993, **8**, 1-30.
134. D. A. Butterfield, S. S. Hardas and M. L. Lange, *J Alzheimers Dis*, 2010, **20**, 369-393.
135. G. Leriche, L. Chisholm and A. Wagner, *Bioorg Med Chem*, 2012, **20**, 571-582.
136. E. A. Runquist and R. J. Havel, *J Biol Chem*, 1991, **266**, 22557-22563.
137. J. Seibel and K. Buchholz, *Adv Carbohydr Chem Biochem*, 2010, **63**, 101-138.
138. K. W. Moremen, R. B. Trimble and A. Herscovics, *Glycobiology*, 1994, **4**, 113-125.
139. G. Davies and B. Henrissat, *Structure*, 1995, **3**, 853-859.
140. R. J. Bernacki, M. J. Niedbala and W. Korytnyk, *Cancer Metastasis Rev*, 1985, **4**, 81-101.
141. B. L. Whitaker, *Br J Cancer*, 1960, **14**, 471-477.
142. D. H. Kim and Y. H. Jin, *Arch Pharm Res*, 2001, **24**, 564-567.
143. U. Schumacher, E. Adam, U. Zangemeister-Wittke and R. Gossrau, *Acta Histochem*, 1996, **98**, 381-387.
144. V. Vlacha, M. Eliopoulou, S. Haidas and N. G. Beratis, *Pediatr Blood Cancer*, 2004, **42**, 350-356.
145. F. E. Brot, C. E. Bell, Jr. and W. S. Sly, *Biochemistry*, 1978, **17**, 385-391.
146. M. R. Islam, S. Tomatsu, G. N. Shah, J. H. Grubb, S. Jain and W. S. Sly, *J Biol Chem*, 1999, **274**, 23451-23455.
147. A. W. Wong, S. He, J. H. Grubb, W. S. Sly and S. G. Withers, *J Biol Chem*, 1998, **273**, 34057-34062.

148. T. L. Cheng, W. C. Chou, B. M. Chen, J. W. Chern and S. R. Roffler, *Biochem Pharmacol*, 1999, **58**, 325-328.
149. L. F. Tietze, H. J. Schuster, K. Schmuck, I. Schuberth and F. Alves, *Bioorg Med Chem*, 2008, **16**, 6312-6318.
150. A. El Alaoui, F. Schmidt, C. Monneret and J. C. Florent, *J Org Chem*, 2006, **71**, 9628-9636.
151. T. Legigan, J. Clarhaut, B. Renoux, I. Tranoy-Opalinski, A. Monvoisin, J. M. Berjeaud, F. Guilhot and S. Papot, *J Med Chem*, 2012, **55**, 4516-4520.
152. P. J. Burke, J. Z. Hamilton, T. A. Pires, J. R. Setter, J. H. Hunter, J. H. Cochran, A. B. Waight, K. A. Gordon, B. E. Toki, K. K. Emmerton, W. Zeng, I. J. Stone, P. D. Senter, R. P. Lyon and S. C. Jeffrey, *Mol Cancer Ther*, 2016, **15**, 938-945.
153. P. J. Burke, J. Z. Hamilton, S. C. Jeffrey, J. H. Hunter, S. O. Doronina, N. M. Okeley, J. B. Miyamoto, M. E. Anderson, I. J. Stone, M. L. Ulrich, J. K. Simmons, E. E. McKinney, P. D. Senter and R. P. Lyon, *Mol Cancer Ther*, 2017, **16**, 116-123.
154. B. Renoux, F. Raes, T. Legigan, E. Peraudeau, B. Eddhif, P. Poinot, I. Tranoy-Opalinski, J. Alsarraf, O. Koniev, S. Kolodych, S. Lerondel, A. Le Pape, J. Clarhaut and S. Papot, *Chem Sci*, 2017, **8**, 3427-3433.
155. M. Talelli, K. Morita, C. J. Rijcken, R. W. Aben, T. Lammers, H. W. Scheeren, C. F. van Nostrum, G. Storm and W. E. Hennink, *Bioconjug Chem*, 2011, **22**, 2519-2530.
156. A. V. Stachulski and X. Meng, *Nat Prod Rep*, 2013, **30**, 806-848.
157. A. V. Stachulski and G. N. Jenkins, *Nat Prod Rep*, 1998, **15**, 173-186.
158. F. M. de Groot, A. C. de Bart, J. H. Verheijen and H. W. Scheeren, *J Med Chem*, 1999, **42**, 5277-5283.
159. A. Alouane, R. Labruere, T. Le Saux, I. Aujard, S. Dubruille, F. Schmidt and L. Jullien, *Chemistry*, 2013, **19**, 11717-11724.
160. R. Erez and D. Shabat, *Org Biomol Chem*, 2008, **6**, 2669-2672.
161. F. M. de Groot, C. Albrecht, R. Koekkoek, P. H. Beusker and H. W. Scheeren, *Angew Chem Int Ed Engl*, 2003, **42**, 4490-4494.
162. M. Shamis and D. Shabat, *Chemistry*, 2007, **13**, 4523-4528.
163. A. Warnecke and F. Kratz, *J Org Chem*, 2008, **73**, 1546-1552.
164. K. M. Schmid, L. Jensen and S. T. Phillips, *J Org Chem*, 2012, **77**, 4363-4374.
165. S. Cao, R. Christiansen and X. Peng, *Chemistry*, 2013, **19**, 9050-9058.
166. E. E. Weinert, R. Dondi, S. Colloredo-Melz, K. N. Frankenfield, C. H. Mitchell, M. Freccero and S. E. Rokita, *J Am Chem Soc*, 2006, **128**, 11940-11947.
167. J. S. Robbins, K. M. Schmid and S. T. Phillips, *J Org Chem*, 2013, **78**, 3159-3169.
168. B. M. Sykes, M. P. Hay, D. Bohinc-Herceg, N. A. Helsby, C. J. O'Connor and W. A. Denny, *Journal of the Chemical Society, Perkin Transactions 1*, 2000, DOI: 10.1039/B000135J, 1601-1608.
169. C. Coll, A. Bernardos, R. Martinez-Manez and F. Sancenon, *Acc Chem Res*, 2013, **46**, 339-349.
170. M. Xue, X. Zhong, Z. Shaposhnik, Y. Qu, F. Tamanoi, X. Duan and J. I. Zink, *J Am Chem Soc*, 2011, **133**, 8798-8801.
171. A. Bolhassani, S. Javan zad, T. Saleh, M. Hashemi, M. R. Aghasadeghi and S. M. Sadat, *Hum Vaccin Immunother*, 2014, **10**, 321-332.
172. K. K. Coti, M. E. Belowich, M. Liong, M. W. Ambrogio, Y. A. Lau, H. A. Khatib, J. I. Zink, N. M. Khashab and J. F. Stoddart, *Nanoscale*, 2009, **1**, 16-39.
173. T. Chen and J. Fu, *Nanotechnology*, 2012, **23**, 235605.
174. Z. Li, D. L. Clemens, B. Y. Lee, B. J. Dillon, M. A. Horwitz and J. I. Zink, *ACS Nano*, 2015, **9**, 10778-10789.
175. J. Liu, X. Du and X. Zhang, *Chemistry*, 2011, **17**, 810-815.
176. J. El Haskouri, J. M. Morales, D. Ortiz de Zarate, L. Fernandez, J. Latorre, C. Guillem, A. Beltran, D. Beltran and P. Amoros, *Inorg Chem*, 2008, **47**, 8267-8277.
177. J. D. Bargh, A. Isidro-Llobet, J. S. Parker and D. R. Spring, *Chemical Society Reviews*, 2019, **48**, 4361-4374.
178. G. Leriche, L. Chisholm and A. Wagner, *Bioorganic & Medicinal Chemistry*, 2012, **20**, 571-582.
179. Y. Xue, H. Bai, B. Peng, B. Fang, J. Baell, L. Li, W. Huang and N. H. Voelcker, *Chemical Society Reviews*, 2021, DOI: 10.1039/D0CS01061H.
180. Y.-J. Cheng, S.-Y. Qin, Y.-H. Ma, X.-S. Chen, A.-Q. Zhang and X.-Z. Zhang, *ACS Biomaterials Science & Engineering*, 2019, **5**, 1878-1886.

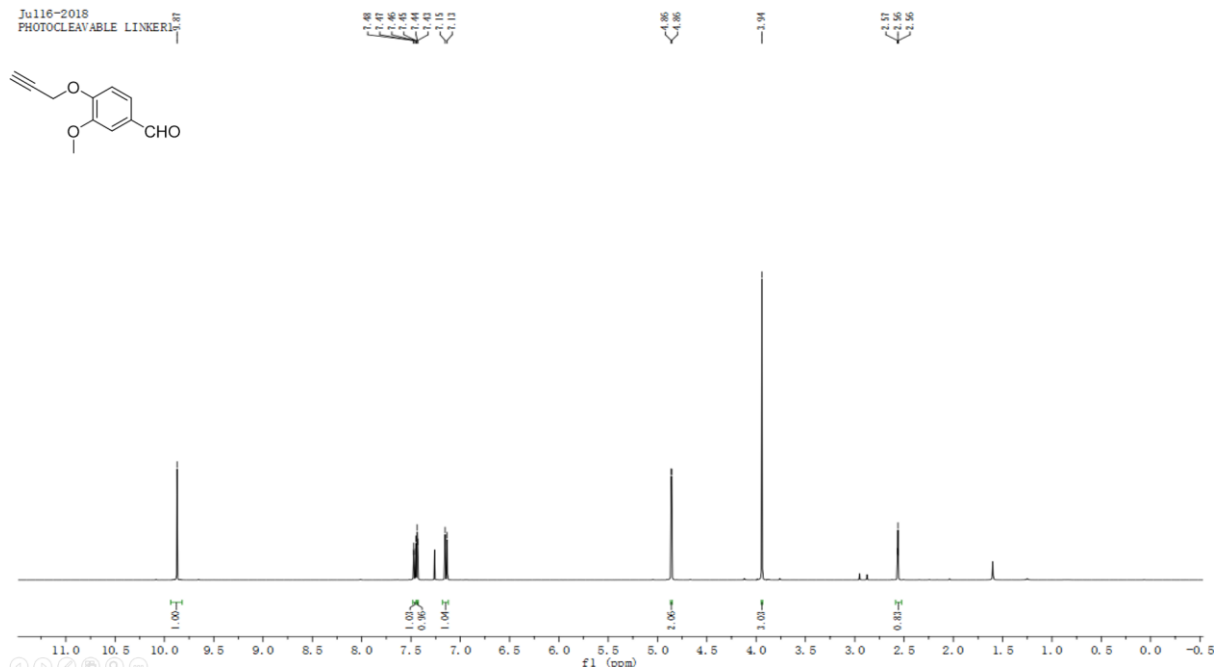
181. J. Chen, S. Chen, X. Zhao, L. V. Kuznetsova, S. S. Wong and I. Ojima, *Journal of the American Chemical Society*, 2008, **130**, 16778-16785.
182. G. Wu, R. F. Barth, W. Yang, S. Kawabata, L. Zhang and K. Green-Church, *Molecular Cancer Therapeutics*, 2006, **5**, 52-59.
183. X. Chen and Z. Liu, *Journal of Materials Chemistry B*, 2016, **4**, 4382-4388.
184. B. M. Cooper, J. Iegre, O. D. DH, M. Olwegard Halvarsson and D. R. Spring, *Chem Soc Rev*, 2021, **50**, 1480-1494.
185. J. Lu, F. Jiang, A. Lu and G. Zhang, *Int J Mol Sci*, 2016, **17**, 561.
186. A. Janaszewska, J. Lazniewska, P. Trzepinski, M. Marcinkowska and B. Klajnert-Maculewicz, *Biomolecules*, 2019, **9**.
187. C. G. Bavnhoj, M. M. Knopp, C. M. Madsen and K. Lobmann, *Int J Pharm X*, 2019, **1**, 100008.
188. T. Tieu, S. Dhawan, V. Haridas, L. M. Butler, H. Thissen, A. Cifuentes-Rius and N. H. Voelcker, *ACS Appl Mater Interfaces*, 2019, **11**, 22993-23005.
189. M. Ruike, M. Houzouji, A. Motohashi, N. Murase, A. Kinoshita and K. Kaneko, *Langmuir*, 1996, **12**, 4828-4831.
190. M. Luo, G. Lewik, J. C. Ratcliffe, C. H. J. Choi, E. Makila, W. Y. Tong and N. H. Voelcker, *ACS Appl Mater Interfaces*, 2019, **11**, 33637-33649.
191. N. Jain, S. W. Smith, S. Ghone and B. Tomczuk, *Pharm Res*, 2015, **32**, 3526-3540.
192. J. D. Bargh, A. Isidro-Llobet, J. S. Parker and D. R. Spring, *Chem Soc Rev*, 2019, **48**, 4361-4374.
193. H. L. Perez, P. M. Cardarelli, S. Deshpande, S. Gangwar, G. M. Schroeder, G. D. Vite and R. M. Borzilleri, *Drug Discov Today*, 2014, **19**, 869-881.
194. Y. Zhou, G. Quan, Q. Wu, X. Zhang, B. Niu, B. Wu, Y. Huang, X. Pan and C. Wu, *Acta Pharm Sin B*, 2018, **8**, 165-177.
195. E. Aznar, M. Oroval, L. Pascual, J. R. Murguía, R. Martínez-Manez and F. Sancenon, *Chem Rev*, 2016, **116**, 561-718.
196. J. M. Chan, P. M. Valencia, L. Zhang, R. Langer and O. C. Farokhzad, *Methods Mol Biol*, 2010, **624**, 163-175.
197. C. I. Crucho, *ChemMedChem*, 2015, **10**, 24-38.
198. X. Liu, Y. Yang and M. W. Urban, *Macromol Rapid Commun*, 2017, **38**.
199. P. Klán, T. Šolomek, C. G. Bochet, A. Blanc, R. Givens, M. Rubina, V. Popik, A. Kostikov and J. Wirz, *Chemical Reviews*, 2013, **113**, 119-191.
200. A. Jiménez-Balsa, S. Pinto, E. Quartin, M. M. Lino, V. Francisco and L. Ferreira, *Bioconjugate Chemistry*, 2018, **29**, 1485-1489.
201. C. Park, K. Lee and C. Kim, *Angewandte Chemie International Edition*, 2009, **48**, 1275-1278.
202. S. K. Choi, M. Verma, J. Silpe, R. E. Moody, K. Tang, J. J. Hanson and J. R. Baker, *Bioorganic & Medicinal Chemistry*, 2012, **20**, 1281-1290.
203. C.-H. Lee, S.-H. Cheng, I.-P. Huang, J. S. Souris, C.-S. Yang, C.-Y. Mou and L.-W. Lo, *Angewandte Chemie International Edition*, 2010, **49**, 8214-8219.
204. J. D. Wallat, J. K. Harrison and J. K. Pokorski, *Molecular Pharmaceutics*, 2018, **15**, 2954-2962.
205. S. C. Jeffrey, J. B. Andreyka, S. X. Bernhardt, K. M. Kissler, T. Kline, J. S. Lenox, R. F. Moser, M. T. Nguyen, N. M. Okeley, I. J. Stone, X. Zhang and P. D. Senter, *Bioconjugate Chemistry*, 2006, **17**, 831-840.
206. I. Tranoy-Opalinski, T. Legigan, R. Barat, J. Clarhaut, M. Thomas, B. Renoux and S. Papot, *European Journal of Medicinal Chemistry*, 2014, **74**, 302-313.
207. S. C. Jeffrey, J. De Brabander, J. Miyamoto and P. D. Senter, *ACS Medicinal Chemistry Letters*, 2010, **1**, 277-280.
208. O. Tacar, P. Sriamornsak and C. R. Dass, *J Pharm Pharmacol*, 2013, **65**, 157-170.
209. P. T. Wong, D. Chen, S. Tang, S. Yanik, M. Payne, J. Mukherjee, A. Coulter, K. Tang, K. Tao, K. Sun, J. R. Baker, Jr. and S. K. Choi, *Small*, 2015, **11**, 6078-6090.
210. C. S. McKay and M. G. Finn, *Chem Biol*, 2014, **21**, 1075-1101.
211. H. C. Kolb, M. G. Finn and K. B. Sharpless, *Angew Chem Int Ed Engl*, 2001, **40**, 2004-2021.
212. R. Liu, J. Zhao, G. Han, T. Zhao, R. Zhang, B. Liu, Z. Liu, C. Zhang, L. Yang and Z. Zhang, *ACS Appl Mater Interfaces*, 2017, **9**, 38222-38229.

213. Y. Chen, O. Tezcan, D. Li, N. Beztsinna, B. Lou, T. Etrych, K. Ulbrich, J. M. Metselaar, T. Lammers and W. E. Hennink, *Nanoscale*, 2017, **9**, 10404-10419.
214. V. V. Rostovtsev, L. G. Green, V. V. Fokin and K. B. Sharpless, *Angew Chem Int Ed Engl*, 2002, **41**, 2596-2599.
215. C. D. Hein, X. M. Liu and D. Wang, *Pharm Res*, 2008, **25**, 2216-2230.
216. M. P. VanBrunt, K. Shanebeck, Z. Caldwell, J. Johnson, P. Thompson, T. Martin, H. Dong, G. Li, H. Xu, F. D'Hooge, L. Masterson, P. Bariola, A. Tiberghien, E. Ezeadi, D. G. Williams, J. A. Hartley, P. W. Howard, K. H. Grabstein, M. A. Bowen and M. Marelli, *Bioconjug Chem*, 2015, **26**, 2249-2260.
217. A. Nouredine, M. Gary-Bobo, L. Lichon, M. Garcia, J. I. Zink, M. Wong Chi Man and X. Cattoen, *Chemistry*, 2016, **22**, 9624-9630.
218. Y. Chen, Y. Xianyu and X. Jiang, *Acc Chem Res*, 2017, **50**, 310-319.
219. V. O. Rodionov, S. I. Presolski, S. Gardinier, Y. H. Lim and M. G. Finn, *J Am Chem Soc*, 2007, **129**, 12696-12704.
220. W. G. Lewis, F. G. Magallon, V. V. Fokin and M. G. Finn, *J Am Chem Soc*, 2004, **126**, 9152-9153.
221. S. A. Jongkees and S. G. Withers, *J Am Chem Soc*, 2011, **133**, 19334-19337.
222. B. Sarmento, D. Mazzaglia, M. C. Bonferoni, A. P. Neto, M. do Céu Monteiro and V. Seabra, *Carbohydrate Polymers*, 2011, **84**, 919-925.
223. W. Zhang, *Adv Exp Med Biol*, 2014, **811**, 19-43.
224. S. Shen, Y. Wu, Y. Liu and D. Wu, *Int J Nanomedicine*, 2017, **12**, 4085-4109.
225. S. C. Jeffrey, J. De Brabander, J. Miyamoto and P. D. Senter, *ACS Med Chem Lett*, 2010, **1**, 277-280.
226. Y. Li, J. Jeon and J. H. Park, *Cancer Lett*, 2020, **490**, 31-43.
227. D. Liang, X. Wu, B. B. Hasinoff, D. E. Herbert and G. K. Tranmer, *Molecules*, 2018, **23**, 2041.
228. H. E. Gottlieb, V. Kotlyar and A. Nudelman, *J. Org. Chem.*, 1997, **62**, 7512-7515.

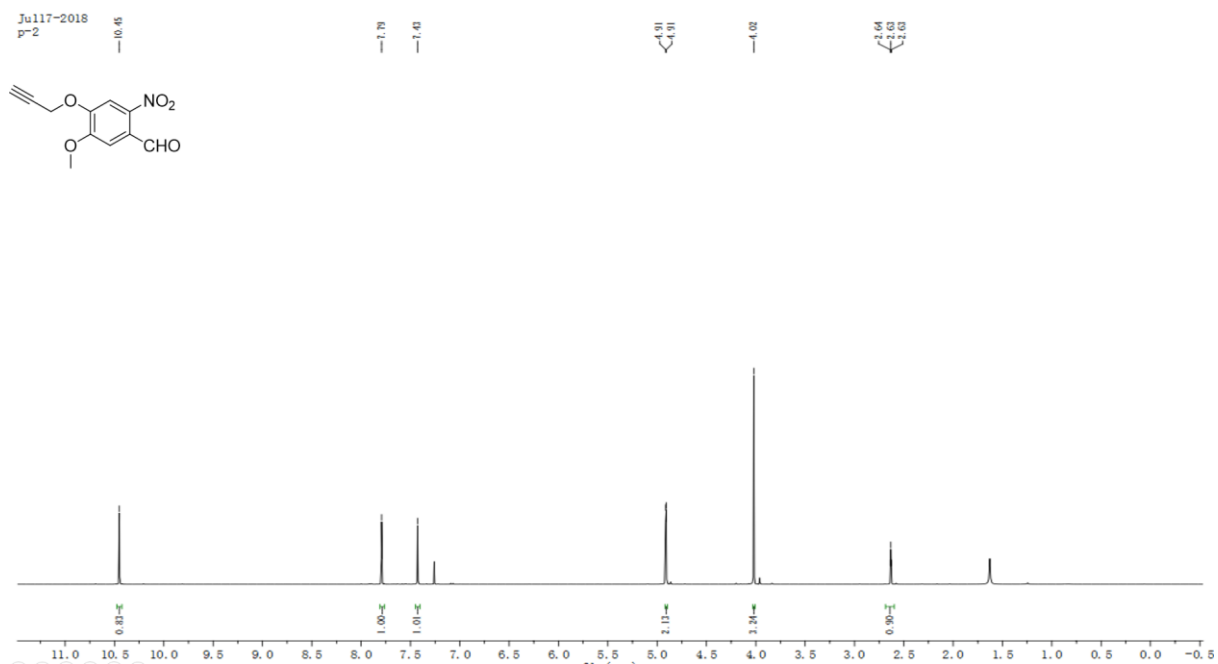
# Appendix

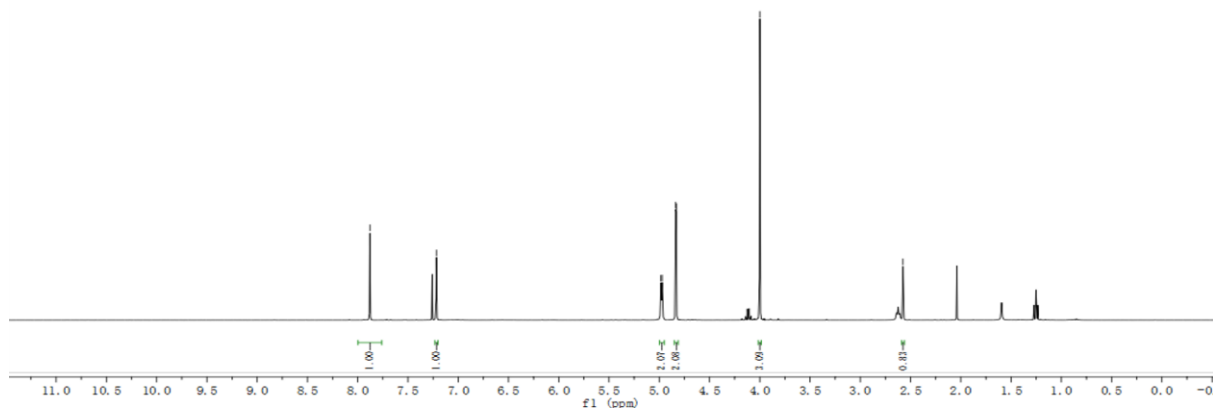
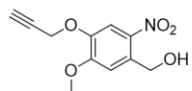
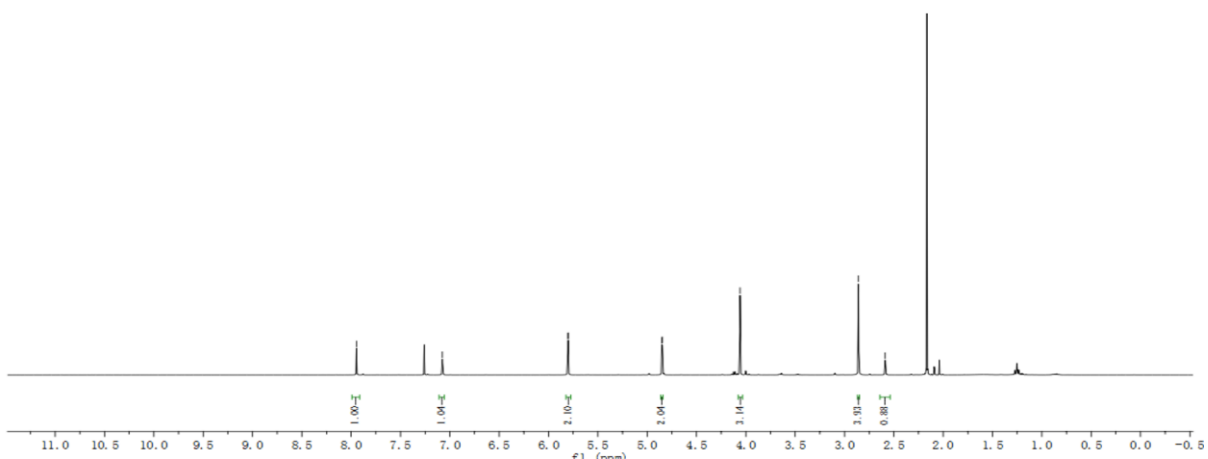
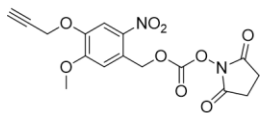
## $^1\text{H}$ NMR spectra

### 3-methoxy-4-(prop-2-yn-1-yloxy)benzaldehyde (30)



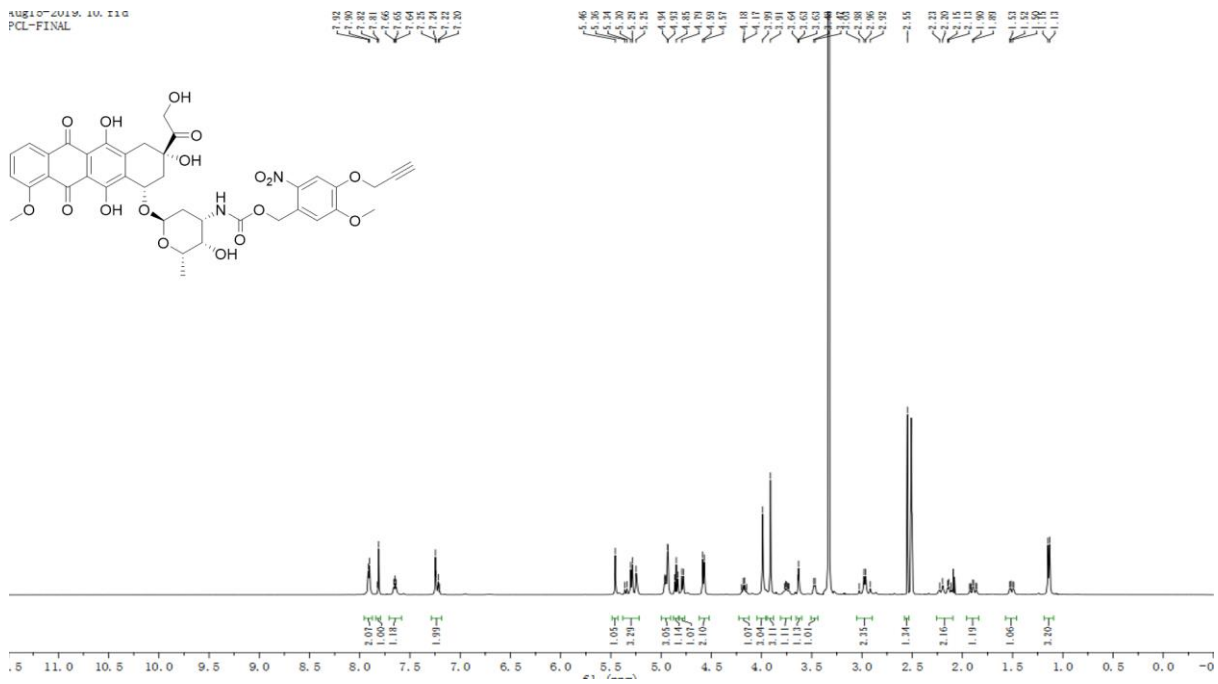
### 5-methoxy-2-nitro-4-(prop-2-yn-1-yloxy)benzaldehyde (31)



**(5-methoxy-2-nitro-4-(prop-2-yn-1-yloxy)phenyl)methanol (32)**Jul109-2018  
1**2,5-dioxopyrrolidin-1-yl (5-methoxy-2-nitro-4-(prop-2-yn-1-yloxy)benzyl) carbonate (34)**Aug31-2018  
JO-PCL-SUCC

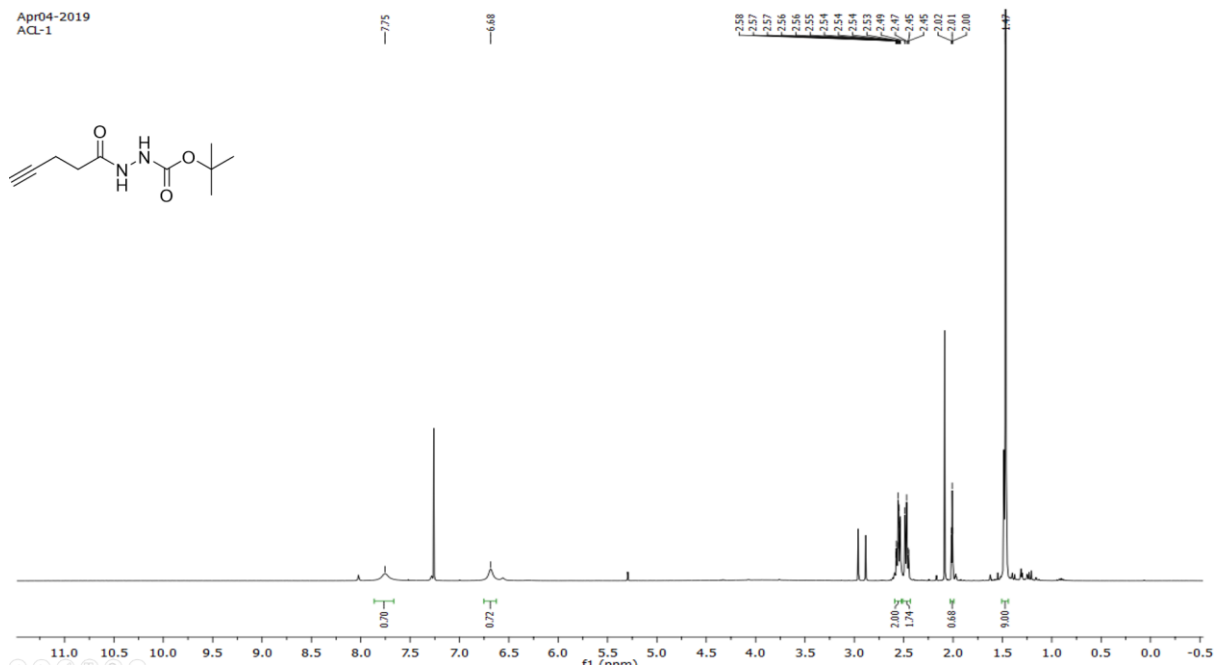
## PCL-DOX

Aug10-2019, 10, 11 G  
PCL-FINAL



## tert-butyl 2-(pent-4-ynoyl)hydrazine-1-carboxylate (36)

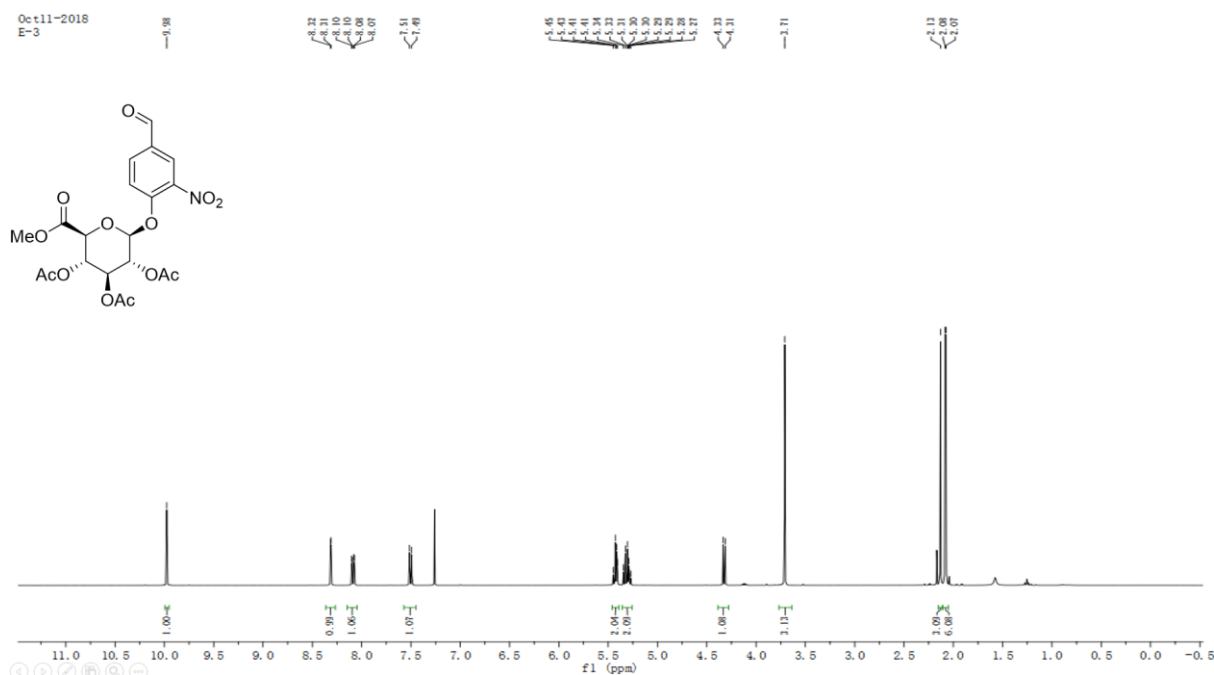
Apr04-2019  
AQL-1



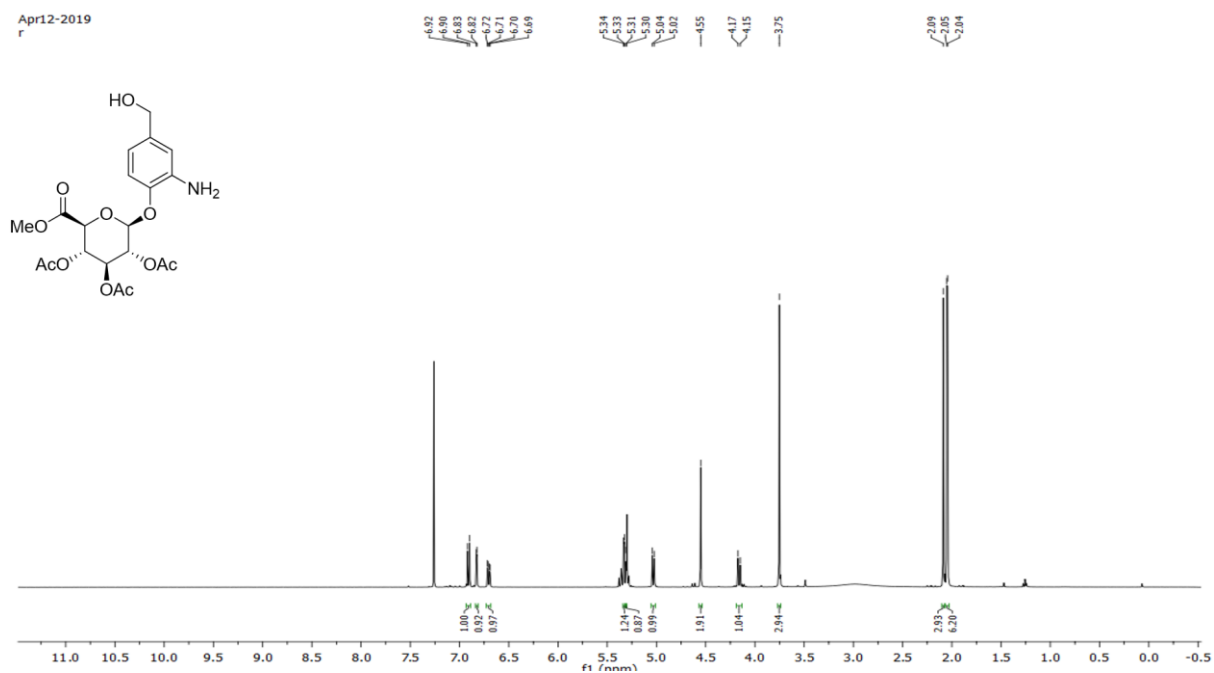




**(2S,3R,4S,5S,6S)-2-(4-formyl-2-nitrophenoxy)-6-(methoxycarbonyl)tetrahydro-2H-pyran-3,4,5-triyl triacetate (41)**

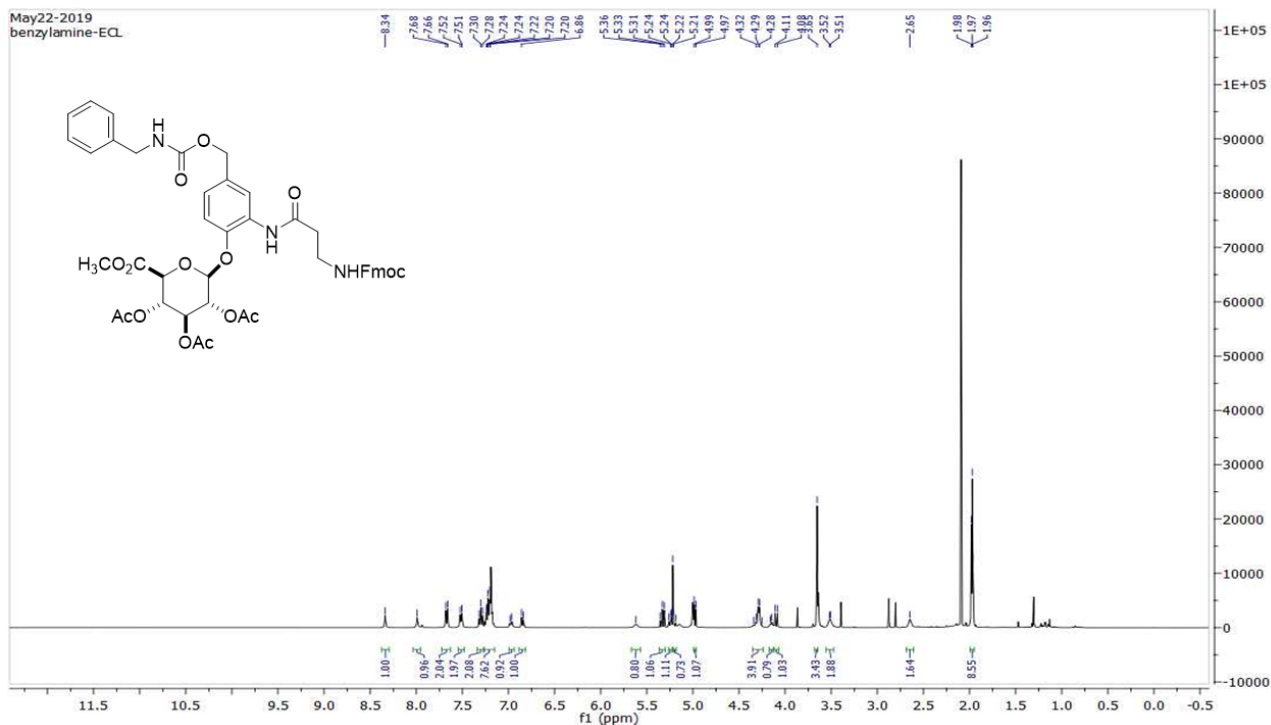


**(2S,3R,4S,5S,6S)-2-(2-amino-4-(hydroxymethyl)phenoxy)-6-(methoxycarbonyl)tetrahydro-2H-pyran-3,4,5-triyl triacetate (42)**

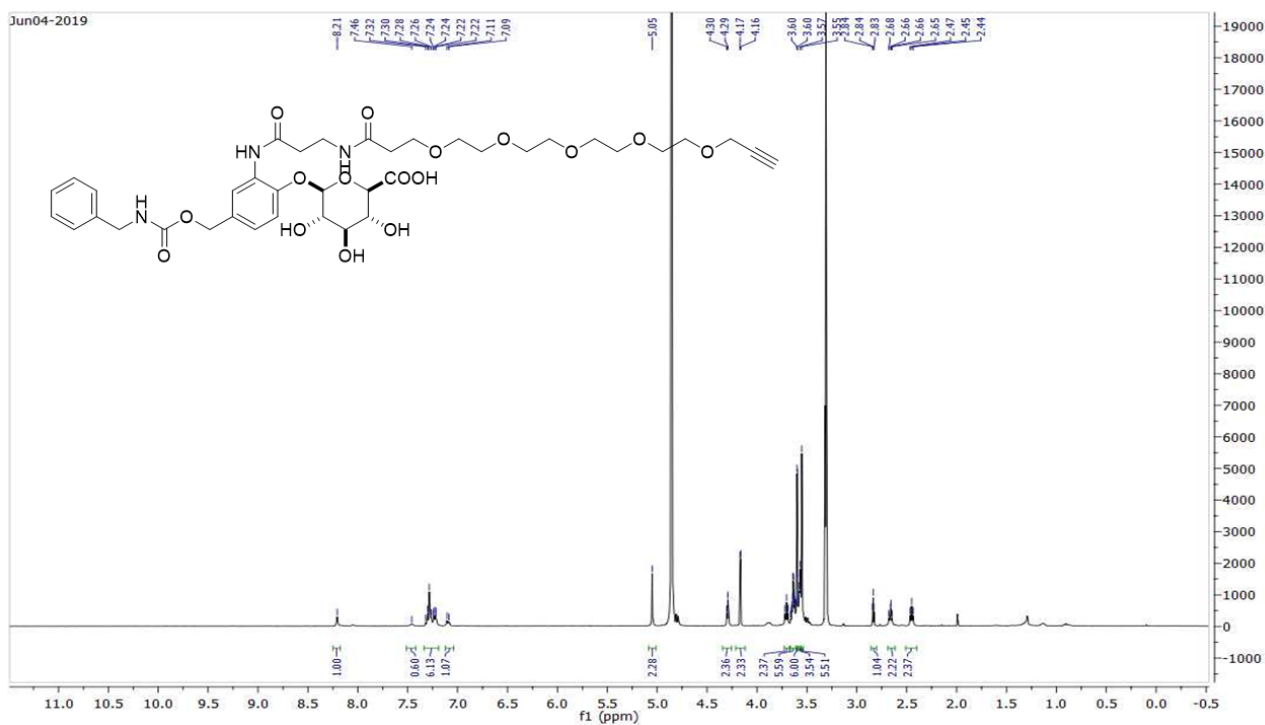




**(((benzylcarbamoyl)oxy)methyl)phenoxy)-6-(methoxycarbonyl)tetrahydro-2H-pyran-3,4,5-triyl triacetate (45)**

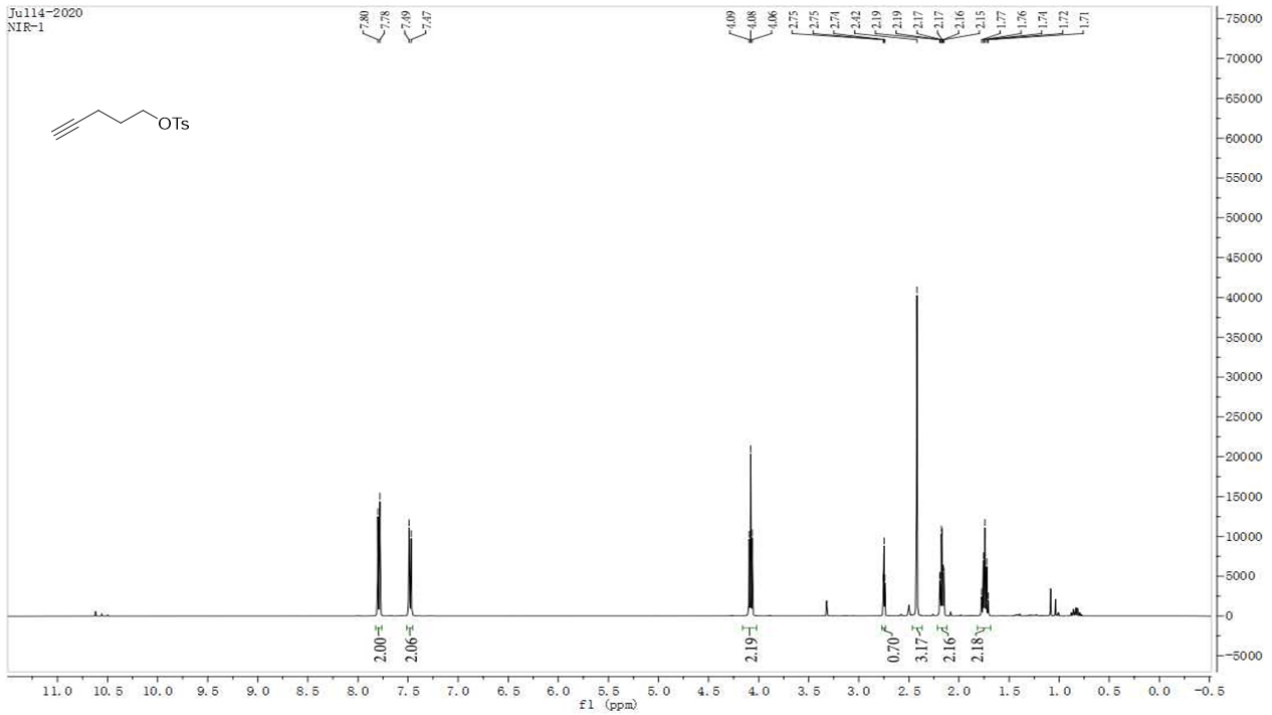


**ECL-benzylamine**

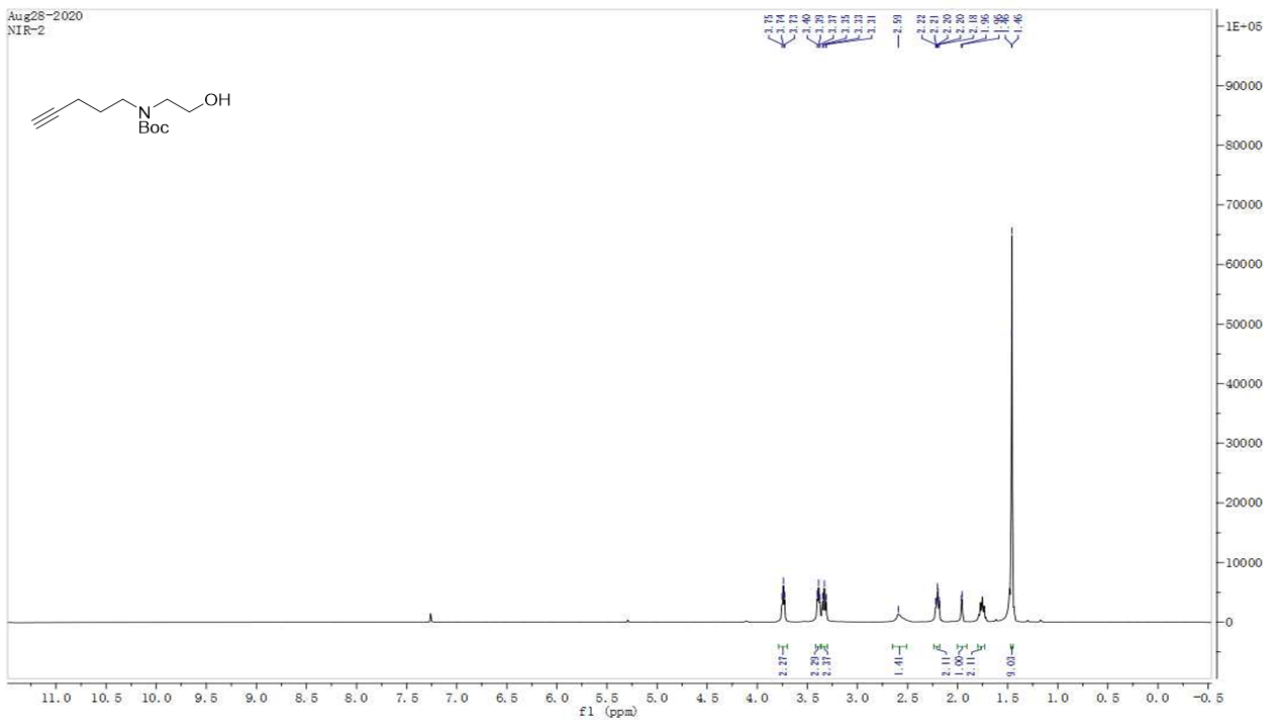




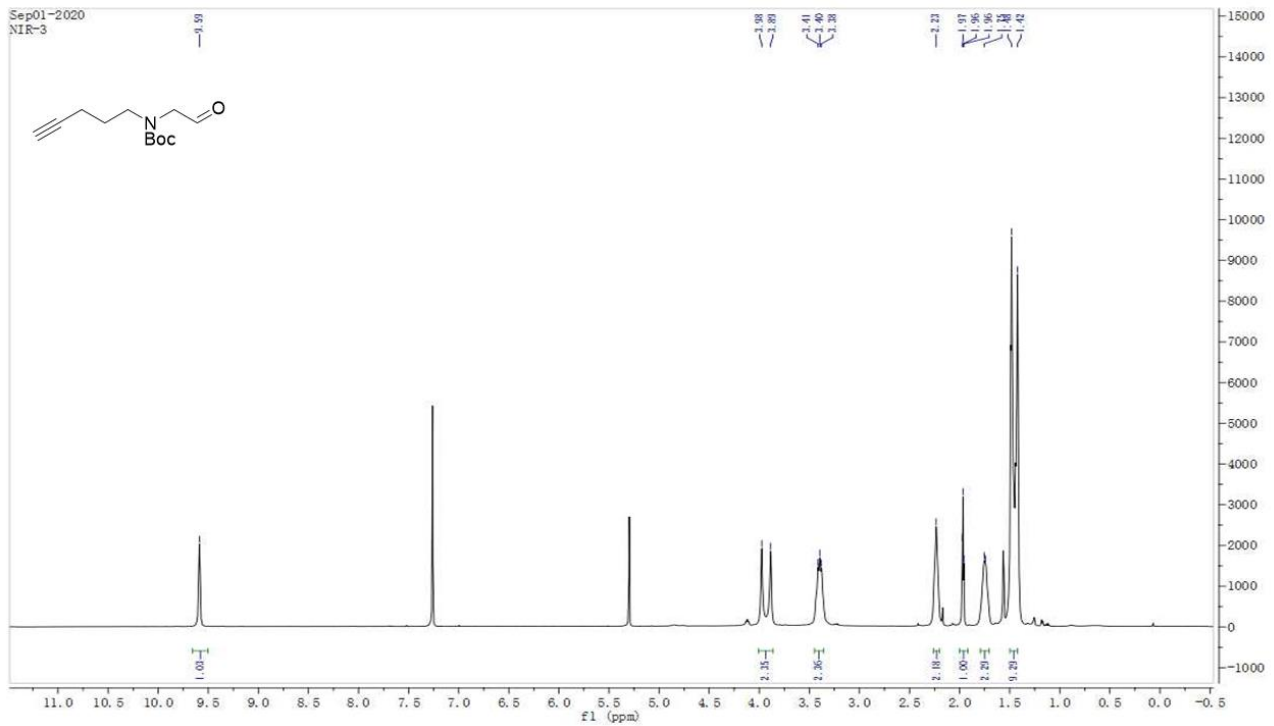
**pent-4-yn-1-yl 4-methylbenzenesulfonate (50)**



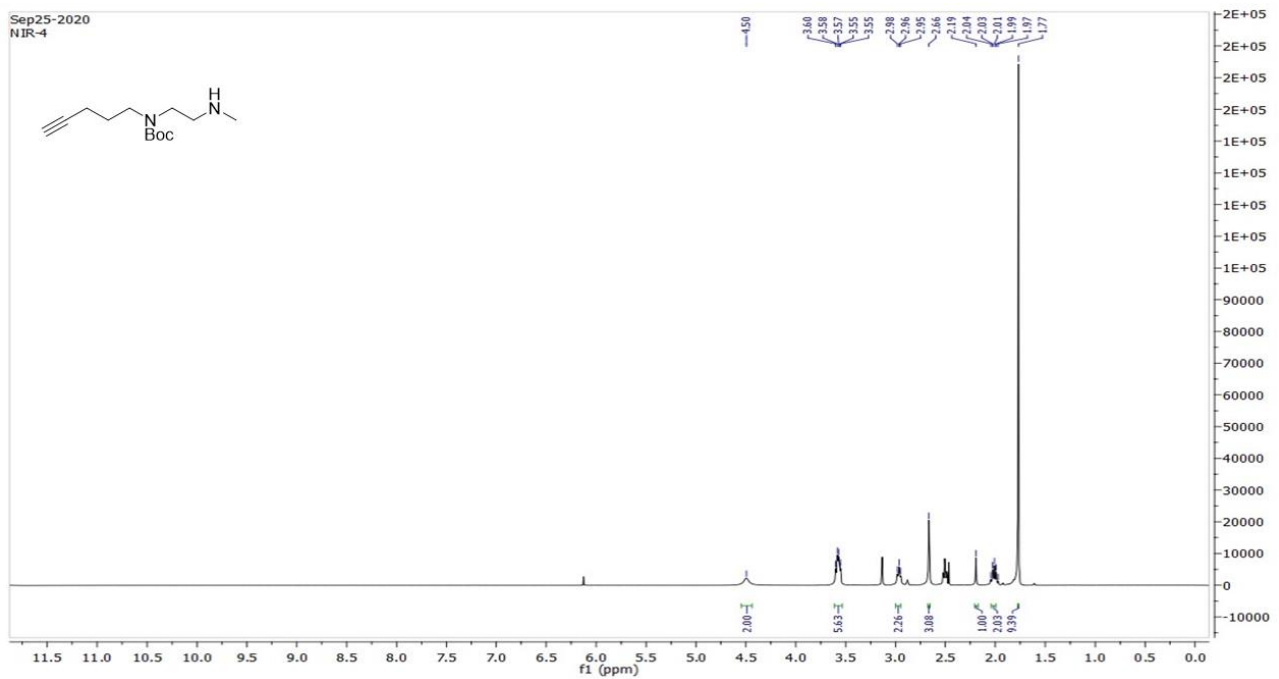
**tert-butyl (2-hydroxyethyl)(pent-4-yn-1-yl)carbamate (52)**



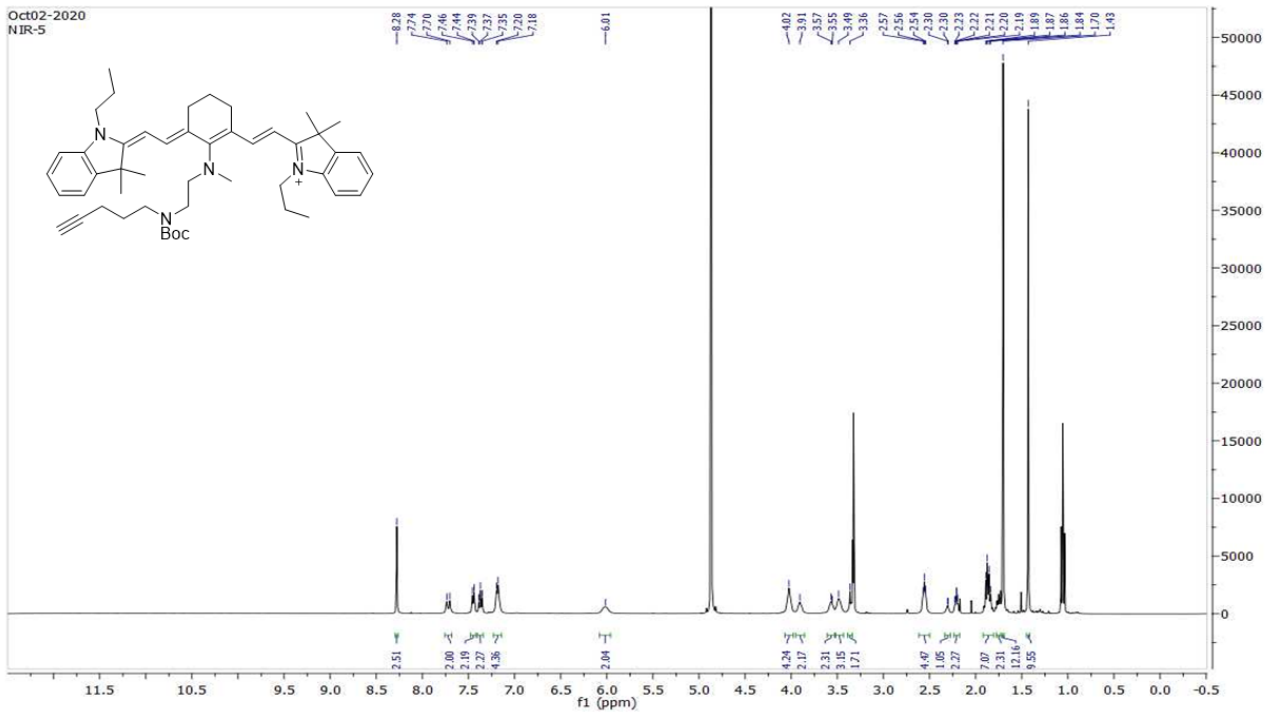
**tert-butyl (2-oxoethyl)(pent-4-yn-1-yl)carbamate (53)**



**tert-butyl (2-(methylamino)ethyl)(pent-4-yn-1-yl)carbamate (54)**

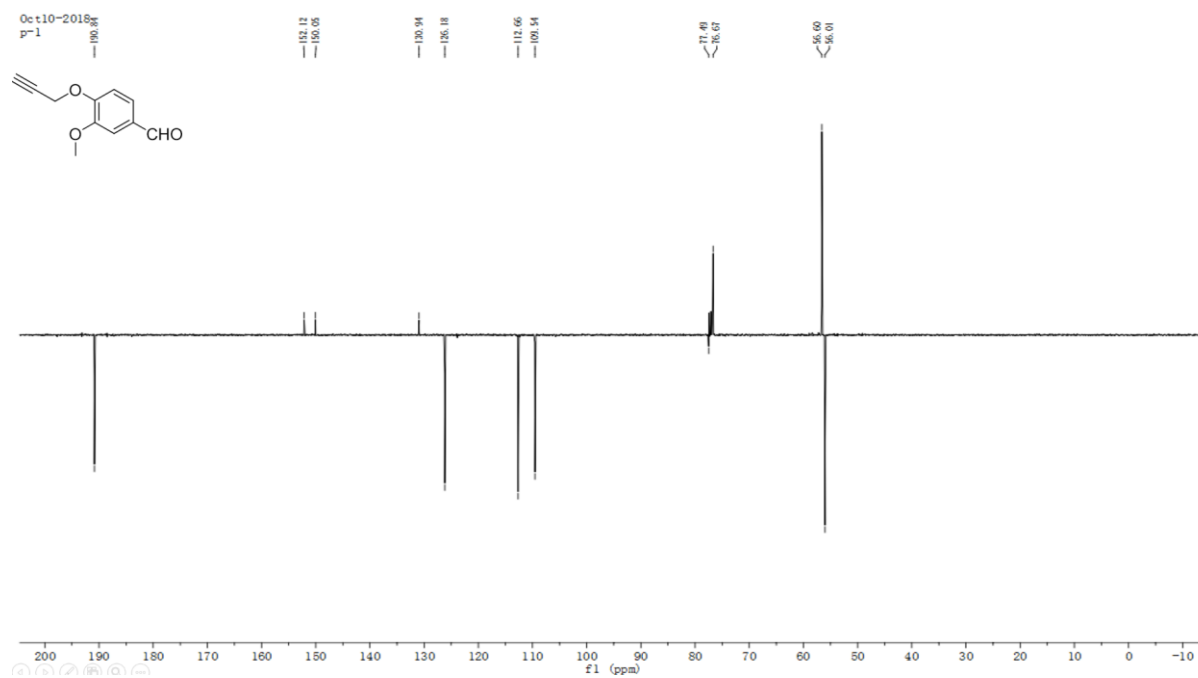


**2-((E)-2-((E)-2-((2-((tert-butoxycarbonyl)(pent-4-yn-1-yl)amino)ethyl)(methyl)amino)-3-(2-((E)-3,3-dimethyl-1-propylindolin-2-ylidene)ethylidene)cyclohex-1-en-1-yl)vinyl)-3,3-dimethyl-1-propyl-3H-indol-1-ium (55)**

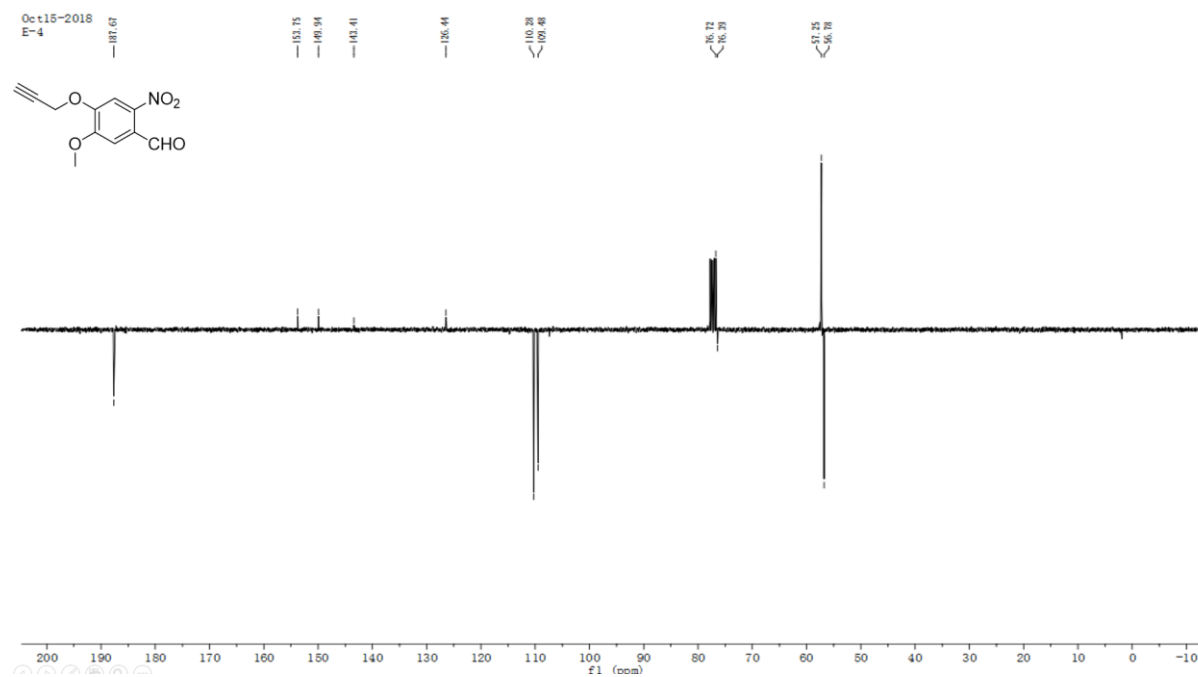


## $^{13}\text{C}$ NMR spectra

### 3-methoxy-4-(prop-2-yn-1-yloxy)benzaldehyde (30)

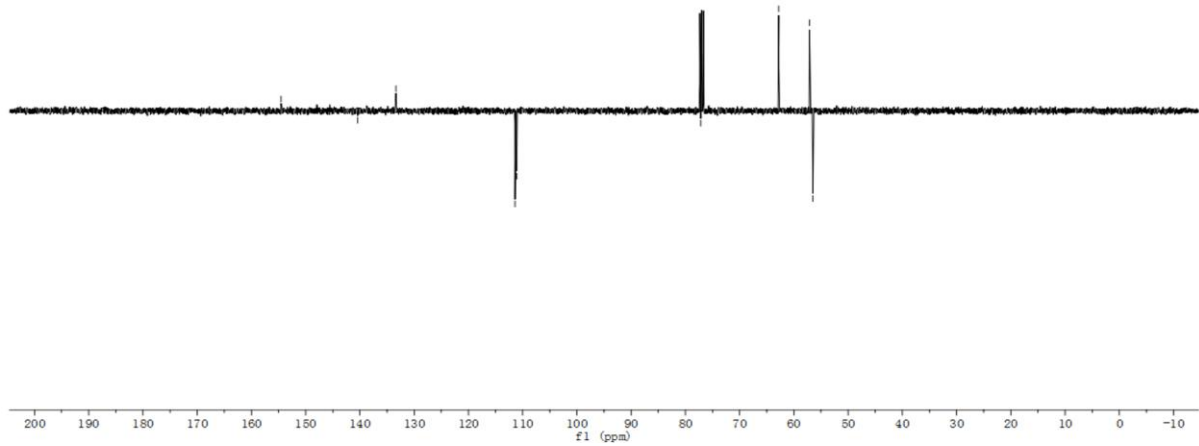
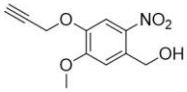


### 5-methoxy-2-nitro-4-(prop-2-yn-1-yloxy)benzaldehyde (31)

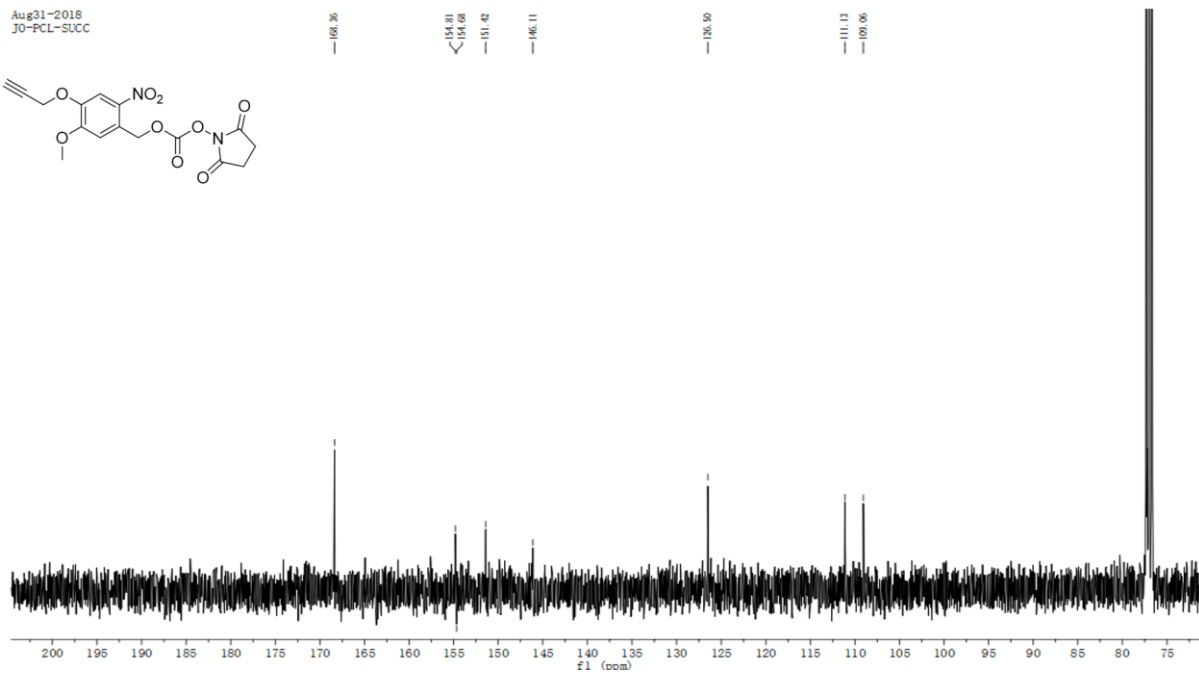
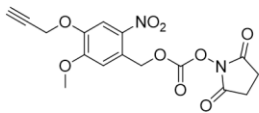


**(5-methoxy-2-nitro-4-(prop-2-yn-1-yloxy)phenyl)methanol (32)**Nov05-2018  
P-3

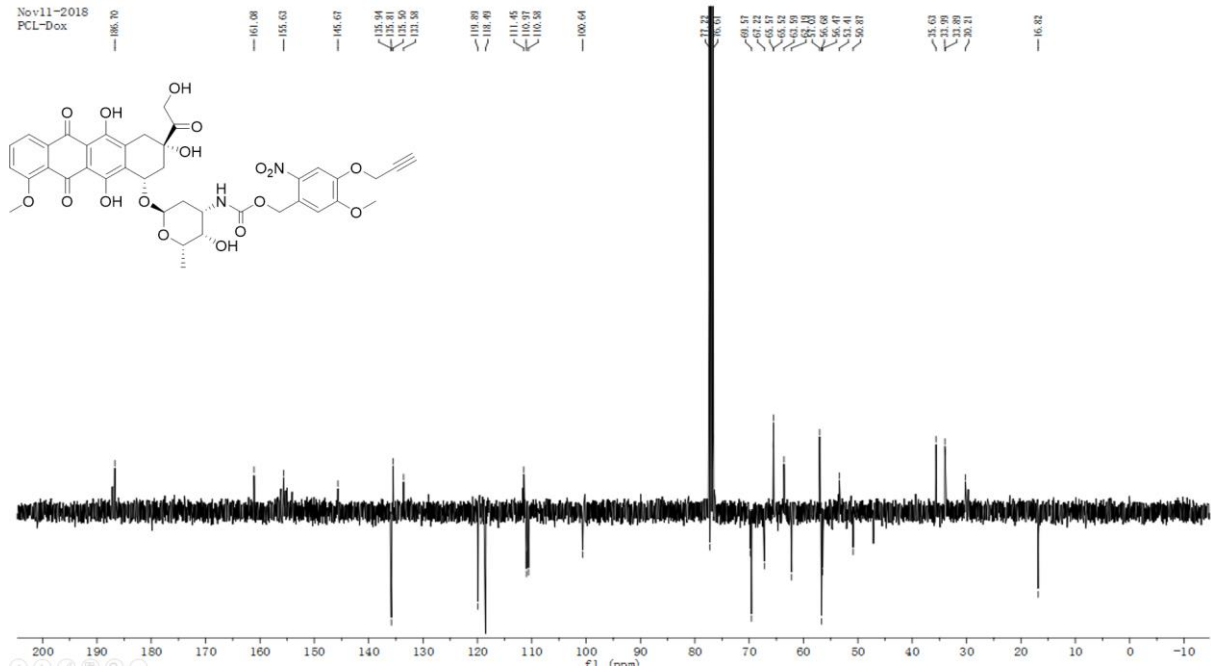
154.53      140.41      133.36      111.40      110.09      77.16      76.98      62.78      57.11      55.49

**2,5-dioxopyrrolidin-1-yl (5-methoxy-2-nitro-4-(prop-2-yn-1-yloxy)benzyl) carbonate (34)**Aug31-2018  
JO-PCL-SUCC

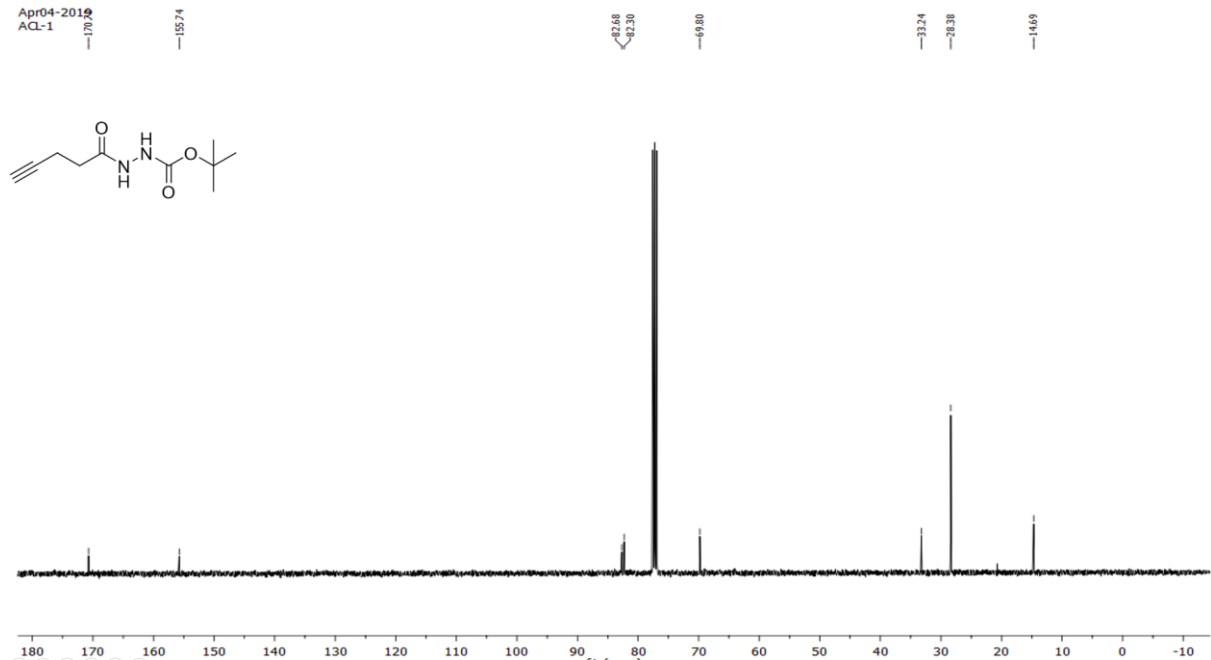
168.36      154.81      154.68      151.41      146.11      126.50      111.13      109.06



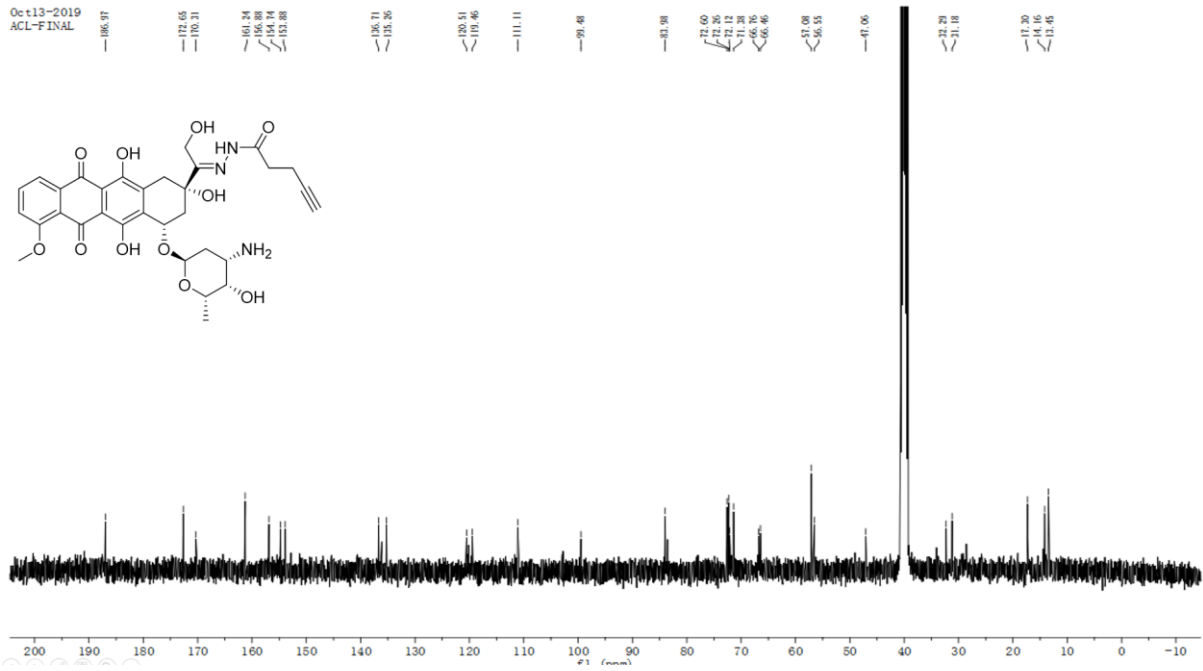
## PCL-DOX



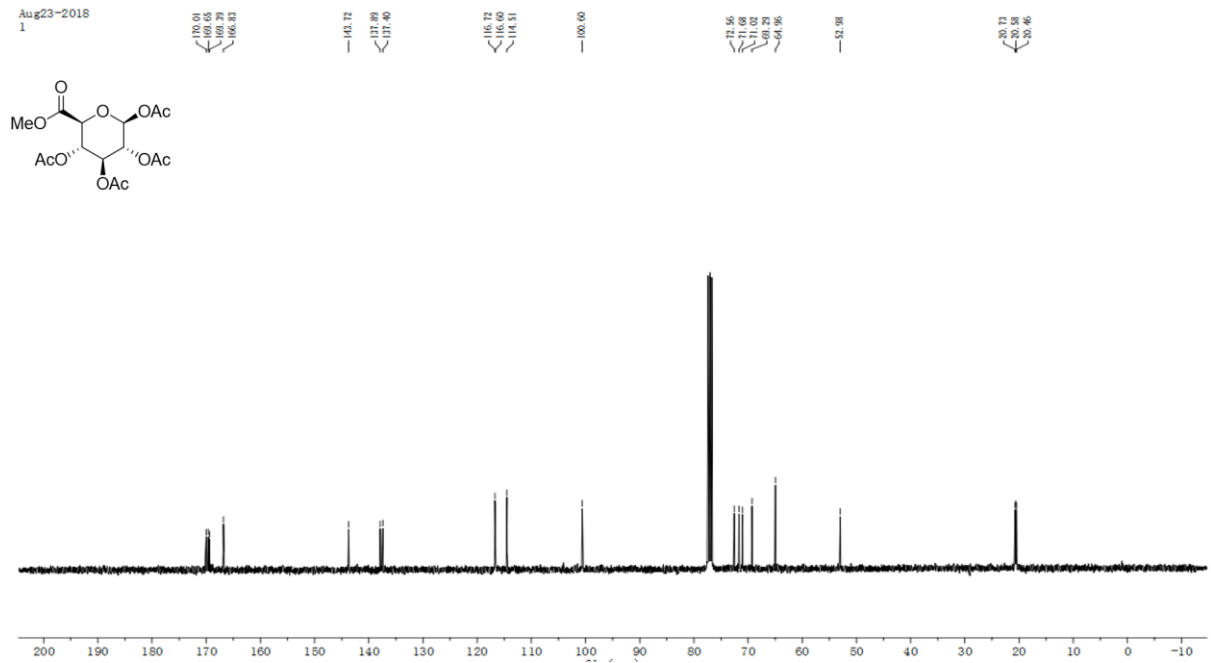
## tert-butyl 2-(pent-4-ynoyl)hydrazine-1-carboxylate (36)



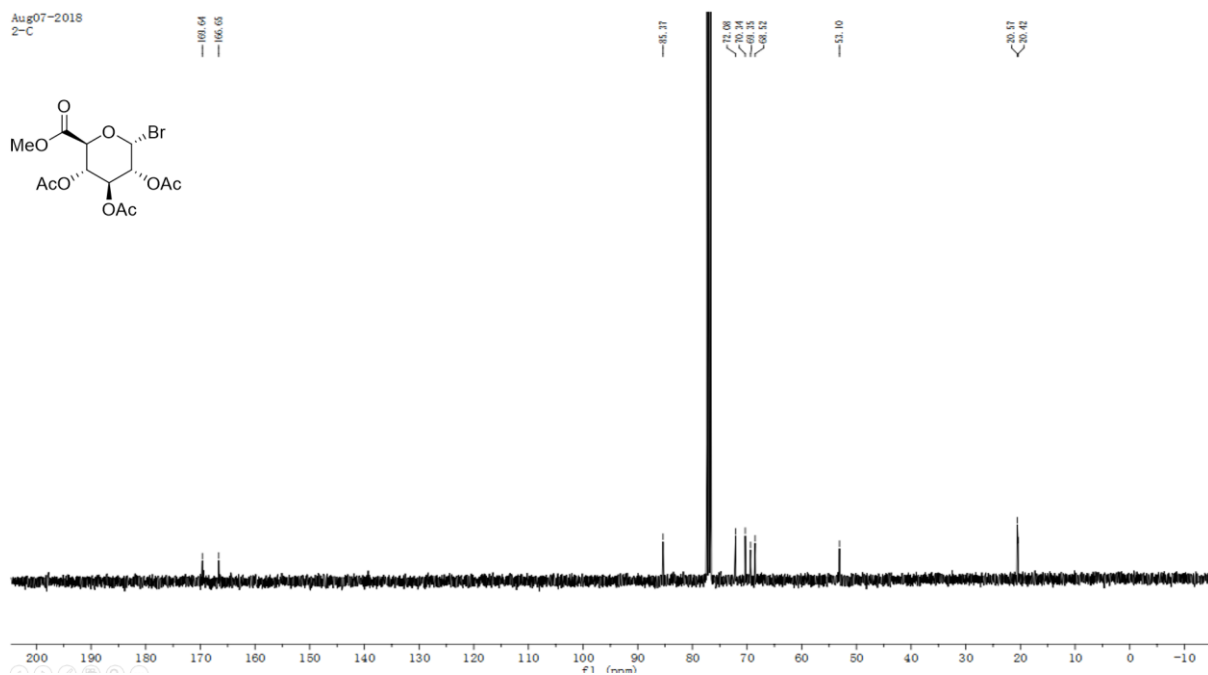
## ACL-DOX

Oct13-2019  
ACL-FINAL

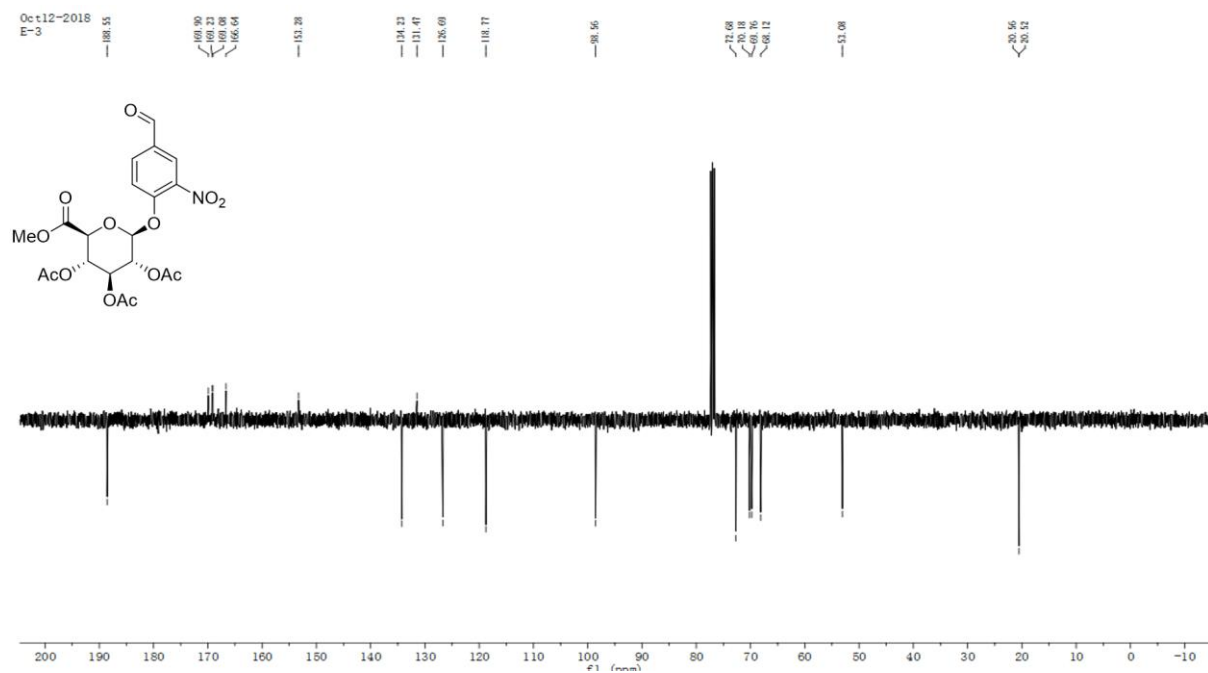
## (2S,3R,4S,5S,6S)-6-(methoxycarbonyl)tetrahydro-2H-pyran-2,3,4,5-tetrayl tetraacetate (39)

Aug23-2018  
1

**(2R,3R,4S,5S,6S)-2-bromo-6-(methoxycarbonyl)tetrahydro-2H-pyran-3,4,5-triyl triacetate (40)**

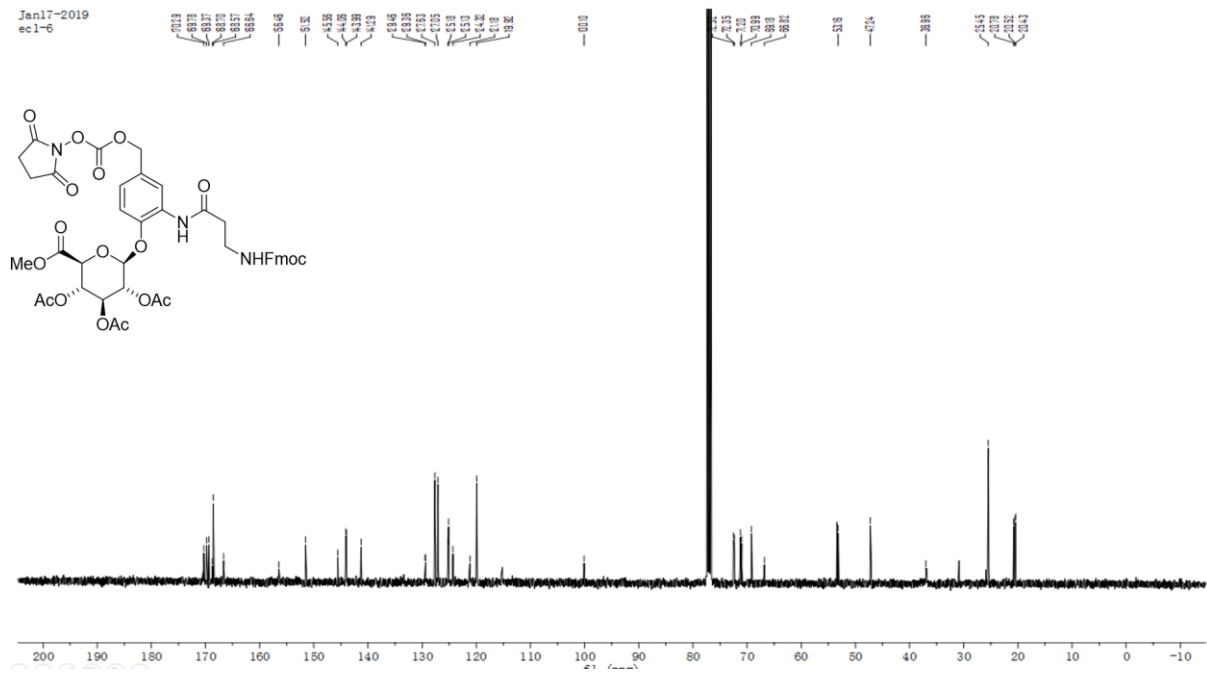


**(2S,3R,4S,5S,6S)-2-(4-formyl-2-nitrophenoxy)-6-(methoxycarbonyl)tetrahydro-2H-pyran-3,4,5-triyl triacetate (41)**

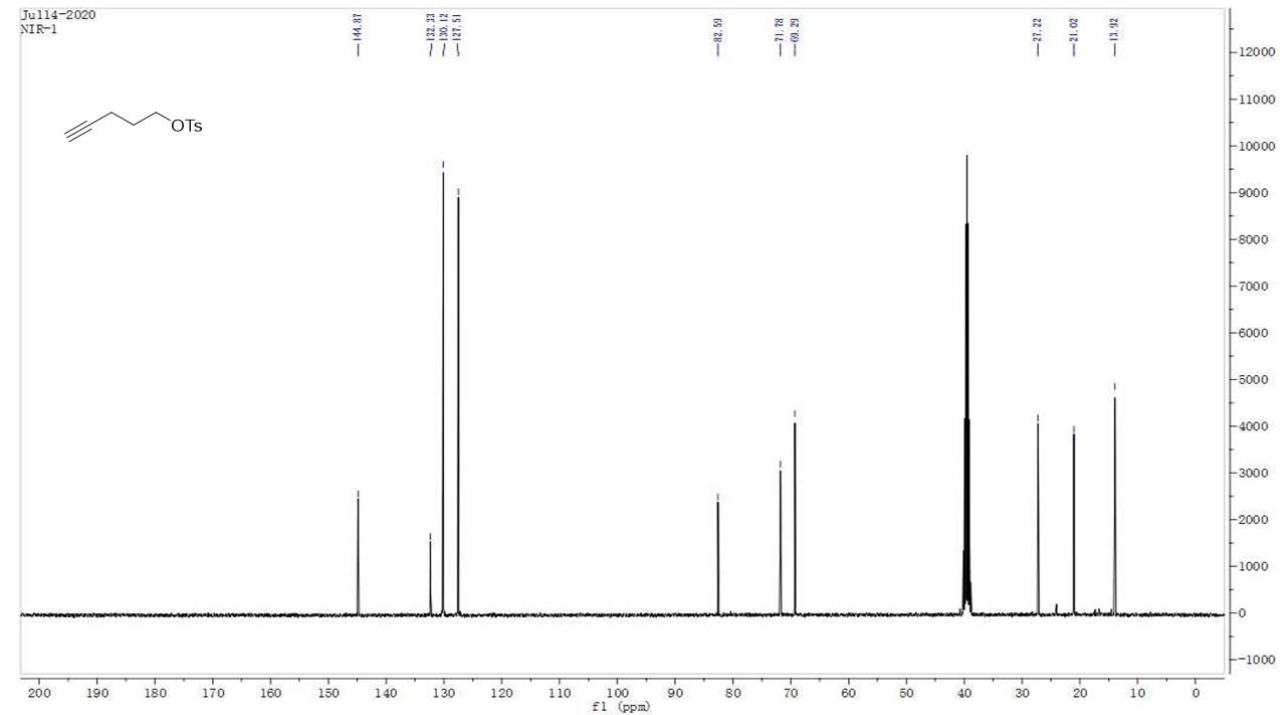


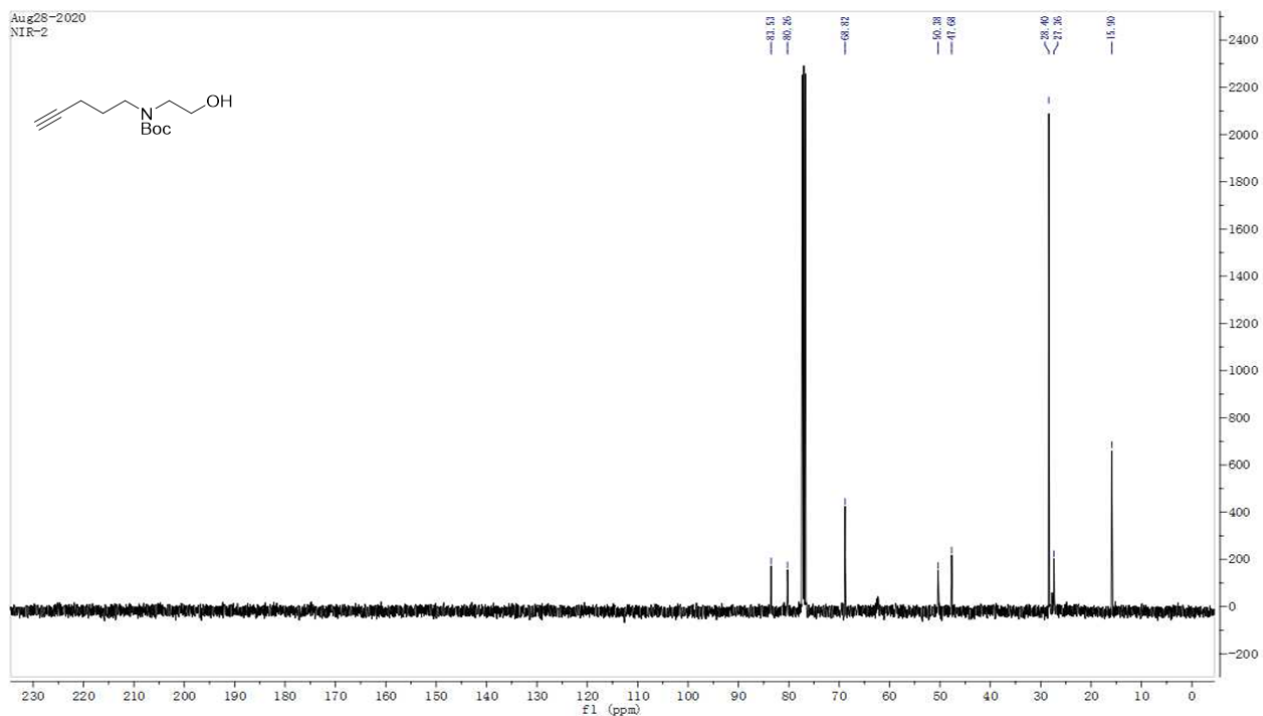
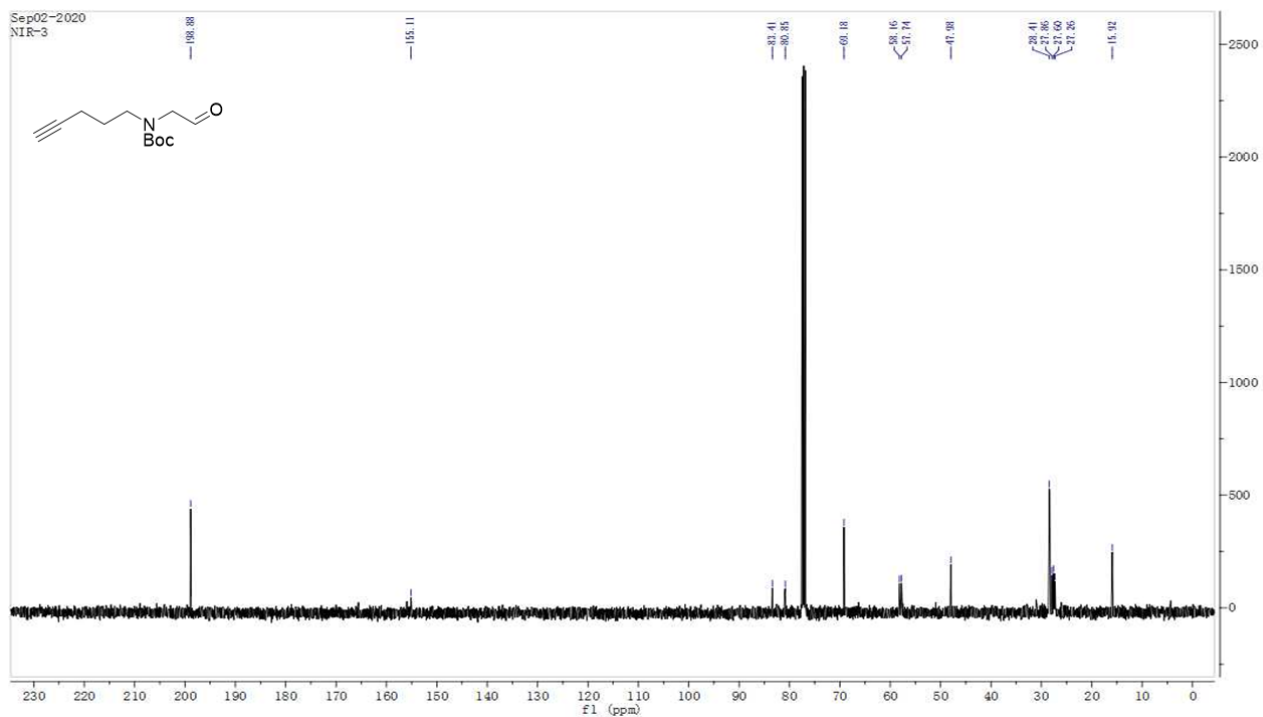


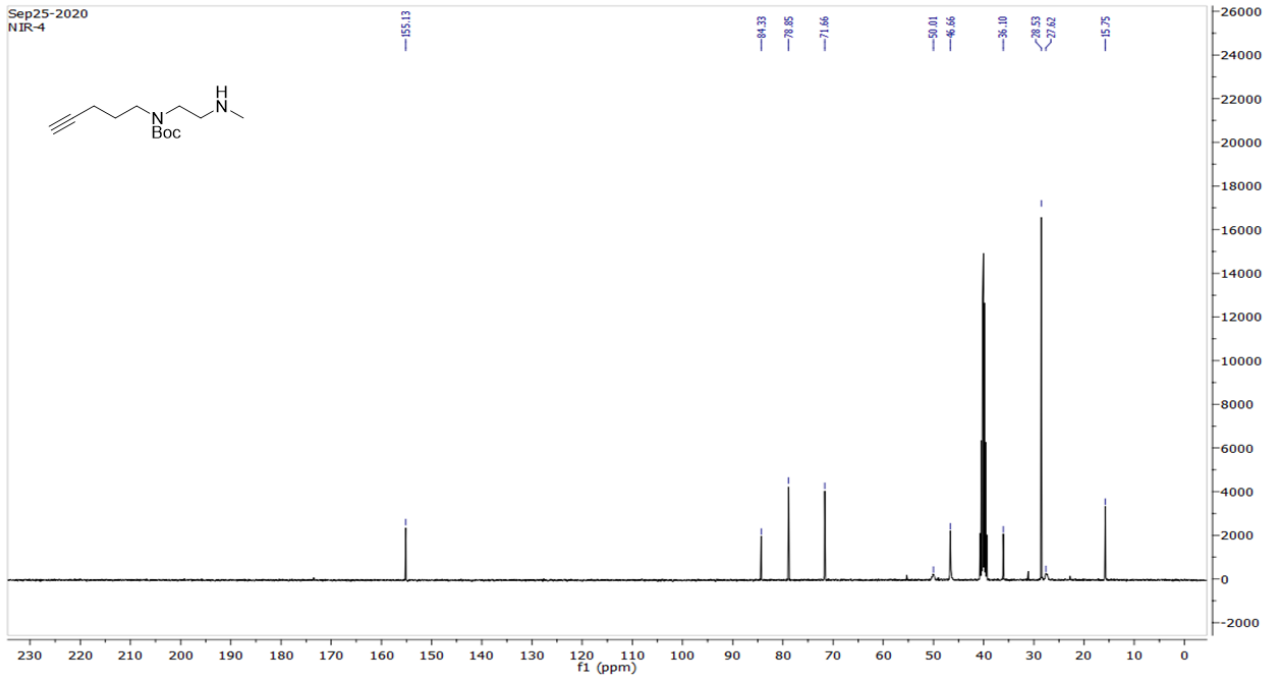
**(2S,3R,4S,5S,6S)-2-(2-(3-(((9H-fluoren-9-yl)methoxy)carbonyl)amino)propanamido)-4-(((2,5-dioxypyrrolidin-1-yl)oxy)carbonyl)oxy)methyl)phenoxy)-6-(methoxycarbonyl)tetrahydro-2H-pyran-3,4,5-triyl triacetate (44)**



**pent-4-yn-1-yl 4-methylbenzenesulfonate (50)**

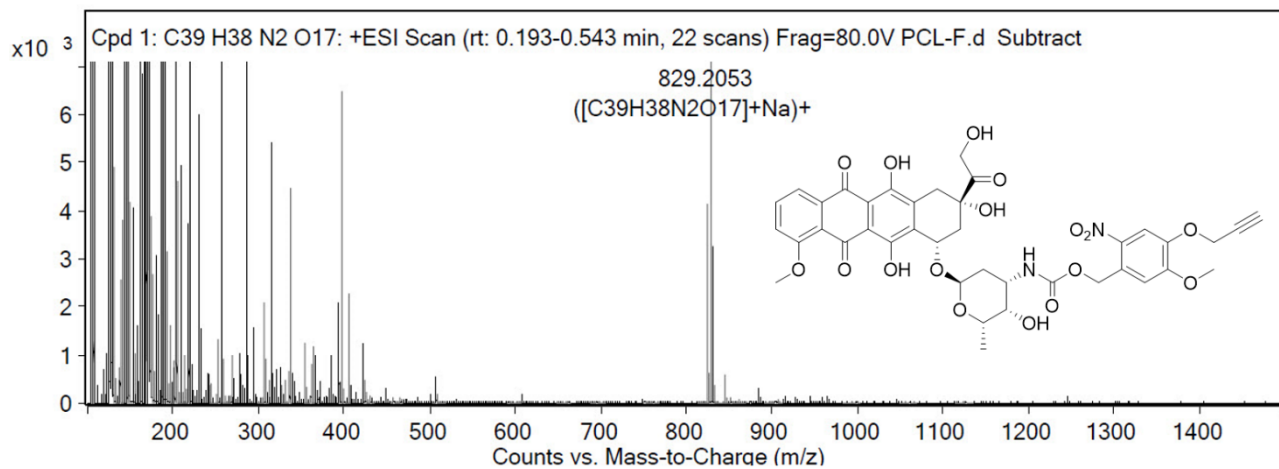


**tert-butyl (2-hydroxyethyl)(pent-4-yn-1-yl)carbamate (52)****tert-butyl (2-oxoethyl)(pent-4-yn-1-yl)carbamate (53)**

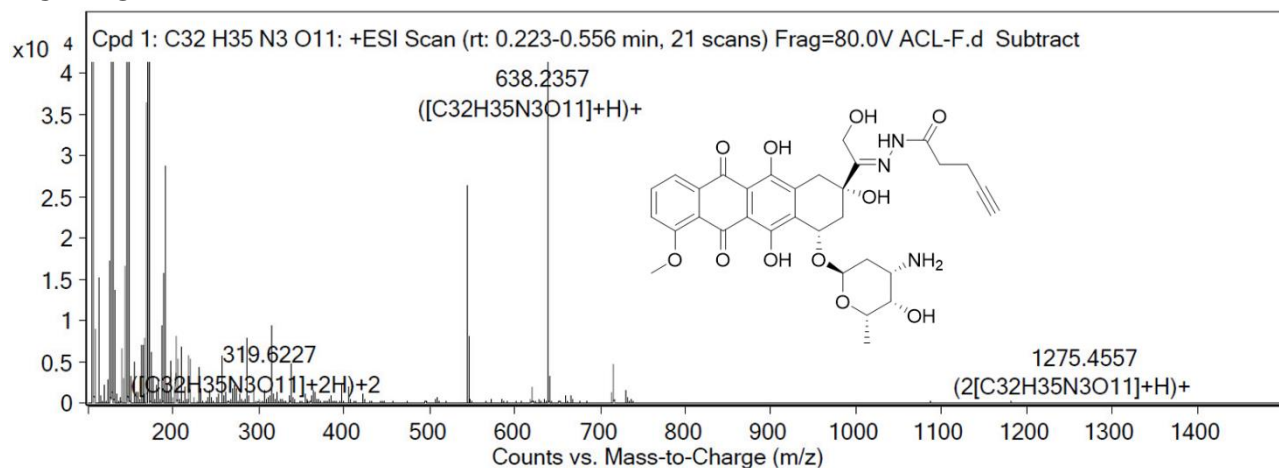
**tert-butyl (2-(methylamino)ethyl)(pent-4-yn-1-yl)carbamate (54)**

## HRMS spectra

### PCL-DOX



### ACL-DOX



### ECL-DOX

